Synthesis, photophysicochemical properties and photodynamic therapy activities of indium and zinc phthalocyanines when incorporated into Pluronic polymer micelles.

A thesis submitted in fulfilment of the requirements of the degree of

Masters degree of Science

At Rhodes University

By

Banele Mike Motloung

March 2020

Dedication

This work is dedicated to Mam Mnisi gwadlagwadla nkophe ezimayakaya ……

Acknowledgments

My utmost and sincere appreciation goes to the **Dist. Professor Tebello Nyokong**, for affording me the opportunity to work under her wing. Thank you for your unwavering guidance, support and encouragement throughout the programme.

Special thanks to Drs Balaji, Managa and Sekhosana for helping me out with the running of experiments and for being patient with me.

I would like to thank Prof John Mack, Dr Jonathan Britton, Ms Gail Cobus and Mr Francis Chindeka for their support and for making the Institute for Nanotechnology Innovation a pleasurable environment to work in. I am also grateful for the support from Prof Earl Prinsloo, Shirley, Marvin and members of staff in the Chemistry Department. To the S22 family, thank you for the enjoyable moments during the three years.

A special thanks to my family and friends for the sacrifices made on my behalf, imithandazo yenu ingigcine kwaze kwala. Financial support from the National Research Fund is greatly appreciated.

Udumo lonke kuye

Abstract

This thesis reports on the syntheses, photophysicochemical properties and photodynamic therapy activities of symmetrical metallophthalocyanines (MPcs) when alone or when incorporated into Pluronic polymer micelles. The Pcs contain either zinc or indium as central metals and have phenyldiazenylphenoxy, pyridine-2-yloxy and benzo[d]thiazol-2-ylthio as ring substituents. Spectroscopic and microscopic techniques were used to confirm the formation MPcs with micelles. The photophysics and photochemistry of the Pcs were assessed when alone and with micelles. All the studied Pcs showed good photophysicochemical behavior with relatively high triplet and singlet oxygen quantum yields corresponding to their low fluorescence quantum yields. The Pcs with indium in their central cavity exhibited higher triplet and singlet oxygen quantum yields in comparison to their zinc counterparts due to the heavy atom effect obtained from the former.

The *in vitro* dark cytotoxicity and photodynamic therapy of the Pc complexes and conjugates against MCF7 cells was tested. All studied Pc complexes alone and with micelles showed minimum dark toxicity making them applicable for PDT. All complexes displayed good phototoxicity < 50% cell viability (except for complex **2** > 50% cell viability) at concentrations ≤100 μg/mL, however the conjugates showed < 45% cell viability at concentrations ≤ 100 μg/mL, probably due to the small micellar size and EPR effect.

The findings from this work show the importance of incorporating photosensitizers such as phthalocyanines into Pluronic polymers micelles and making them water soluble and ultimately improving their photodynamic effect.

Table of Contents

Contents **Page**

List of abbreviations

^{1}H NMR	Proton Nuclear Magnetic Resonance
ADMA	Tetrasodium α, α-(anthracene-9,10-diyl) dimethylmalonate
DBU	1, 8-Diazabicyclo- [5.4.0]-undec-7-ene
DMF	Dimethyl Formamide
DMSO	Dimethyl Sulfoxide
DMSO-d_6	Deuterated Dimethyl Sulfoxide
DPBF	1,3 -Diphenylisobenzofuran
F	Fluorescence
FTIR	Fourier Transform Infrared
HOMO	Highest Occupied Molecular Orbital
IC	Internal conversion
ISC	Intersystem crossing
IR	Infrared
LUMO	Lowest Occupied Molecular Orbital
MPcs/Pcs	Metallophthalocyanines/Phthalocyanines
MX	Metal Salt
P	Phosphorescence
PDT	Photodynamic Therapy
PACT	Photodynamic Antimicrobial Chemotherapy
R	Substituents
ROS	Reactive Oxygen Species
THF	Tetrahydrofuran

TCSPC	Time Correlated Single Photon Counting
TEM	Transmission Electron Microscope
Uv-Vis	Ultraviolet- Visible
RT	Room Temperature

List of symbols

α	Non-peripheral position
β	Peripheral position
ΔAS	Change in singlet state absorbance
ΔAT	Change in triplet state absorbance
Ɛ	Molar extinction coefficient
$Ɛ_S$	Singlet state molar extinction coefficient
$Ɛ_T$	Triplet state molar extinction coefficient
λ	Lambda
τ_F	Fluorescence lifetime
τ_T	Triplet state lifetime
Φ_F	Fluorescence quantum yield
Φ_T	Triplet state quantum yield
Φ_Δ	Singlet Oxygen quantum yield
A/abs	Absorbance/absorption
S_0	Singlet ground state
S_1	Singlet excited
T_1	Triplet excited state
T_2	Second triplet excited state

Preface

The thesis describes the synthesis of symmetrical phthalocyanines (Pcs) containing zinc and indium as central metals. The Pcs are physically entrapped into Pluronic micelles. The photophysical and photochemical properties of the Pcs and their conjugates are studied together with photodynamic therapy behavior against epithelial breast cancer cell lines (MCF7).

CHAPTER 1
INTRODUCTION

This chapter highlights the basic structure of phthalocyanines (Pcs), their application and syntheses. Basic background on Pluronic micelles, their syntheses and applications are also presented.

1.1 Phthalocyanines (Pcs)

1.1.1 Brief history and general applications

Phthalocyanines (Pcs) are planar aromatic macrocycles consisting of an 18 π – electron conjugated ring with four isoindole units connected via nitrogen atoms **[1, 2]**. The Pc macrocycle can be substituted with different functional groups on the nonperipheral (α) and peripheral (β) positions (shown in **Scheme 1.1,** to be discussed later), to influence their physicochemical properties which are crucial for their applications.

At the same time the central cavity of Pcs can coordinate different metals to form metallophthalocyanines (MPcs) and these metals are known to influence their photophysical behaviour.

Pc derivatives have attracted attention as second generation photosensitizers (PS) for diverse applications such as photodynamic therapy (PDT) **[3-5]**, photodynamic antimicrobial chemotherapy (PACT) **[6-8]**, photodegradation of pollutants **[9]** and nonlinear optics **[10]** to mention but a few. Their applicability could be attributed to their ease of structural modifications, absorption in the infra-red region, good optical, chemical and thermal properties **[11 – 15]**.

1.1.2 Electronic Absorption spectral behaviour of MPcs

The ground state electronic absorption spectra of MPcs are often influenced by factors such as nature of the central metal, ring substituents, the solvent used, point of substitution and ring expansion **[16–19]**. MPcs are characterised by two distinct absorption bands as shown in **Figure 1.1.**

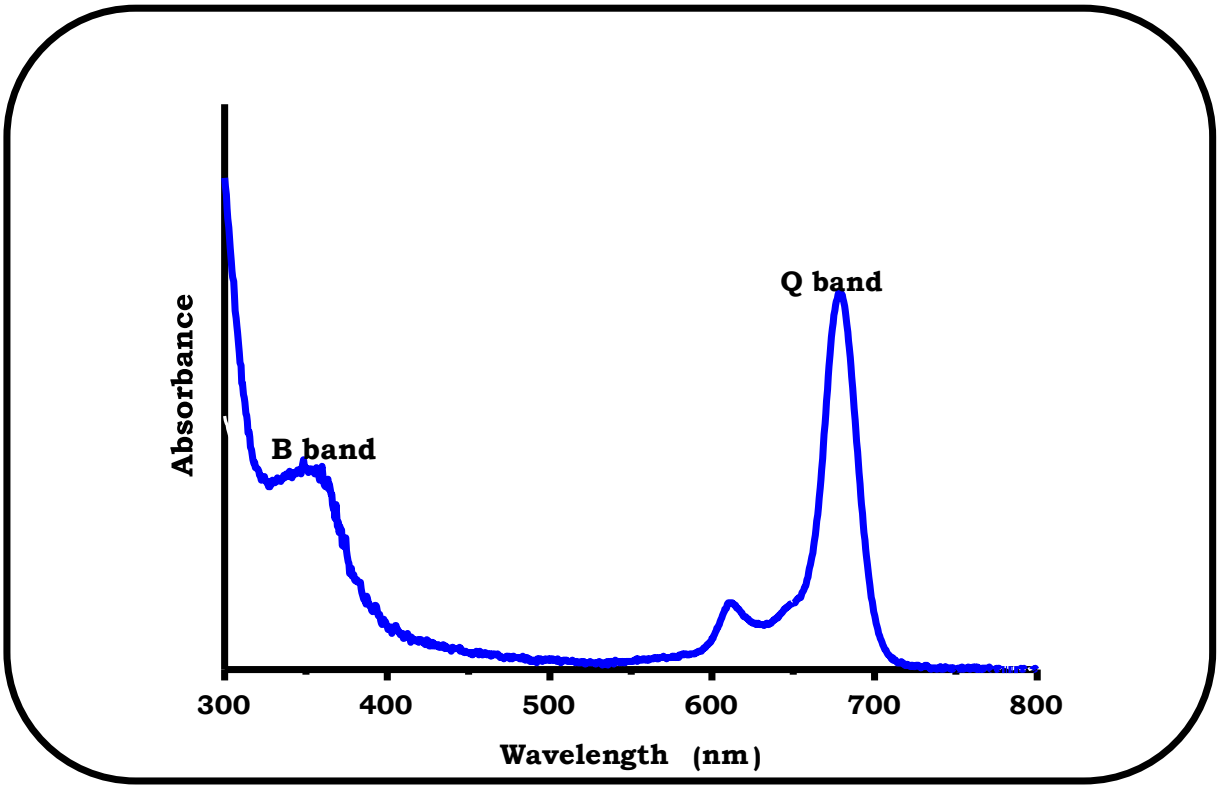

Figure 1.1: Ground state electronic absorption spectrum for MPcs.

The Q-band is the most intense peak found in the visible and near infra-red region depending on the structural properties of the MPcs, while the B-band, found between 300–400 nm, consists of two less intense, overlapping peaks due to B_1 and B_2 hence it is broad **[20]**.

Using Gouterman's four orbital model **[21]**, the Q-band is assigned to the doubly degenerate π-π* transition between the ground state a_{1u} of the highest occupied molecular orbital (HOMO) to the degenerate e_g of the lowest unoccupied molecular orbital (LUMO), while the B-bands (B_1 and B_2) correspond to the π-π* transitions from a_{2u} and b_{2u} of the HOMO to the e_g of the LUMO, **Figure 1.2 [20–23]**.

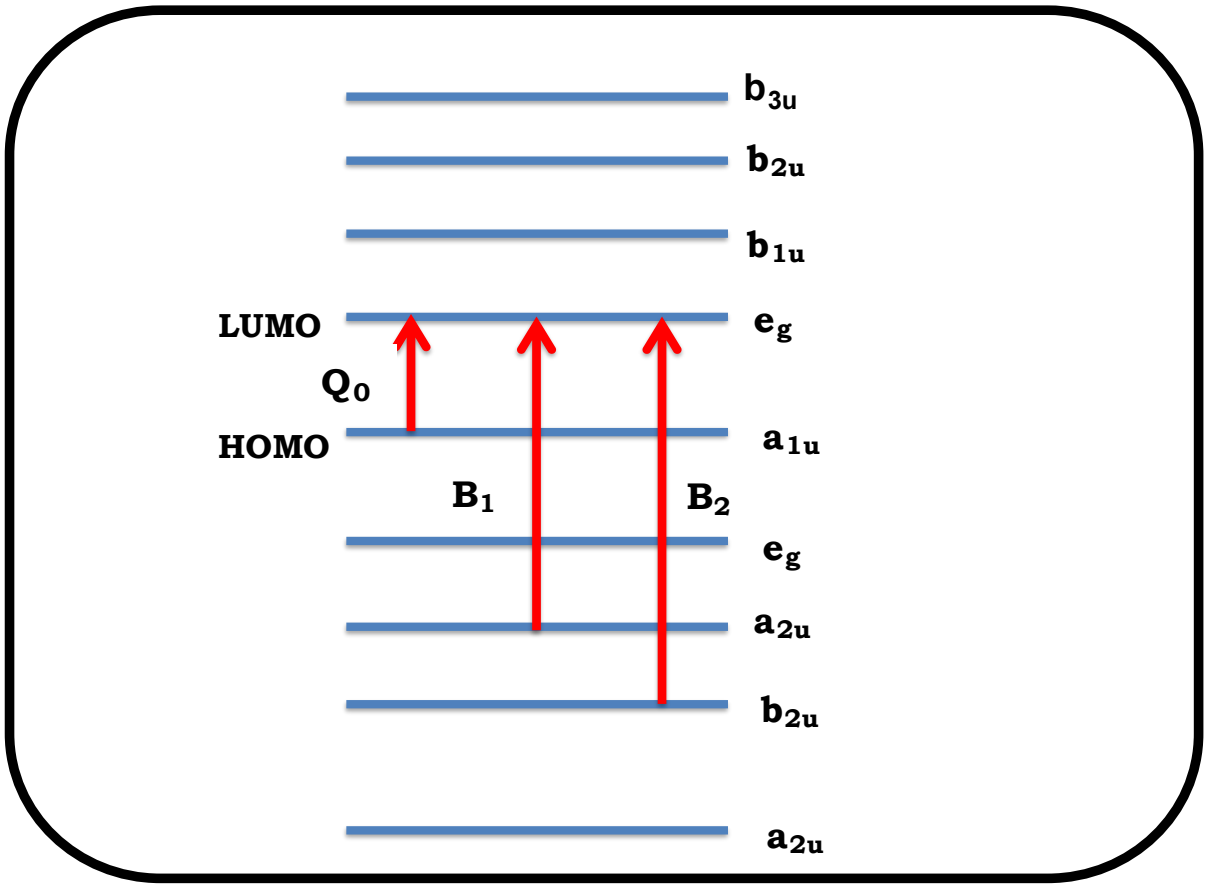

Figure 1.2: Electronic transitions in metallated Pcs showing the origin of the Q_0, B_1 and B_2 absorption bands

1.1.3 Synthesis

The synthesis of phthalocyanines can be achieved using different precursors such as: phthalimide, phthalic acid, phthalic anhydride, o-cyanobenzamide, odibromobenzene, diiminoisondole and phthalonitrile. The most commonly used precursor being the phthalonitriles because they produce higher yields of MPcs, and pure compounds compared to other precursors **[24]**.

For the synthesis of α and β substituted Pcs, 3-nitrophthalonitrile and 4nitrophthalonitrile, respectively are used as precursors. The nitro groups of these phthalonitriles are modified to afford the desired substituted phthalonitriles for the synthesis of Pcs. Symmetrically tetra-substituted Pcs are synthesized by cyclocondensation of mono-substituted phthalonitriles as precursors **[25-27], Scheme 1.1**

Mono-substituted phthalonitriles always result in a mixture of four possible isomers of tetrasubstituted phthalocyanines with D_{2h}, C_{4h}, C_{2v} and C_s symmetry as shown in

Figure 1.3 (using β substituted Pcs as examples). Similar isomers are obtained for the α substituted Pcs. Attempts have been made to isolate these isomers and a few have been isolated using column chromatography **[28,29]**, however in most cases specially designed high-performance liquid chromatography (HPLC) columns are required and the yield is low. Isomeric mixtures have been shown to be suitable for many applications including PDT **[30]**.

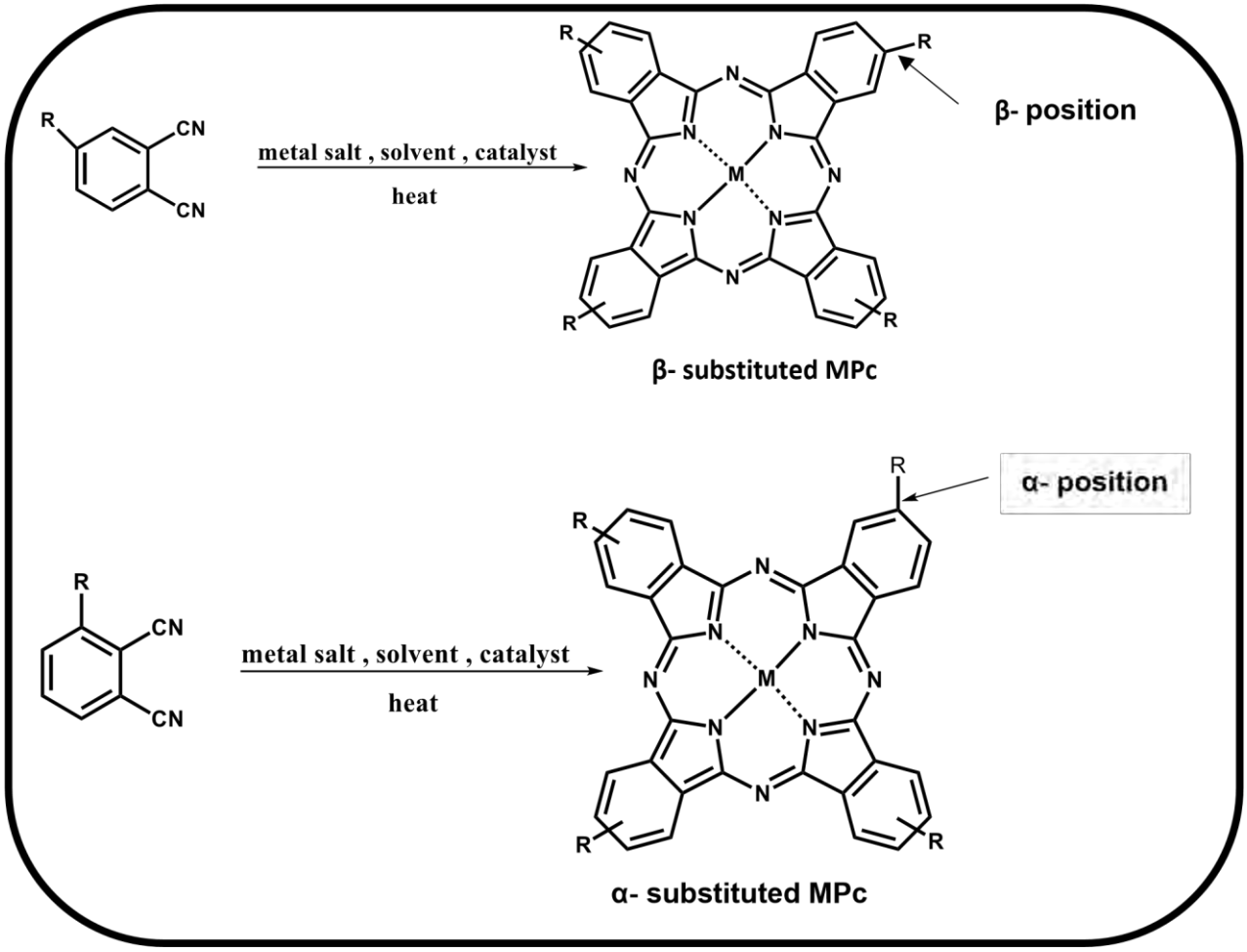

Scheme 1.1: Synthetic route for tetrasubstituted MPcs (R represents the substituent).

Statistical condensation of two differently substituted phthalonitriles is generally utilized for the synthesis of A_3B-type asymmetrical Pcs, which are characterized by three identical (A) isoindole subunits and one different (B) subunit, **Scheme 1.2**. The phthalonitrile precursors are combined in mole ratios of 3:1 up to 9:1 (A: B) depending on the reactivity of the substituents **[31-34]**. A mixture of six products could be obtained as shown in **Scheme 1.2** and these are separated chromatographically to isolate the desired Pc (A_3B or AB_3). Symmetrical Pcs are employed in this thesis.

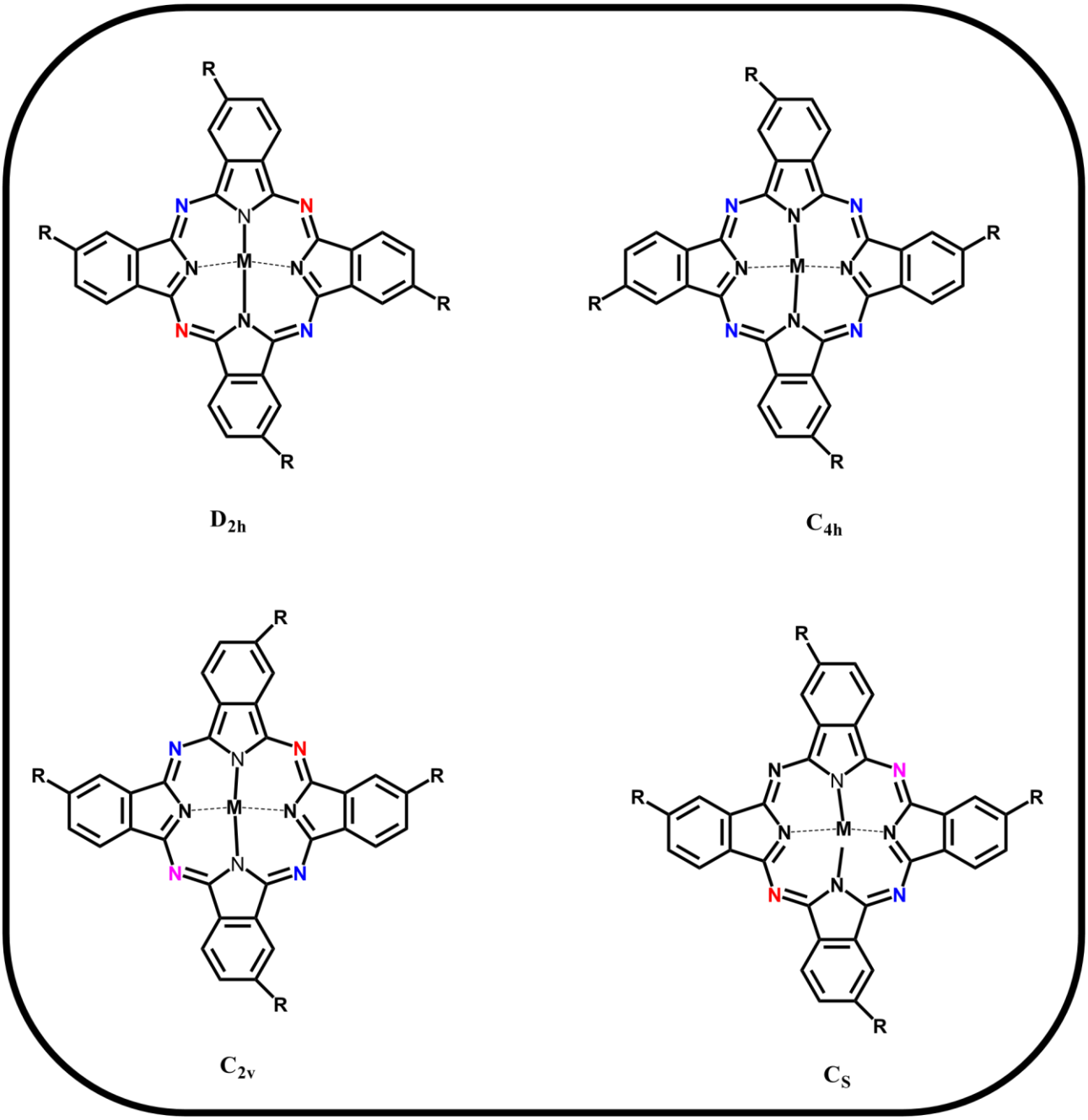

Figure 1.3: Constitutional isomers of tetrasubstituted phthalocyanines (For each isomer symmetrically non-equivalent nitrogen atoms are shown in different colours and R represents different substituents).

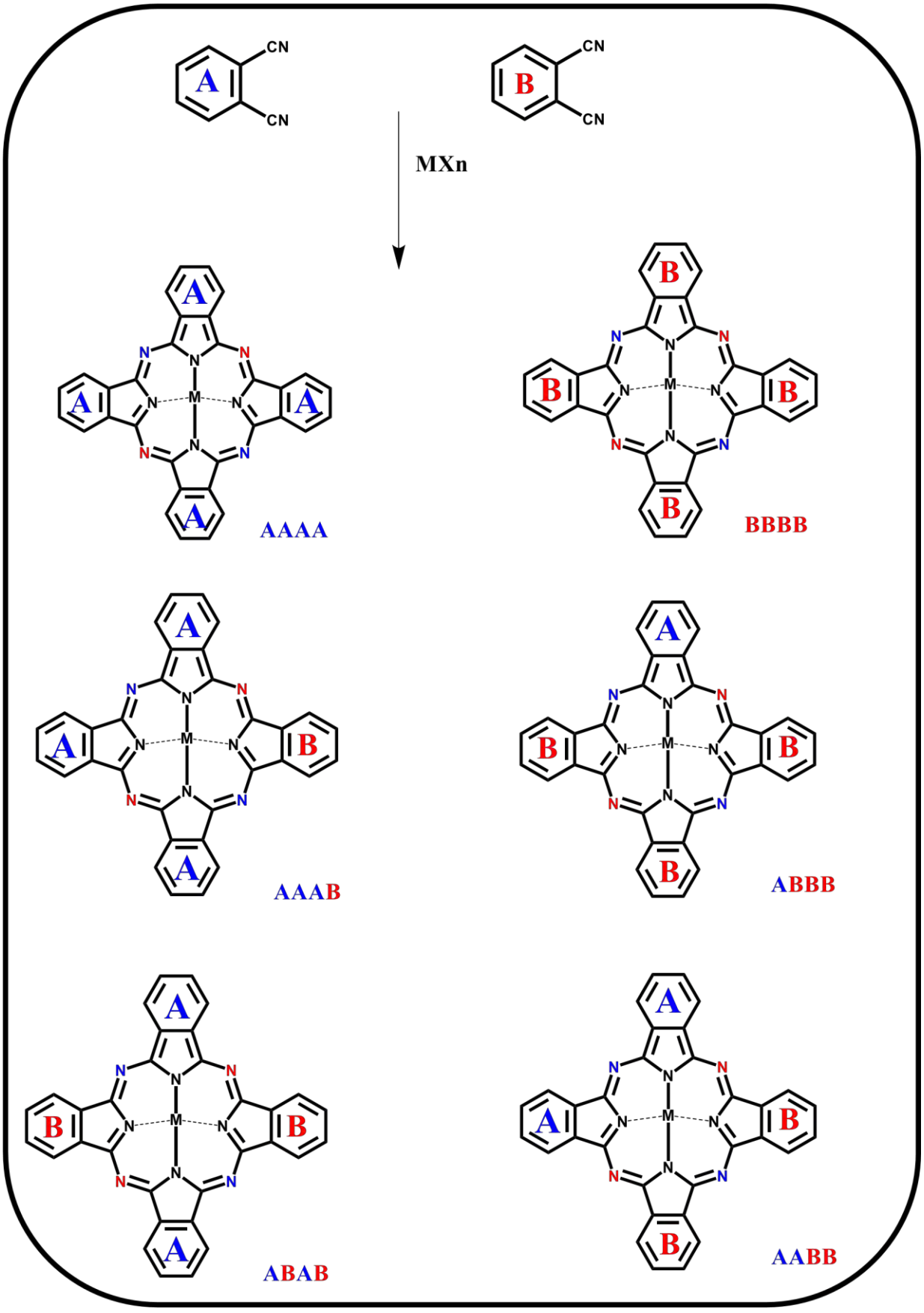

Scheme 1.2: Statistical mixed condensation products of phthalonitriles A and B.

1.1.4. MPcs synthesized and studied in this work

In this work symmetrical peripherally substituted MPcs are synthesized containing either indium or zinc as central metals and with benzo[d]thiazol-2-ylthio, phenyldiazenylphenoxy and pyridyloxy as ring substituents, **Table 1.1,** Complexes **4**, **5** and **6** have been reported before **[35-37]**, however their photophysicochemical behaviour in the presence of Pluronic polymer micelles are explored for the first time in this work. Complexes **1**, **2** and **3** are reported for the first time in this work.

1.1.4.1 Choice of central metal

Metal centres influence photophysical and photochemical properties of Pcs. In and Zn were chosen because they are diamagnetic hence, they have a closed shell structure which results in enhanced photophysical properties. Furthermore, as heavy atoms they promote intersystem crossing to populate the triplet state through the spin orbit coupling (SOC) also termed as heavy atom effect. SOC is most common in atoms whose nuclei are large and enhances the kinetics of both radiative and non-radiative transitions between states with different spin **[38, 39]**.

1.1.4.2 Choice of substituents

Substituents greatly influence the behaviour of MPcs in particular their photophysical and photochemical properties together with their applications **[40,41]**.

i) The azo groups (in complexes **1** and **2**) were chosen as a ring substituent due to the promising anticancer properties displayed by compounds containing azo groups **[42]**.

ii) The pyridyloxy substituents (in complexes **3** and **4**) were chosen because of the reported anticancer potential for pyridine derivatives **[43, 44]**. Phenyl rings are reported to contribute to effective population of the triplet state **[45]**

iii) The benzo[d]thiazol-2-ylthio substituents (in complexes **5** and **6**) were chosen since benzothiazole derivatives have been found to have antitumor activities **[46-48]** which could be advantageous for PDT applications. Additionally, phenyl rings could be advantageous as mentioned before.

Table 1.1: MPcs synthesized in this work.

Molecular Structure	Phthalocyanine	Pluronic polymer micelle	Studies	Complex number.
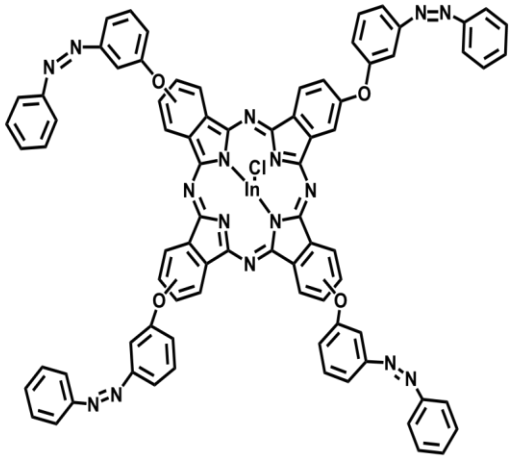	indium (III) chloride tris(3-((Z)-phenyldiazenyl) phenoxy) phthalocyanine	F – 127	Photophysics and PDT	**1** (New)
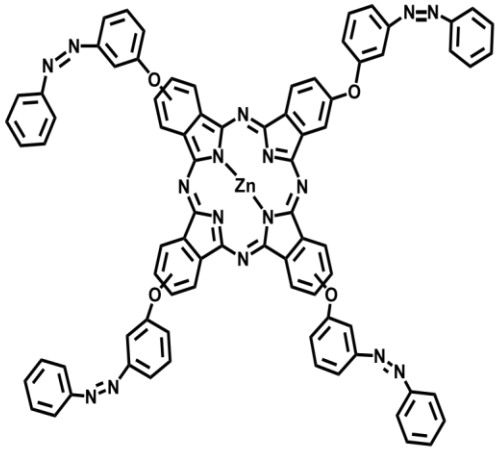	zinc (II) tris(3-((Z)-phenyldiazenyl) phenoxy) phthalocyanine	F – 127	Photophysics and PDT	**2** (New)
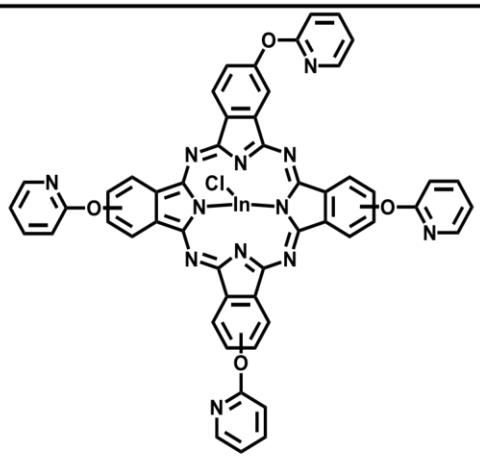	indium (III) chloride tetrakis (pyridin-2-yloxy) phthalocyanine	F – 127	Photophysics and PDT	**3** (New)

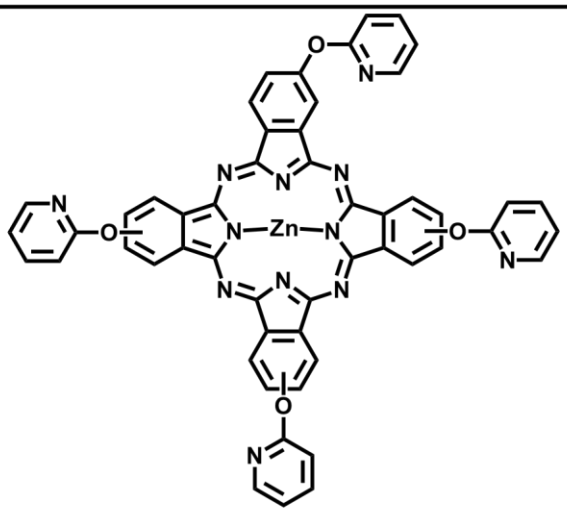	zinc (II) tetrakis (pyridin-2-yloxy) phthalocyanine **[35]**	F – 127	Photophysics and PDT	**4**
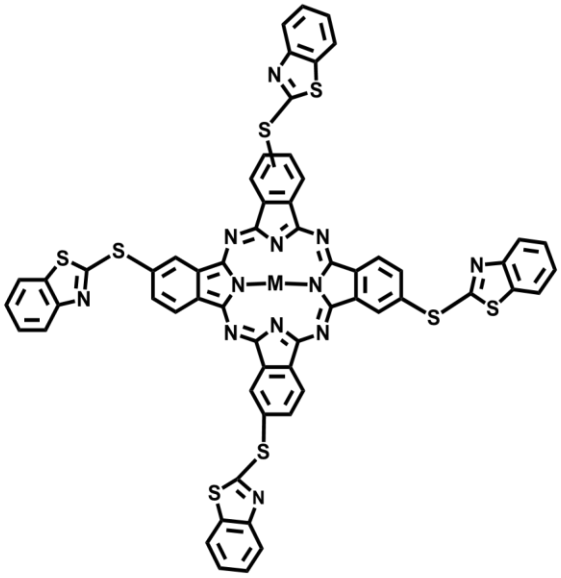	indium (III) chloride tetrakis [benzo[d]thiazol-2-ylthio) phthalocyaninato] **[36, 37]** zinc (II) tetrakis [benzo[d]thiazol-2-ylthio) phthalocyaninato] **[36,37]**	F – 127 L121/F127 F – 127 L121/F127	Photophysics and PDT Photophysics and PDT	**5** **6**

1.2 Photodynamic therapy (PDT) and Pluronic Micelles

PDT is a clinically approved, minimally invasive cancer treatment modality which requires a photosensitizer (PS) and light of appropriate wavelength in the presence of ground state molecular oxygen to elicit selective destruction of the tumor cells **[4]**. The three components (a PS, visible light and molecular oxygen) are nontoxic when separate, however when the PS is activated by visible light, the excited PS reacts with molecular oxygen leading to the production of reactive oxygen species (ROS), capable of inducing stress on tumorigenic cells **[4,49–51]**.

PDT is useful for the treatment of early and localised tumours, due to the selective delivery of the PS to cancerous tissue **[5, 52]**. However, complete cure of metastatic tumours is more challenging since irradiation of the whole body is not possible **[5, 53]**. MPcs have proven to be an efficacious PS for PDT of cancer and some of them have been approved in countries such as Russia, United States of America and United Kingdom, for the treatment of cancer. **Figure 1.4** shows the phthalocyanines that are in clinical trials **[54, 55]**.

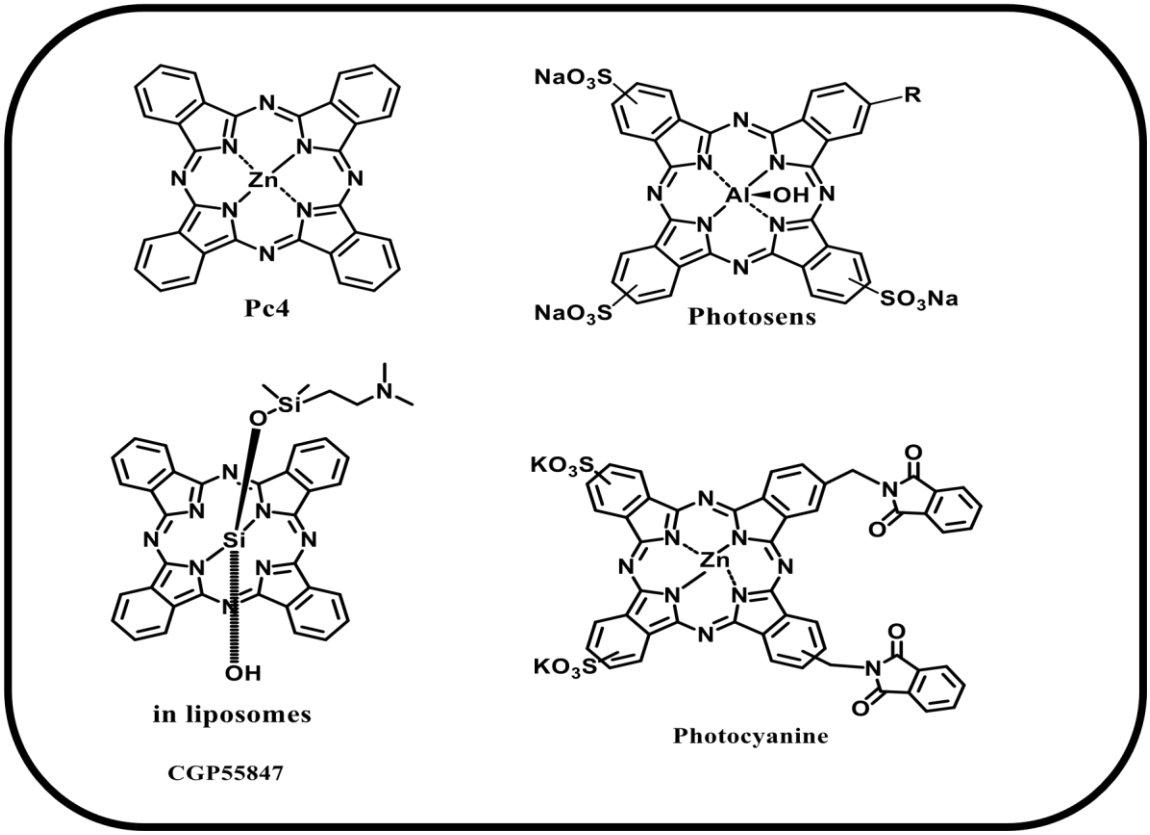

Figure 1.4. Some MPcs in clinical trials as PS for PDT

1.2.1. PDT mechanisms when using MPcs as PSs.

During photosensitisation as shown in **Figure 1.5**, the MPc (as a PS) is irradiated with light of a specific wavelength, usually between 600 – 800 nm **[51]**. The MPc in the ground state (S_0) absorbs light, which provides energy for the MPc to reach an electronically excited singlet state (S_1). The S_1 state has an unstable and short half-life (10^{-9} s) **[53]**, leading to fast deactivation through either radiative (such as fluorescence) or non-radiative processes, like intersystem crossing (ISC). Ideal MPcs undergo deactivation through ISC to a triplet excited state (T_1). The longer half-life (10^3 s) of the T_1 state **[53]** compared to S_1, allows for enough time for photosensitisation by the excited MPc.

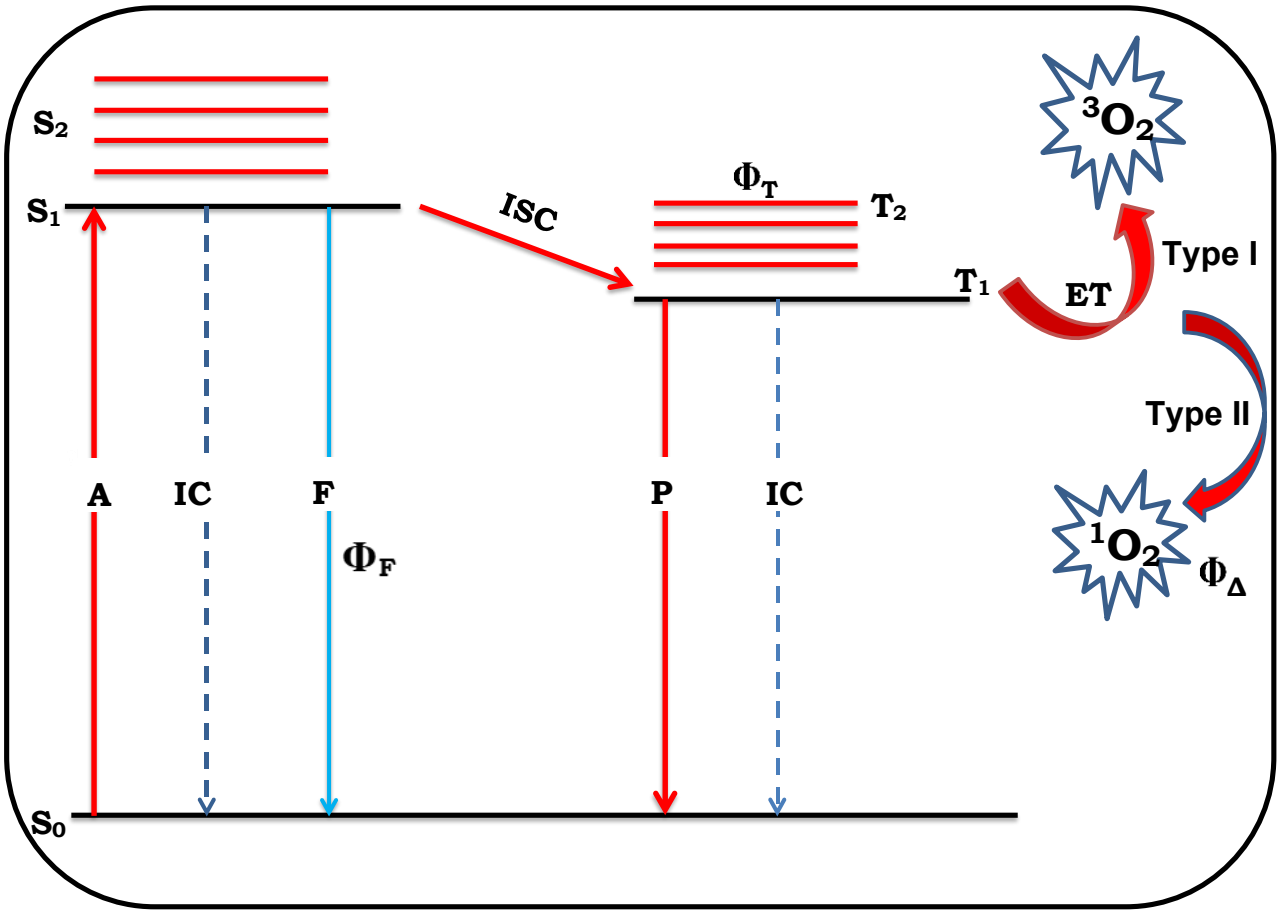

Figure 1.5: A modified Jablonski diagram showing the transitions between ground state (S0) and electronic excited states (S1 and T1). S1= singlet excited state, T1= first triplet state, A= absorption, F= fluorescence, IC = internal conversion, ISC= intersystem crossing, P= phosphorescence, ET = energy transfer

The excited MPc molecule in the triplet excited transfers its energy to ground state oxygen O_2 ($^3\sum_g$), generating excited state oxygen, O_2 ($^1\Delta_g$), the main cytotoxic species, which subsequently oxidizes the substrate. This is the type II mechanism **[51, 52, 56, 57]**.

Type I mechanism involves the interaction of the excited triplet state of the MPc with ground state molecular oxygen or substrate molecules generating superoxide and hydroperoxyl radicals, which subsequently afford oxidation of the substrate. It has been reported **[51, 52, 56, 57]** that the Type II mechanism is more common in photoinitiated oxidation reactions; hence the magnitude of the singlet oxygen quantum yield (Φ_Δ), which expresses the amount of singlet oxygen generated per quanta of light, is often employed as the main criterion in choosing the photosensitizers to be used in photocatalytic reactions **[52,53,58,59].** Even though phthalocyanines are well

– known photosensitizers for PDT, their applications as photosensitizers in PDT are often hampered by their hydrophobicity, as this complicates their formulation and results in an unfavourable biodistribution. Hence the use of Pluronic polymer micelles.

1.2.2. Pluronic micelles

Pluronic^{TM} block copolymers (also known as 'poloxamers') are non-ionic polymers comprised of two blocks of poly (ethylene oxide) (PEO) separated by a central block of poly (propylene oxide) (PPO) arranged in A-B-A triblock structure as illustrated **(Fig. 1.6)**.

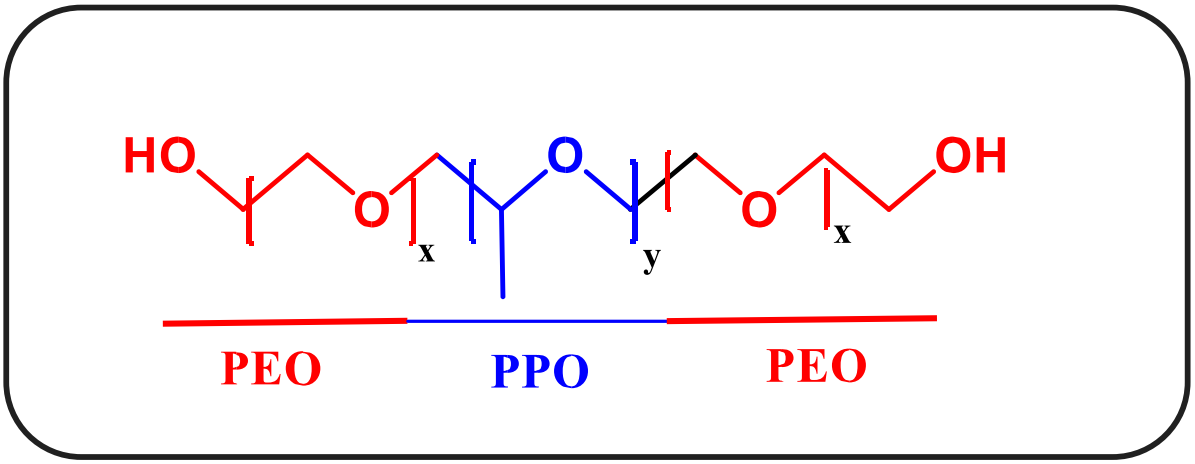

Figure 1.6: Schematic representation of the arrangement of Pluronic polymer.

The PEO and PPO segments on the micelles act as hydrophilic corona and hydrophobic core, respectively **[59-63]**. Pluronic^{TM} block copolymers are appealing because their physicochemical properties are tuneable. The advantages of Pluronic block copolymers are that they are commercially available in very broad compositions and they are regarded as being cost effective. A defining property of amphiphilic block copolymers is the ability of individual block copolymer termed 'unimers', to self-assemble into micelles in aqueous solutions. The formed micelles can have an estimated diameter of 30–50 nm at concentrations equal to or above the critical micelle concentration (CMC) **[64-66]**. The CMC is very important because it determines the stability of micelles against possible dilution of the drug delivery system and specifies the maximal achievable concentration of Pluronic unimers to the targeted cells **[65, 67]**. Micelles can be spherical, rod-like, or lamellar depending on the length of the ethylene oxide (EO) and propylene oxide (PO) blocks, concentration of the block copolymers, and the temperature **[68]**. Polymer micelles are fast becoming a powerful

nanomedicine platform for cancer therapeutic applications because of their biocompatibility and relatively small size, which help to prevent them from being recognized by proteins and macrophages therefore allowing a greater circulation time **[69]**. Polymer micelles also can solubilize water insoluble drugs **[70]**. Several Pluronics have been approved by Food and Drug Administration (FDA) for oral or intravenous administration because they are widely employed as solubilizers, emulsifiers or coating agents due to their biocompatibility and high drug loading ability **[69, 71- 73]**.

1.2.3. Incorporation of phthalocyanines into Pluronic polymers

There are different methods that can be used to incorporate drugs into polymer micelles such as dialysis, emulsion and evaporation **[74]** under the evaporation methods there is solid dispersion and film formation **[75]**. Solid dispersion method involves solubilization of copolymer with the phthalocyanine/drug **(Fig. 1.7)**, followed by rotative evaporation. The mixtures are then placed on a sonicator at room temperature and the solvent is removed **[76]**. The achieved solid products are left in a vacuum desiccator, followed by hydration and vigorous stirring. The solutions are transferred onto test tubes and left undisturbed for precipitation of drugs/Pcs which were not bound onto the polymer, which are then filtered **[76,77]**. This method was employed in this work.

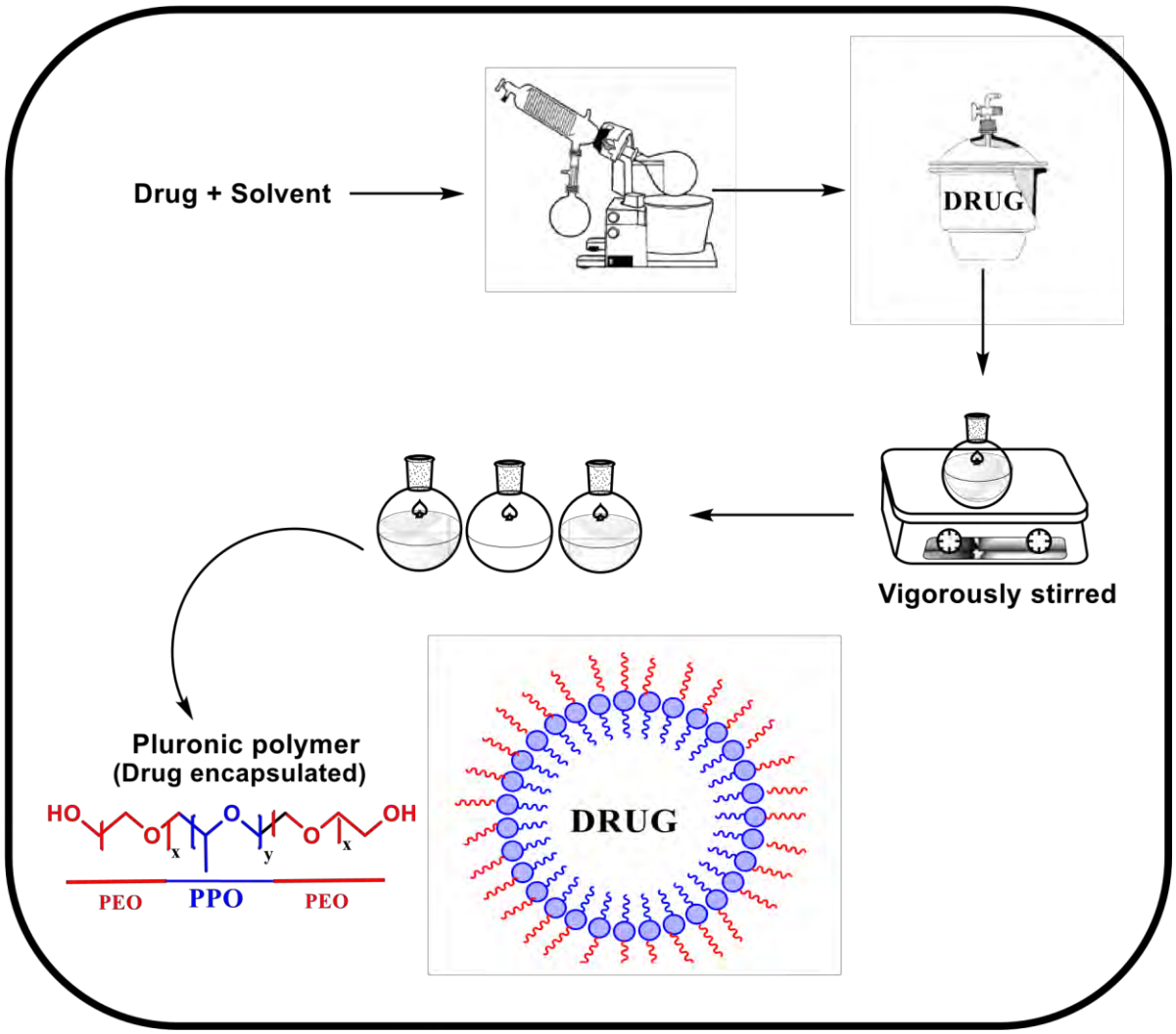

Figure 1.7: Schematic representation of incorporation of drugs into Pluronic polymers.

Porphyrins and phthalocyanines that have been embedded into different Pluronic polymers micelles reported in literature **[78-87],** are shown in **Table 1.2**.

Table 1.2 Some Porphyrins and Phthalocyanines embedded in individual Pluronic micelles.

Compound	Pluronic Polymer	studies /PDT	Reference
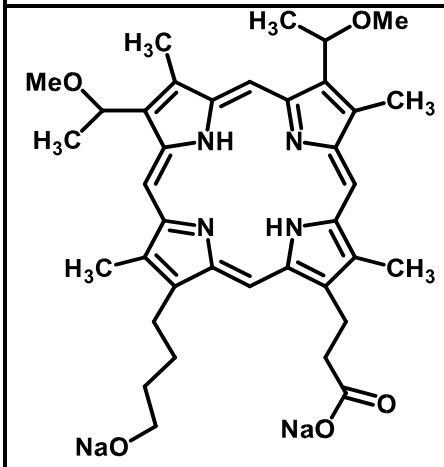	F108, F127, P85, P123, L61 and L64	Singlet Oxygen quantum yields and PDT	**[78,79]**
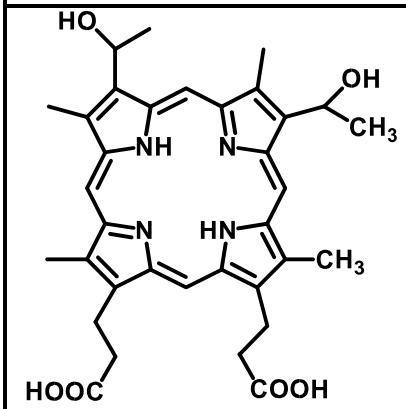	F127, P108 and L122	Fluorescence quantum yields and Singlet oxygen quantum yields	**[80]**
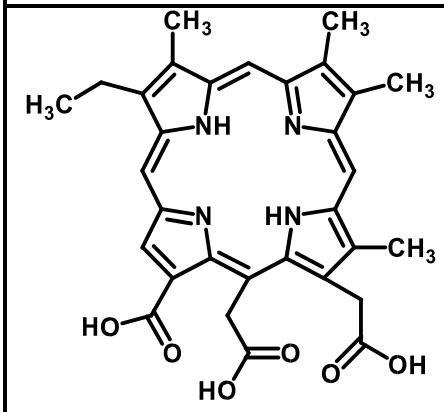	F127	Singlet Oxygen quantum yields and PDT	**[81]**

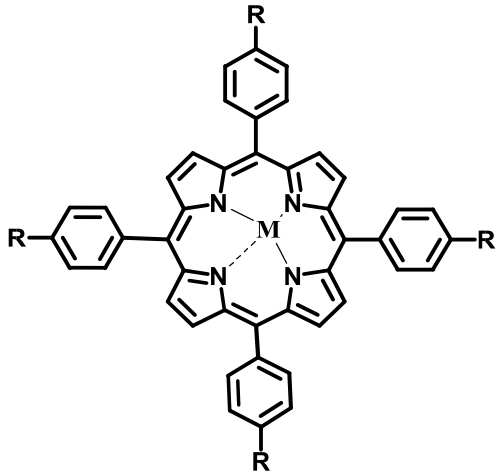 **M = H_2** **R= H**	F127	Singlet Oxygen quantum yields	**[78,82]**
M = H_2 **R= OH**	F127, P108 and L122	Fluorescence quantum yields	**[81]**
M = H_2 **R = $N(CH_3)^+$)** **= OH** **= SO_3H** **= COOH**	F68, F127, P123 and L44	PDT	**[83]**
M = H_2			

R = 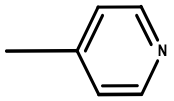 = 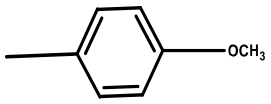	and F127 P123	-	**[84]**
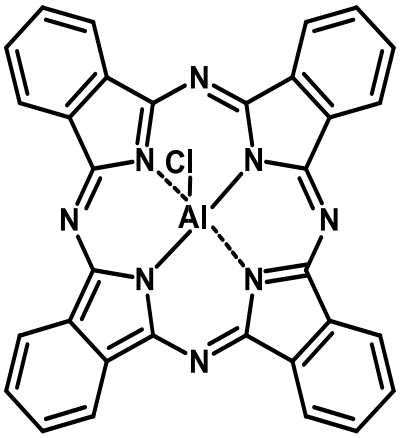	and F127 P123	PDT and PACT	**[85,86]**
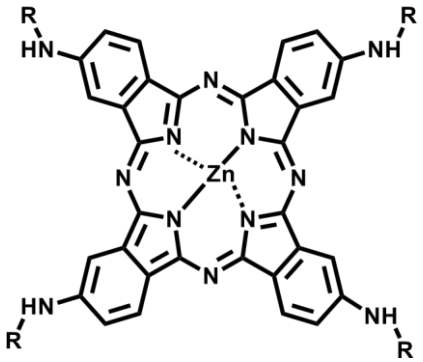	P123	Chemotherapy and PACT	**[87]**
R = 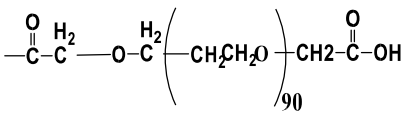			

As shown in **Table 1.2** Many porphyrins have been embedded in Pluronic polymer micelles and there are very few metallated and ring substituted phthalocyanines embedded into Pluronic polymer micelles and used as photosensitizers in PDT, hence complexes **1 – 6** were synthesized in this work. Ring substituted MPcs are preferable since solubility is improved and aggregation is reduced; hence bulky substituents are employed in this work. There are reports of unsubstituted chloroaluminumphthalocyanine embedded in Pluronic F-127 for use in PDT **[85]** and photoactivation of microorganisms **[86]**. A substituted zinc phthalocyanine has been cross- linked to Pluronics for chemotherapy but not for PDT **[87]**. The current work reports for the first time on the encapsulation (physically entrapped and not cross linked) of the ring substituted phthalocyanines into Pluronics and their use as photosensitizers. Physical entrapment in micelles releases dyes much faster than cross linking **[88],** hence the former is employed in this work rather than cross linking reported in literature **[87]**. Encapsulation of phthalocyanines into Pluronic polymer micelles results in water solubility of the phthalocyanines in micelles**.** Complexes **1-4, 5** and **6** became water soluble upon encapsulation to Pluronic polymer micelles. It has been demonstrated that binary mixture of Pluronics may compensate for drawbacks of a single Pluronic system. Binary mixtures also allow for higher loading capacity than mono systems **[89]**. **Table 1.3** shows porpyrins that have been embedded into a binary mixture of micelles **[90-93]**.

Table 1.3 Porphyrins and Phthalocyanines embedded in individual Pluronic micelles.

Compound	Pluronic Polymer	Studies/PDT	Reference
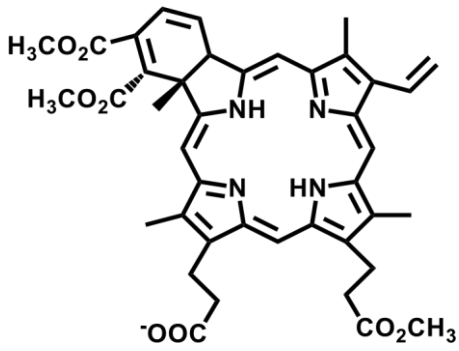	P123/F127	Fluorescence quantum yields and Singlet quantum yields	**[90,91]**

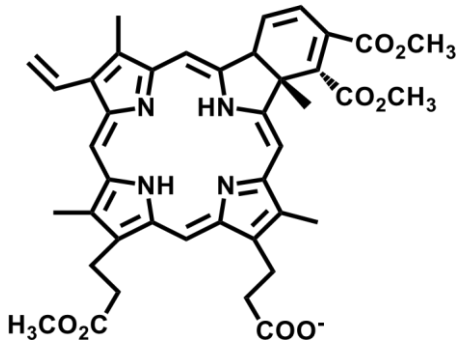 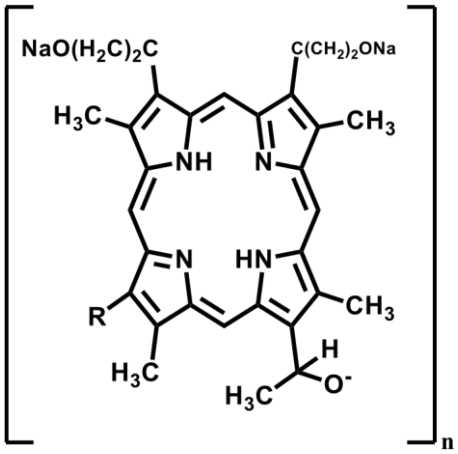 n = 0 – 6 R = 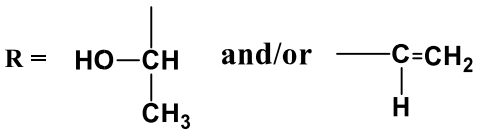	P123/F127	Singlet Oxygen quantum yields	**[92]**

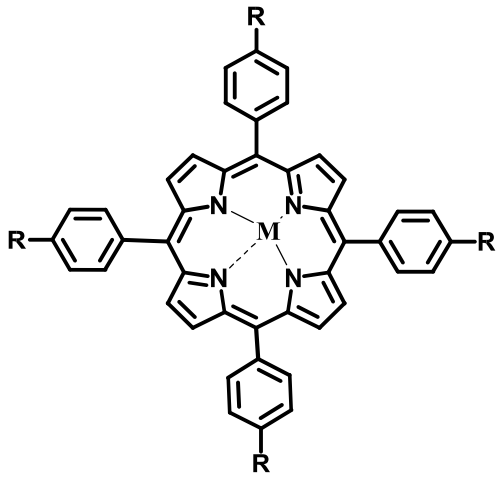 **M = H_2** **= Zn** **R =** 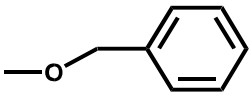	P123/F127	Fluorescence quantum yields, lifetimes and singlet oxygen quantum yields Fluorescence quenching	**[93]**

Table 1.3 Shows that there are no phthalocyanines that have been embedded into binary mixtures hence reported for the first time in this work using complexes **5** and **6** as examples. Pluronic F127 and L121 have similar length of hydrophobic block but different hydrophilic length **[94]**. It has been reported that mixed L121/F127 exhibit higher solubilization capacity compared to F127 micelles alone **[95],** hence the former is employed in this work (using complexes **5** and **6** as examples).

1.3 Photophysical and Photochemical properties of Pcs

Photophysico-chemical properties of MPcs are best described using the modified Jablonski diagram. **Figure 1.5** discussed above.

The photophysicochemical parameters of phthalocyanines are fluorescence quantum yield (Φ_F) and lifetime (τ_F), triplet quantum yield (Φ_T) and lifetime (τ_T) and the singlet oxygen quantum yield (Φ_Δ). These are important in the determination of the suitability of the molecules as photosensitisers **[96, 97]**.

1.3.1. Fluorescence quantum yield (Φ_F) and lifetimes (τ_F)

Fluorescence quantum yield is the ratio of absorbed photons to the emitted photons through fluorescence. Fluorescence quantum yields can be determined by comparative or absolute methods **[98, 99]**. The comparative method uses fluorescence quantum yields of a standard as a reference and was used in this work. The fluorescence quantum yields can be determined using equ. (1.1)

$$\Phi_F = \Phi_{F(STD)} \cdot \frac{F \cdot A_{Std} \cdot n^2}{F_{Std} \cdot A \cdot n^2_{Std}} \qquad (1.1)$$

Where **F** and $\mathbf{F_{STD}}$ are areas under fluorescence emission curves of the sample and the standard, respectively. **A** and $\mathbf{A_{STD}}$ are the absorbances of the sample and standard at the excitation wavelength, respectively, **n** and $\mathbf{n_{STD}}$ are refractive indices of solvents used for sample and standard, respectively. ZnPc in dimethyl sulfoxide (DMSO) was used as a standard, Φ_F = 0.20 **[41]**, in this work for MPcs. For the determination of fluorescence quantum yields, the sample and the standard are both excited at the same wavelength. Factors such as the nature of solvent used, pH, aggregation, temperature, nature of central metal, concentration, nature of substituents and point of substitution have been reported to influence the Φ_F of MPcs. The fluorescence lifetime (τ_F), is the average time a molecule spends in its excited singlet state before reverting to the ground state through fluorescence. The Time Correlated Single-photon Counting (TCSPC) technique **[100,101]** was used to determine the τ_F values of all the MPcs alone and with micelles studied in this work.

1.3.2 Triplet quantum yields (Φ_T) and lifetimes (τ_T)

The triplet quantum yield **(Φ_T)** is used to estimate the efficiency of the molecule to populate the triplet state. There are various methods of studying the properties of a molecule in its triplet state **[102,103]**. The laser flash photolysis technique was used in this thesis through comparative methods where ZnPc was used as a standard and calculations were done using equ. (1.2)

$$\Phi_T = \Phi_T^{STD} \frac{\Delta A_T \cdot \varepsilon_T^{STD}}{\Delta A_T^{STD} \cdot \varepsilon_T} \qquad \textbf{(1.2)}$$

Where $\Delta \mathbf{A}_T$ and and $\Delta \mathbf{A}_T^{STD}$ are the changes in the triplet state absorbance of the sample and the standard, respectively. ε_T and ε_T^{STD} are the triplet state extinction coefficients for the sample and the standard, respectively. Φ_T^{STD} is the triplet state quantum yield for the standard. Unsubstituted ZnPc in DMSO, Φ_T^{STD} = 0.65 **[102]** was used as a standard. ε_T and ε_T^{STD} were calculated from the molar extinction coefficients of their respective ground singlet state ε_S, the changes in absorbances of the ground state ($\Delta \mathbf{A}_S$) or the triplet state ($\Delta \mathbf{A}_T$) using equ. (1.3a) and (1.3b)

$$\varepsilon_T = \varepsilon_S \cdot \frac{\Delta A_T}{\Delta A_S} \qquad \textbf{(1.3 a)}$$

$$\varepsilon_T^{STD} = \varepsilon_S^{STD} \cdot \frac{\Delta A_T^{STD}}{\Delta A_S^{STD}} \qquad \textbf{(1.3 b)}$$

The triplet lifetimes are obtained from the triplet decay curve by fitting using

Origin Pro 8 software.

1.3.3. Singlet oxygen quantum yields (Φ_Δ)

Singlet oxygen ($^1O_2$) is a highly reactive oxygen species that is the primary cytotoxic agent in PDT **[104].** It is formed through an energy transfer process between an

excited triplet state of the MPc and ground state molecular oxygen ($^3O_2$), **Figure 1.5.** The singlet oxygen generation may be experimentally determined by a chemical method that utilises singlet oxygen quenchers **[105]**. The singlet oxygen quenchers react with singlet oxygen (**Scheme 1.3**) as soon as it is produced in an oxygenated MPc solution. The depletion of the singlet oxygen quencher is spectroscopically monitored over predetermined time intervals to assess the singlet oxygen produced by the PS. Singlet oxygen quenchers such as 1,3 diphenylisobenzofuran (DPBF) or anthracene-9,10-bismethylmalonate (ADMA) (**Scheme 1.3**) can be used to quantify singlet oxygen production in organic solvents and aqueous solutions, respectively **[106,107].** Both were employed in this work.

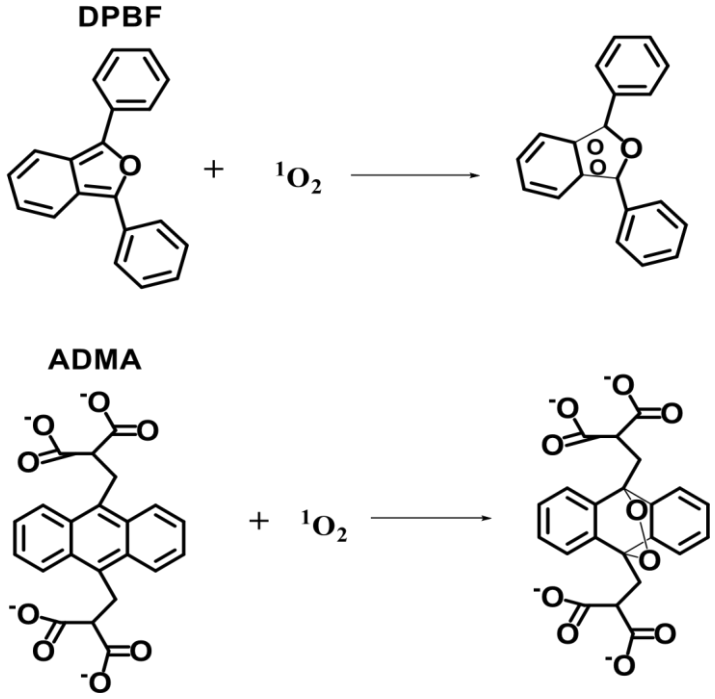

Scheme 1.3: Reaction of singlet oxygen with DPBF and ADMA.

Equ. (1.4) was then used to calculate singlet oxygen quantum yields:

$$\Phi_{\Delta} = \Phi_{\Delta}^{STD} \frac{R^{Sample} . I_{Abs}^{STD}}{R^{STD} . I_{Abs}^{Sample}} \quad \textbf{(1.4)}$$

Where Φ_{Δ}^{STD} is the singlet oxygen quantum yield for the standard (ZnPc, Φ_{Δ}= 0.67 in DMSO) **[107]**. AlPcSmix (containing a mixture of sulfonated phthalocyanine derivatives) was employed as a standard in aqueous media ($\Phi_{\Delta}{}^{STD}$ = 0.42) **[108]**. R^{Sample} and R^{STD} are the DPBF and ADMA photobleaching rates in the presence of the sample under investigation and the standard, respectively. . I_{Abs}^{Sample} and I_{Abs}^{STD}

are rates of light absorption by the sample and the standard, respectively and calculated using equ. (1.5a) and (1.5b) **[109]**.

$$\mathbf{I_{Abs}^{Sample}} = \frac{\alpha.A.I}{N_A} \qquad \textbf{(1.5a)}$$

$$\mathbf{I_{Abs}^{STD}} = \frac{\alpha.A.I}{N_A} \qquad \textbf{(1.5b)}$$

Where $\alpha = 1 - 10^{-(\lambda)}$, A (λ) is the absorbance of the sensitizer at the irradiation wavelength, A is the irradiated area, I is the intensity of light expressed as photons ($cm^{-2}\,s^{-1}$) and N_A is Avogadro's constant **[108 -110]**.

1.4 Summary of aims

The aims of this thesis include:

- Synthesis and characterization of symmetrical, metallophthalocyanines with azo groups (phenyldiazenylphenoxy), pyridyloxy and benzo[d]thiazol-2-ylthio as substituents.
- Synthesis of Pluronic Polymer micelles (F127 and F127/L121).
- Encapsulation of metallophthalocyanines to F127 or F127/L121 composites.
- Study the spectroscopic (ground state electronic absorption, excitation and emission) properties of the synthesized MPcs when alone and when embedded to F127 or F127/L121 composites.
- Study the photophysical (fluorescence quantum yield and lifetime, triplet quantum yield and lifetime) and photochemical (singlet oxygen quantum yield) properties of the synthesized MPcs when alone and when embedded to F127 or F127/L121 composites.
- *In vitro* dark cytotoxicity and photodynamic therapy activities of selected MPcs and conjugates against MCF7 breast cancer cells.

CHAPTER 2
Experimental Section

2. Experimental section

This chapter assimilates the details of the materials, instrumentation and experimental procedures used for the synthesis and characterisation of the complexes and pluronic micelles, as well the complexes with micelles studied, together with *in vitro* dark cytotoxicity and PDT studies.

2.1 Equipment

- Proton-nuclear magnetic resonance (^{1}H NMR) spectra were recorded on a Bruker AVANCE II 600 MHz NMR spectrometer using tetramethylsilane (TMS) as an internal reference.
- Elemental analyses of MPcs were carried out using a Vario Elementar Microcube ELIII CHNS instrument analyzer.
- Mass spectra data were acquired on a Bruker AutoFLEX III Smartbeam TOF/TOF mass spectrometer using α-cyano-4-hydrocinnamic acid as the matrix.
- Infrared spectra were acquired on a Bruker ALPHA FT–IR spectrometer with universal attenuated total reflectance (ATR) sampling accessory.
- Ground state electronic absorption was measured using a Shimadzu UV-2550 spectrophotometer.
- Fluorescence excitation and emission spectra were measured on a Varian Eclipse spectrofluorimeter using a 360–1100 nm filter. Excitation spectra were recorded at the wavelength of the emission maxima.
- Fluorescence lifetimes were measured using a time correlated single photon counting setup (TCSPC) (FluoTime 300, Picoquant GmbH) with a diode laser (LDH-P-670, Picoquant GmbH, 20 MHz repetition rate, 44 ps pulse width). Fluorescence was detected under the magic angle with a peltier cooled photomultiplier tube (PMT) (PMA-C 192-N-M, Picoquant GmbH) and integrated electronics (PicoHarp 300E, Picoquant GmbH). A monochromator with a spectral width of about 4 nm was used to select the required emission wavelength. The response function of the system, which was measured with a scattering Ludox solution (DuPont), had a full width at half-maximum (FWHM) of about 300 ps. The ratio of stop to start pulses was kept low (~0.05) to ensure good statistics. All fluorescence decay curves were measured at the wavelength of emission maxima. The data were analysed with the FluoFit software (Picoquant®). The support plane approach was used to estimate the errors of the decay times **[111]**. The layout of the TCSPC is shown in **Figure 2.1.**

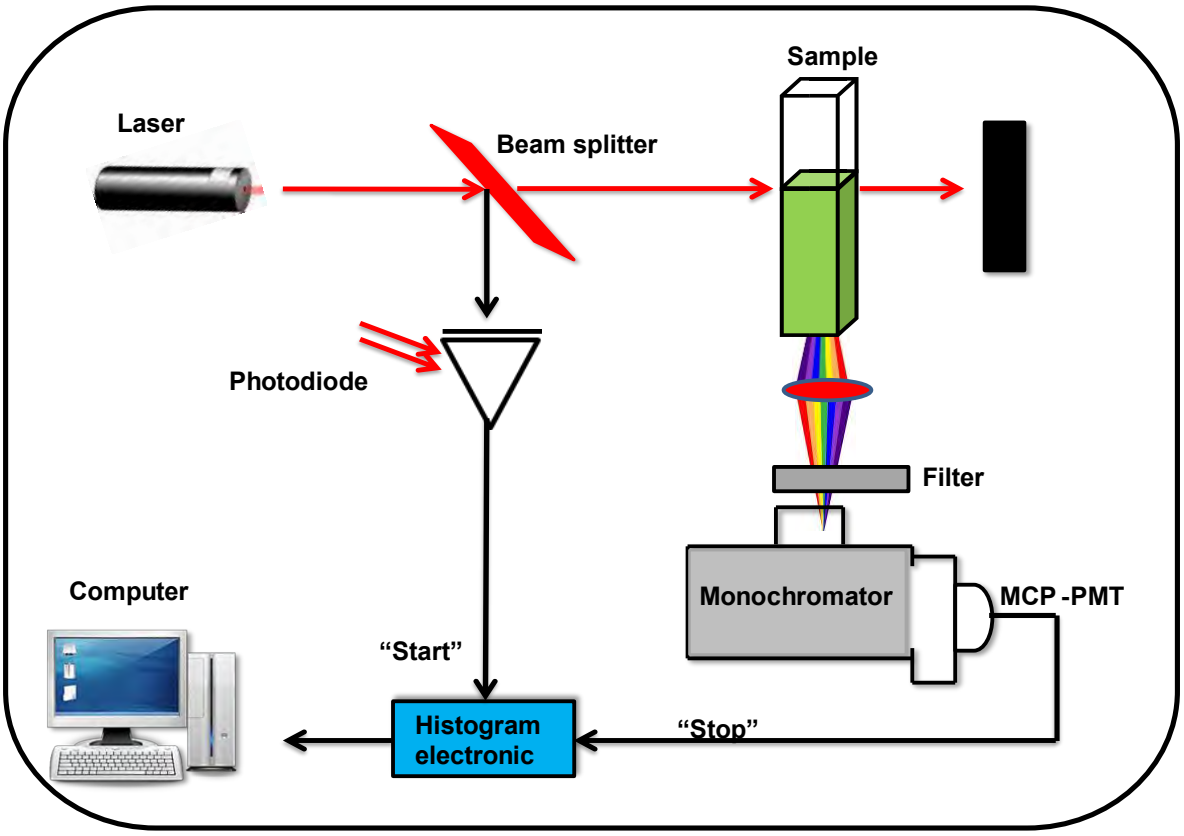

Figure 2.1: Schematic representation of time correlated single photon counting (TCSPC) set–up. (MCP)–PMT = (Multichannel plate detector) Monochromator Photomultiplier Tube.

- A laser flash photolysis system was used to determine the triplet quantum yields. The excitation pulses were produced using a tunable laser system consisting of an Nd: YAG laser (355 nm, 135 mJ/4–6 ns) pumping an optical parametric oscillator (OPO, 30 mJ/3–5 ns) with a wavelength range of 420–2300 nm (NT-342B, Ekspla). The signal from a PMT detector was recorded on an oscilloscope. A new system consisting a LP980 spectrometer with a PMT-LP detector, Tektronix digital storage oscilloscope and an ICCD camera (Andor DH320T-25F03) was also used. The absorbance of the sample solution and the standard were ~1.5 at the Q–band. The solution was introduced into a 1 cm path length quartz cell and deaerated using argon for 15 min. Thereafter the solution was sealed and illuminated using an appropriate excitation wavelength source (the crossover wavelength of the sample and the standard is utilized as the laser excitation source wavelength). The maximum triplet absorption detection wavelength was determined from the transient curve. The triplet lifetimes were determined by exponential fitting of the kinetic curves using OriginPro® 8 software.

- Irradiation for singlet oxygen quantum yield was performed using a general electric quartz lamp (300 W) as irradiation source. A 600 nm cut-off glass filter (Schott) for ultraviolet radiation and a water filter for infrared radiation were used. An interference filter, 670 nm with a band of 40 nm was additionally used before the sample chamber. Light intensity was measured with a POWER MAX 5100 (Molelectron detector incorporated) power meter. Solutions of photosensitizer containing DPBF in DMSO or ADMA in aqueous media, were prepared in the dark and irradiated in the Q-band region. DPBF and ADMA degradation at 417 nm and 380 respectively, was monitored during irradiation to quantify the singlet oxygen quantum yield with reference to a standard. The layout of the photochemical set–up is shown in **Figure 2.2**.

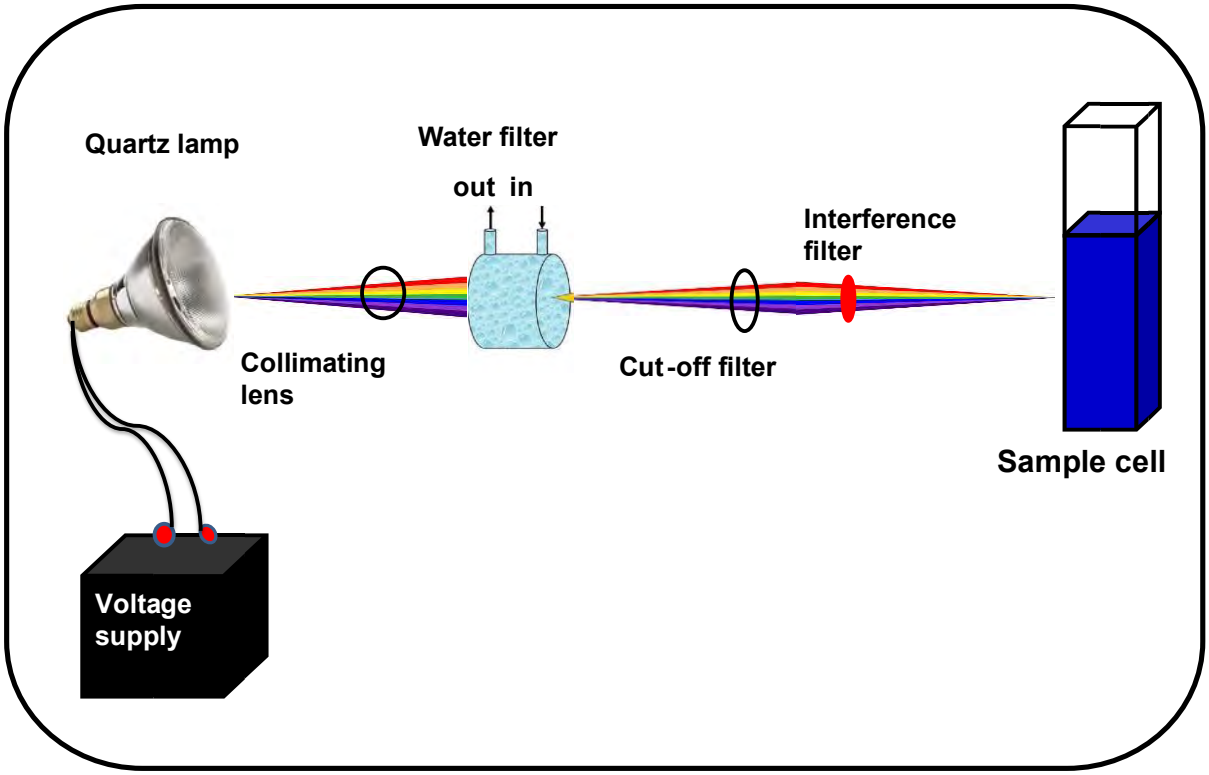

Figure 2.2. Schematic illustration of photochemical set–up.

- Transmission electron microscope (TEM) images were obtained using a ZEISS LIBRA model 120 operated at 90 kV and iTEM software was used for TEM micrographs processing.
- Dynamic light scattering (DLS) experiments were done on a Malvern Zetasizer nanoseries, Nano-ZS90.
- Illumination for PDT studies of Pcs and conjugates were performed using a Modulight Medical Laser system (ML) 7710-680 channel Turnkey laser system coupled with 2 × 3W channels at 680 nm, cylindrical output channels, aiming

beam, integrated calibration module, foot/hand switch pedal, fibre sensors (subminiature version A) connectors and safety interlocks. The iIllumination kit for in *vitro* PDT studies with capacity to hold 127.76 × 85.48 mm 96 well tissue culture plate was used.

- The MCF7 cells were cultured in a humidified atmosphere incubator with ~5% CO_2 and temperature at 37 °C (Heal Force).
- The cells were viewed under phase contrast using a Zeiss AxioVert.A1 Fluorescence LED (FL-LED) inverted microscope.
- The cell viability was measured with Synergy 2 multi-mode microplate reader (BioTek).

2.2. Materials

2.2.1 Solvents

Dimethyl sulfoxide (DMSO, spectroscopy grade), 1–pentanol, 1–hexanol, deuterated (DMSO–d6, chloroform–d), and 25% ammonium hydroxide were obtained from Sigma Aldrich®. Absolute ethanol, methanol, dimethylformamide (DMF), cyclohexane, tetrahydrofuran (THF), nitric acid (55%), acetonitrile, acetone, octanol, chloroform and toluene were obtained from SAARCHEM®. Highly purified water was obtained through installed water purifying system from ELGA, Veolia water PURELAB, Flex system (Marlow, UK).

2.2.2 Reagents

Zinc (II) acetate dihydrate, indium (III) chloride, 1,8-diazobicylo [5.4.0]undec-7-ene (DBU), unsubstituted zinc phthalocyanine (ZnPc), 1, 3 diphenylisobenzofuran (DPBF), silica gel, anthracene-9,10-bismethylmalonate (ADMA), 4-nitrophthalonitrile, potassium hydroxide pellets and poly(ethylene glycol)- block- poly(propylene glycol)block – poly(ethylene glycol) Pluronic® L-121 and F-127, 4-amino-2,5-di-tertbutylphenol were purchased from Sigma–Aldrich. E-4-(4-(phenyldiazenyl) phthalonitrile **(a) [42]**, 4-(2-pyridyloxy) phthalonitrile **(b) [35]**, and aluminium sulfonated phthalocyanine (AlPcSmix- mixture of sulfonated phthalocyanine derivatives) have been reported in literature **[112]**.

Cultures of epithelial breast cancer cells (MCF7 cells) were obtained from Cellonex. Trypsin ethylenediaminetetraacetic acid (EDTA), trypan blue, Dulbecco's

phosphatebuffered saline (DPBS) and Dulbecco's modified Eagle's medium (DMEM) were obtained from Sigma Aldrich, heat-inactivated fetal calf serum (FCS), neutral red cell proliferation reagent (WST-1), and 100 µg/mL penicillin-100 unit/mL-streptomycinamphotericin B mixture were obtained from Lonza (Biowest).

2.3 Synthesis

Three MPcs are reported here for the first time and their synthetic details are provided in this section. (E)-4(-4(phenyldiazenyl)phthalonitrile **[42]**, 4-(2-pyridyloxy) phthalonitrile **[35]**, and MPcs zinc(II)-tetra{2-pyridyloxyphthalocyaninato}) phthalocyanine **(4) [35]** indium(III)tetrakis[(4-benzo[d]thiazol-2ylthio)phthalocyaninato] **(5) [36,37]** and zinc(II) tetrakis[(4-benzo[d]thiazol-2ylthio)phthalocyaninato] **(6) [36,37]** are known and were synthesized as reported in literature.

2.3.1 Synthesis of indium(III) tris (3-((Z)- phenyldiazenyl) phenoxy) phthalocyanine (complex 1) - Scheme 4.1.

(E)-4(-4(phenyldiazenyl) phenoxy) phthalonitrile **(a)** (0.200 g, 0.62 mmol) and indium chloride (0.061 g, 3.09 mmol) were placed in a 100 mL beaker. Then DBU (0.50 ml, 3.3 mmol) and 1–hexanol (4 mL) were added into the reaction mixture. The reaction mixture was irradiated in a microwave for 15 min. The obtained product was precipitated out of solution with 1:1 ratio of methanol and Millipore water and then centrifuged and placed to dry in a fume hood overnight. Thereafter the crude product was washed successively with hot ethanol, THF, and chloroform under Soxhlet extraction. The resulting hygroscopic product was dried in the fume hood overnight.

Yield: 74 %; UV/ Vis (DMSO): λ_{max}/nm (log ε): 355 (2.94), 613 (3.36), 697 (5.23) IR (KBr, cm^{-1}) 1701(CO), 1605 (N=N), 1499, 1483, 1266, 1231, and 1091. ^{1}H NMR (600, DMSO–d_6) ppm: 8.03 (s, 2H, phenyldiazenyl), 8.01 (s, 2H, Pc), 7.96 (s, 2H, Pc), 7.91 (s, 4H, Pc), 7.90 (s, 4H, Pc), 7.62 – 7.61 (m, 16H, phenyldiazenyl), 7.60 – 7.59 (m, 13H, phenyldiazenyl), 7.43 (s, H, phenyldiazenyl), 7.37 (s, 2H, phenyldiazenyl) 7.36 (s, 2H, phenyldiazenyl), Calc for $C_{80}H_{48}InClN_{16}O_4$: C, 68.04, H, 3.43, N, 15.87. Found C: 68.18, H 3.48, N 15.48. MALDI TOF MS *m/z*: 1447.72 amu. Found: 1411.27 $[M- Cl]^+$.

2.3.2. Synthesis of zinc (II) tris(3-((Z)- phenyldiazenyl) phenoxy) phthalocyanine (Complex 2) – Scheme 4.1.

The synthesis was as outlined for complex **2** was as outlined for complex **1** except zinc acetate dihydrate (0.135 g, 0.62 mmol) was used instead of indium chloride, and the reaction time was 11 min instead of 15 min. All the other reagents, and the purification methods were as outlined above.

Yield: 77%; UV/ Vis (DMSO): λ_{max}/nm (log ε): 350 (3.75), 627 (4.43), 684 (5.21), IR (KBr, cm^{-1}): 1643(CO), 1589(N=N), 1483, 1232 and 766. ^{1}H NMR (600, $CDCl_3$): 8.05 – 8.04 (s, 3H, phenyldiazenyl), 8.02 – 7.90 (m,13H, phenyldiazenyl), 7.58 – 7.50 (m, 16H, phenyldiazenyl), 7.48 – 7.46 (m, 4H, phenyldiazenyl), 7.11 (s, 7H, Pc), 6.98 (s, 5H, Pc). Calc for $C_{80}H_{48}N_{16}O_4Zn$: (C, 70.51, H 3.55, N 16.45)% Found (C: 70.08, H 3.74, N 16.38)% MALDI TOF MS *m/z*: Calcd: 1362.75 amu. Found: 1362.46 $[M]^+$.

2.3.3. Synthesis of indium (III) tetra{2-pyridyloxyphthalocyaninato}) (Complex 3) - Scheme 4.2

4-(2-Pyridyloxy) phthalonitrile (**b)** (0.200 g, 9.62 mmol) and indium chloride (1.98 g, 9 mmol) was dissolved in 1–hexanol (4 mL) in a 100 mL beaker. Then DBU (0.50 mL) was added into the reaction mixture. The reaction mixture was irradiated in a microwave for 8 min. Thereafter the resulting green product was precipitated out with diethyl ether and washed successively with 1: 1 methanol and water and then placed under sonication and centrifuged with DMSO and thereafter left to dry overnight in the fumehood.

Yield: 70 %; UV/ Vis (DMSO): λ_{max}/nm (log ε): 365 (4.86), 664 (4.92), 688 (5.52). FTIR (KBr, cm^{-1}) 3064 (C–H), 1722, 1634, 1554, 1480, 1344, 1255 (C–O–C) 1183, 1062 and 1011. ^{1}H NMR (600, DMSO–d_6) ppm: 8.28 – 8.20 (m, 4H, Pc), 7.96 (s, 4H, Pc), 7.89 – 7.73 (4H, Pc), 7.46 – 7.38 (s, 2H, Pyridyloxy), 7.26 (m, 2H, Pyridyloxy), 7.19 (m, 2H, Pyridyloxy), 7.09 (m, 4H, Pyridyloxy), 6.83 – 6.75 (m, 2H, pyridyloxy), 6.60 (m, 4H, Pyridyloxy). Calc for $C_{52}H_{28}InClN_{12}O_4$: C, 60.34, H, 2.73, N, 16.24. Found C: 60.28, H 2.71, N 16.28. MALDI TOF MS *m/z*: 1035.43 amu. Found: 1000.33 amu $[M-Cl]^+$

2.3.4 Incorporation of phthalocyanines into Pluronic micelles, Scheme 4.3

A previously reported thin – film hydration method with some modifications was used for the incorporation of complexes **1**, **2**, **3**, **4**, **5** and **6** into Pluronic® F–127 **[113]**. Each Pc complex was co – solubilized with Pluronics (1/40: w/w) in THF (5 mL), and the solution was sonicated for 20 min. Then, the solvent was evaporated *in vacuo* for 1 h at 60 ºC and the product was dried for 12 h in a desiccator. The solid obtained was hydrated with ELGA Type II water (5 mL) and sonicated for 15 min then further stirred for 2 h. The solution was filtered through a 0.2 µm filter to remove the unloaded complexes. The filtrate was freeze-dried to obtain the solid form. The phthalocyanines when loaded into Pluronic F127 are represented as **1**–F127, **2**–F127 etc. for all phthalocyanines (where F127 represents Pluronic F127). Complexes **5** and **6** were also embedded into F127/L127 (1/1: w/w) represented as **5**–F127/L121 and **6**–F127/L121 respectively.

2.4 Cell Studies

2.4.1. Culturing of MCF7 cells.

The MCF7 cells were cultured using Dulbecco's modified Eagle's medium (DMEM) supplemented with 10% (v/v) heat inactivated fetal calf serum (FCS) and 100 unit/mL penicillin–100 µg/mL streptomycin–amphotericin B. The cells were cultured in T75 flasks, incubated at 37 °C and 5% CO_2 in a humidified atmosphere until a cell confluence of 80 % was achieved. The cells were rinsed with Dulbecco's modified phosphate buffer saline (DPBS) before routine trypsinisation. The viable trypsinised cells were counted with the aid of a trypan blue dye exclusion assay (0.40% trypan blue solution) using a hemocytometer. The cells were seeded at a cell density of 10,000 cells/well in supplemented DMEM containing phenol red in 96–well plates. They were further incubated under similar conditions for 24 h to allow cell attachment to the wells. The attached cells were rinsed with 100 µL DPBS once, followed by administration of 100 µL supplemented DMEM containing gradient doses of the respective drugs (complexes and complexes with micelles). The stock drug concentrations were prepared in DMSO and made up to the desired volume with supplemented DMEM. Plates were re-incubated again at 37°C and 5% CO_2 in the dark for 24 h. The effect of DMSO on the cells was investigated by the incubation of

cells with 1% (v/v) DMSO in supplemented DMEM which represents the highest percentage of DMSO in the drug gradient solutions. Control cells were given supplemented DMEM with phenol red without the drug. After 24 h, the cells were rinsed with 100 µL DPBS once and were ready for *in vitro* dark cytotoxicity.

2.4.2. *In vitro* dark cytotoxicity and PDT activity.

For *in vitro* dark toxicity, supplemented DMEM with phenol red was added and the plates were re-incubated for 24 h. For PDT studies, supplemented phenol red free DMEM was added and the plates were subsequently illuminated with fixed light dosimetry of 170 J/cm^2 using a Modulight ML7200 series illumination set–up as a light source. After illumination, the supplemented phenol red free DMEM was replaced with supplemented DMEM with phenol red and the plates were re-incubated for 24 h. For both *in vitro* dark cytotoxicity and PDT activity, each experiment was performed in triplicate replicate and surviving cells were quantified after re–incubation using WST1 viability assay.

2.4.3. Cell viability determination

The WST–1 assay was used to assess the toxicity and cell proliferation in the monolayer of the cells treated with the drugs and the control, respectively. This was performed as specified in the manufacturer's instruction and a Synergy 2 multi–mode microplate reader (BioTek) set at a wavelength of 450 nm was used to quantify the stained viable cells. The percent cell viability was determined using equation 2.1:

$$\%\ \text{cell viability} = \frac{\text{Absorbance of sample at 450 nm}}{\text{Absorbance of control at 450 nm}} \times 100 \qquad (2.1)$$

where the absorbance of sample is for cells containing drugs while absorbance of control is for control cells containing only supplemented DMEM with phenol red.

2.4.4 Statistical analysis

The data obtained from the experiments was statistically analysed. Each sample was run 3 times and each experiment was repeated three times. One–way analysis of variance (ANOVA) for the *in vitro* dark cytotoxicity and PDT data of the drugs against MCF7 cell was evaluated. A p–value < 0.05 was considered statistically significant.

2.4.5 Determination of partition coefficients (K_p)

By monitoring spectral changes, it is possible to quantify the degree of drug/ micelle interaction, which is normally expressed as micelle / water partition coefficient K_p. The elucidation of these constants is key for the understanding of interactions with biomembranes **[114]** and estimating the distribution of drugs. The K_p values were determined in biphasic octanol and water system as previously reported **[115]**. Complexes **1** – F127, **2** – F127, **3** – F127, **4** – F127, **5** – F127, **5** – F127/L121, **6** – F127 and **6** – F127/L121 were added to a mixture of 50 % (v/v) octanol and water, which was vigorously stirred and left to rest in the dark for 48 h. The concentration of **1** – F127, **2** – F127, **3** – F127, **4** – F127, **5** – F127, **5** – F127/L121, **6** –F127 and **6** – F127/L121 the aqueous $[PS]_{water}$ and organic $[PS]_{octanol}$ phases were determined using UV – Vis spectra and the data was fitted using Eq. (2.2) **[84].**

$$K_p = [PS]_{octanol} / [PS]_{water} \qquad (2.2)$$

The values are estimates for comparison purposes only since the extinction coefficients used are that of the Pc complexes in DMSO.

CHAPTER 3
Attempted Synthesis

3. Attempted synthesis to see the effect of bulky substitution

Scheme 3.1: Synthesis of A

The synthesis of **A** (**Scheme 3.1**) was as follows (2.00 g, 1.55 mmol) of 4 nitrophthalonitrile and 4-amino-2,5-di-tert-butylphenol (3.99 g, 1.55 mmol) were dissolved in 50 mL dry DMF and then 10 g of potassium carbonate was added into the reaction mixture. Thereafter the reaction mixture was left to stir for 48 h in an argon environment. The resultant brown product was washed with a mixture of methanol and water (1:1) and left to dry in the fumehood.

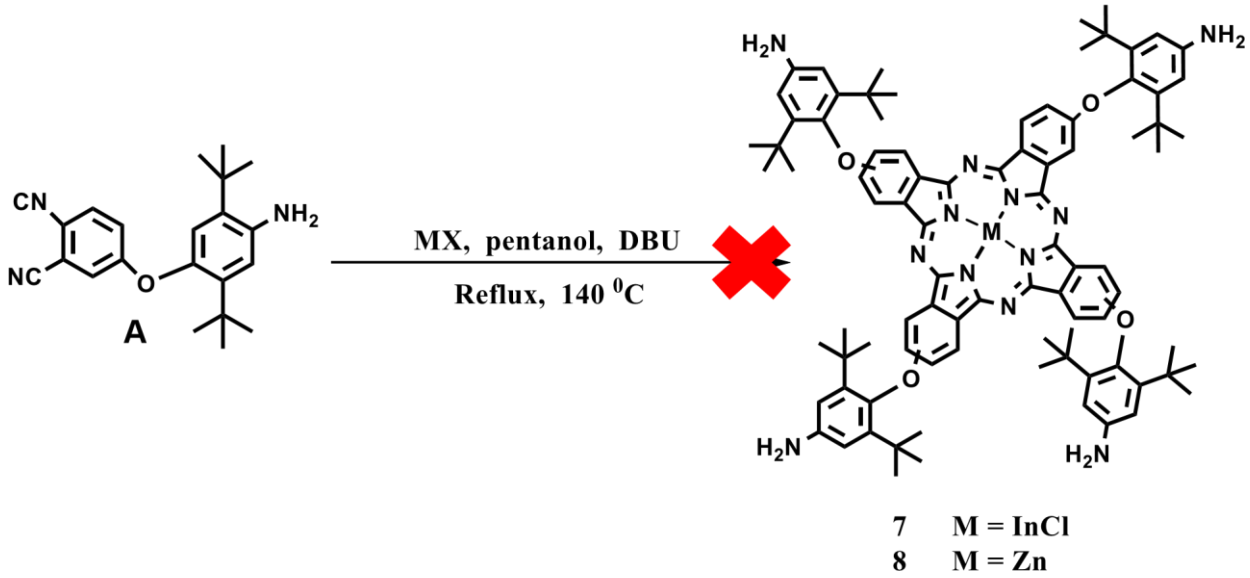

Scheme 3.2: Attempted synthesis of complexes 7 and 8.

3.1 Synthesis of complexes 7 and 8 (Scheme 3.2)

The first attempt for the synthesis of complex **7** was as follows where (100 g, 2.90 mmol) of 5-(4-amino-2,5-di-tert-butylphenoxy)-2-isocyanobenzonitrile **(A)** was dissolved in 1– pentanol (5 mL), then indium chloride (0.64 g, 2.90 mmol) and DBU (0.3 mL, 1.98 mmol) were added. The reaction mixture was refluxed overnight at 160°C in the presence of argon flow. The reaction mixture was precipitated out using 1:1 (v/v) methanol and water which was supposedly meant to afford complex **7**.

A similar procedure was followed for the synthesis of complex **8** but zinc acetate dihydrate (0.63 g, 2.90 mmol) was used instead of indium chloride.

The second attempt for the synthesis of complexes **7** and **8** was done following the same reaction conditions as the above, however 1-hexanol was used as a solvent instead 1-pentanol and the mixtures were irradiated in the microwave instead of refluxing overnight, but no identifiable product was formed.

Rationale behind synthesis

The rationale behind the synthesis of complexes **7** and **8** was to obtain tetrasubstituted substituted phthalocyanines for application in photodynamic therapy, moreover bulky substitution improves solubility **[116]** and reduces aggregation, hence bulky substituents were chosen.

Publications

The results discussed in this thesis have been presented in the articles as listed below that have been published or submitted for publication in peer – reviewed journals.

1. B. M. Motloung, K. E. Sekhosana, M. Managa, E. Prinsloo, T. Nyokong, The photophysicochemical properties and photodynamic therapy activity of phenyldiazenyl phenoxy substituted phthalocyanines when incorporated into Pluronic® F127 micelles, **Polyhedron 174 (2019) 114157**

2. B.M. Motloung, B. Babu, E. Prinsloo, T. Nyokong, The photophysicochemical properties and photodynamic therapy activity of In and Zn phthalocyanines when incorporated into individual or mixed Pluronic® micelles, Polyhedron, Accepted with revision

Results and discussion

4. Syntheses and characterization

5. Photophysicochemical properties

6. Photodynamic Therapy

CHAPTER 4
Syntheses and characterization

4.1. Characterization of phthalocyanines alone

Complexes **4, 5** and **6** have been reported before **[35-37]** and will not be discussed in the following subsections, their characterization is provided in Appendix A. Syntheses and characterisation of complexes **1, 2** and **3** are reported for the first time and will be discussed in the following subsections.

Scheme 4.1 Illustrates the synthesis of symmetrically substituted complexes **1** and **2** using cyclotetramerization of (E)-4(-4(phenyldiazenyl)phenoxy) phthalonitrile **(a)** in the presence of a catalytic amount of DBU, Zn (**2**) or indium (**1**) salts, and 1–hexanol. Good yields were obtained for this synthetic pathway due to a non-extensive purification procedure. A yield of 74% and 77% was obtained for complexes **1** and **2** synthesized in this work. The synthesis of complex **3 (Scheme 4.2)** was achieved by the cyclotetramerization of 4-(2-pyridyloxy) phthalonitrile **(b)** in the presence of a catalytic amount of DBU, indium salt, and 1–hexanol. Good yields were obtained for this synthetic pathway due to a non-extensive purification procedure. A yield of 70% was obtained for complex **3** synthesized in this work.

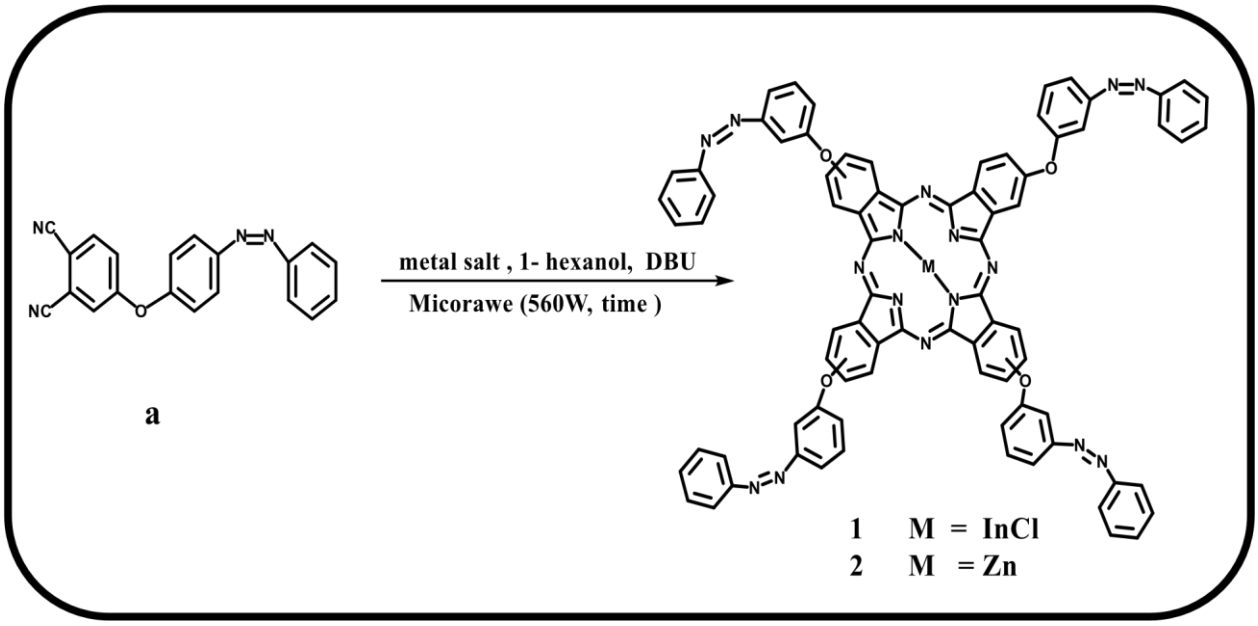

Scheme 4.1: Synthetic pathway for complexes 1 and 2.

Characterization of the Pc complexes **1, 2** and **3** was achieved using infrared, ultraviolet–visible, MALDI-TOF mass and ^{1}H NMR spectroscopies, and elemental analyses.

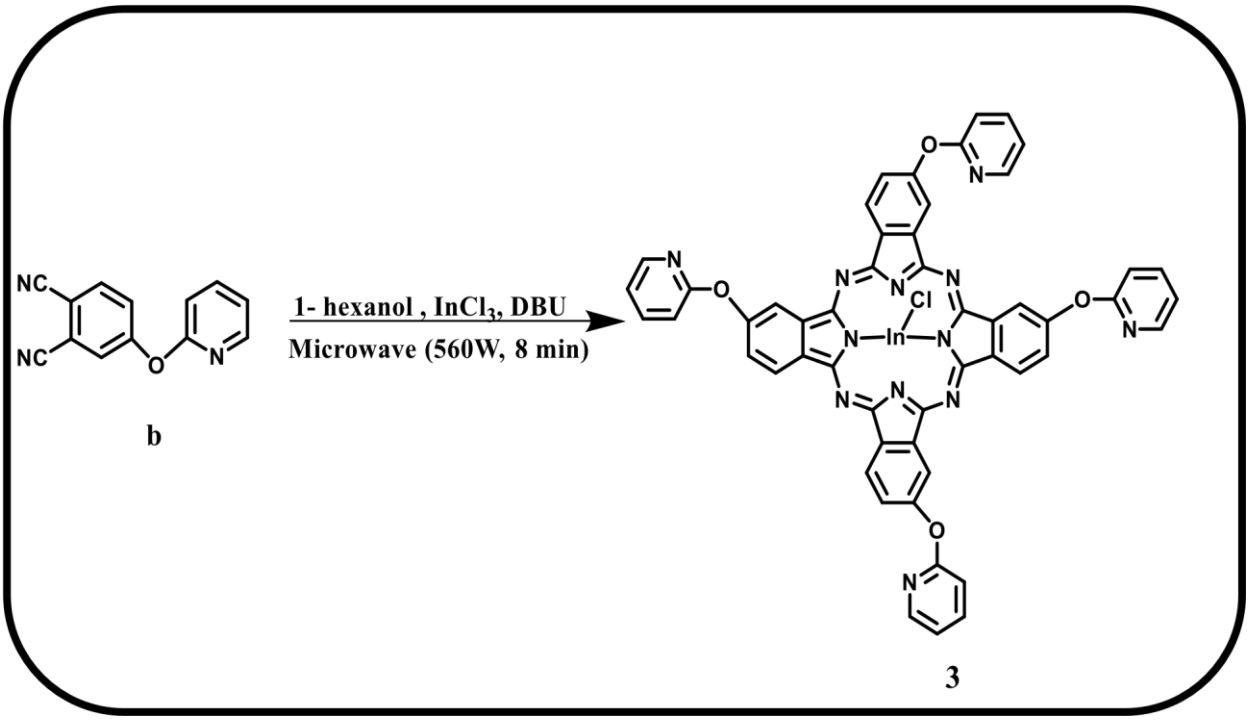

Scheme 4.2: Synthetic pathway of Indium (III) tetra {2pyridyloxyphthalocyaninato} (Complex 3).

The ^{1}H NMR spectra of complexes **1, 2** and **3** (See **Fig. A1**, **A2 and A3**) shows aromatic ring proton peaks between 8.03 – 7.36 ppm, 8.05 – 6.98 and 8.28 – 6.60 ppm, respectively. Peak integration gave the anticipated number of protons for all complexes, confirming their purity. The ^{1}H NMR spectra for the known complexes **4**–**6** are shown in **Figs. A4** – **A6** together with the rest of the data.

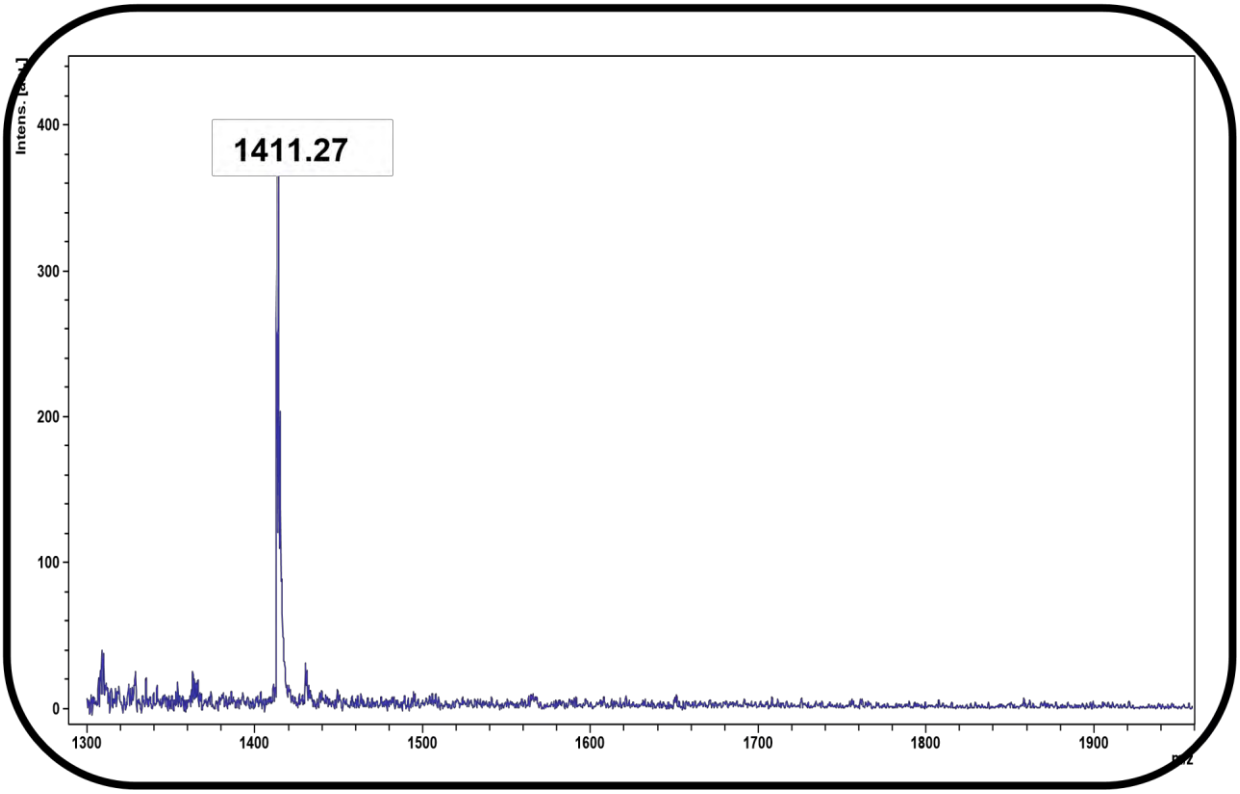

Figure 4.1: The MS (Maldi-TOF) for complex 1.

The mass spectrum of complex **1 (Fig. 4.1)** showed the molecular ion peak at m/z: **1** 1411.27 $[M- Cl]^+$, while that of **2** was found at m/z: 1362.46 $[M]^+$ **(Fig. A7)** and for **3** it was found at m/z: 1000.33 amu $[M- Cl]^+$ (**Fig. A8)** and mass spectra of complexes **4**–**6** are shown in **Figs. A9 – A11** . The obtained elemental analyses agreed with the calculated inferring the purity of the complexes. The electronic ground state absorption spectra provides no evidence of band broadening due aggregation and contain a single Q band at 697 nm, 684 nm and 689 **(Table 4.1)**, for complexes **1**, **2** and **3**, respectively in DMSO **(Fig. 4.2)**, which is what is typically observed for metallated phthalocyanine with degenerate D_{4h} symmetry.

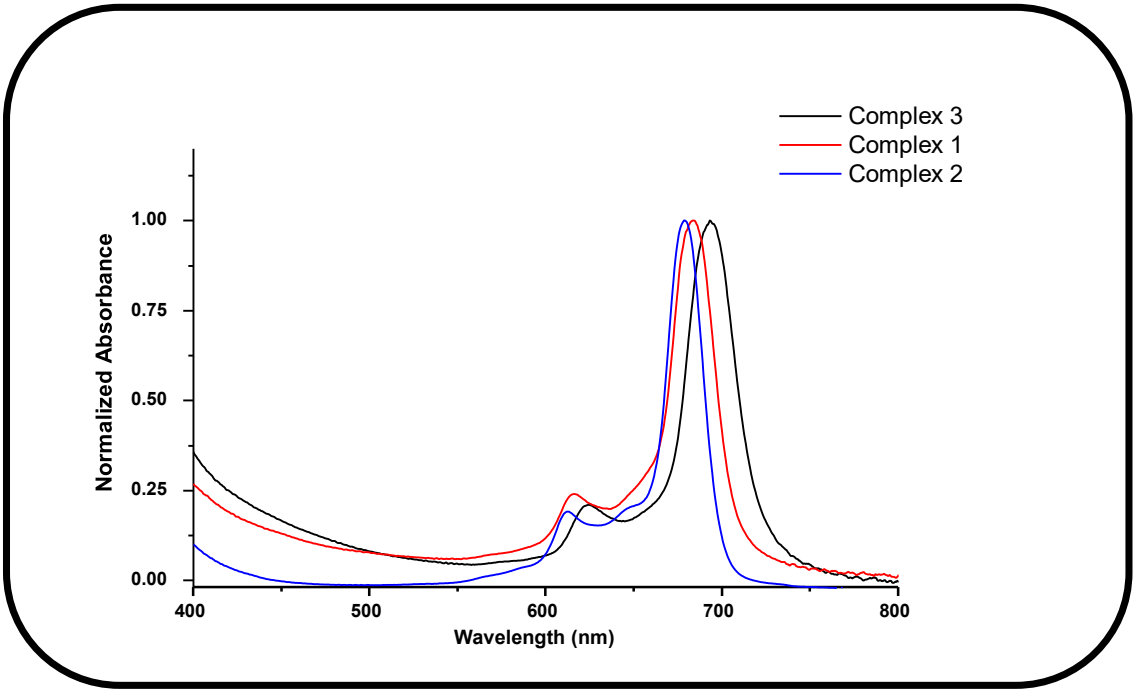

Figure 4.2: The ground state absorption spectra for complexes 1 and 2 in DMSO.

The red shift in the Q band of complex **1** compared to **2**, can be attributed to the effect of the central metal **[117]**. The non-planar effect of the indium (III) ion, with a relatively bigger atomic radius than the zinc (II) as the central metal ion in the Pc cavity results in red shifting of the Q band, the same applies to complexes **3** compared to **4**, and **5** compared to **6.**

Table 4.1: Showing wavelength (λ), partition coefficient (Kp), DLS and TEM **sizes for the complexes alone and with micelles.**

Complex	DMSO λ_{Qband} (nm)	K_p	DLS (nm)	TEM (nm)
1	697	-	-	-
1-F127	693	146	18.52	17.20
2	684	-	-	-
2-F127	683	114	18.25	17.90
3	689	-	-	-
3-F127	686	158	27.14	18.83
4	680	-	-	-
4-F127	675	102	21.23	16.91
5	693	-	-	-
5-F127	690	145	28.13	17.25
5-F127/L121	716	143	36.03	30.74
6	686	-	-	-
6-F127	677	112	20.25	18.31
6-F127/L121	672	128	37.81	31.87

4.2. Characterization of phthalocyanines in micelles

4.2.1 Spectra

Complexes **1**–**6** were further loaded into Pluronic F127 polymer micelles while **5** and **6** were in addition loaded into F127/L121. The incorporation of all phthalocyanines into micelles was carried out using the thin film hydration method **(Scheme 4.3)** which has been described in literature as stated in chapter 2**.** The polymeric micelles of interest in this work are the Pluronic triblock copolymer which are composed of poly(ethylene oxide) (PEO) and poly(propylene oxide) (PPO) with a PEO-PPO-PEO structure **(Scheme 4.3) [62].** The phthalocyanines become water-soluble after incorporation into Pluronic F127 and F127/L121 micelles, hence the studies following incorporation were done in water in this work. No comparison can be made between phthalocyanines alone dissolved in organic solvents and when they are embedded in micelles since different solvents are used.

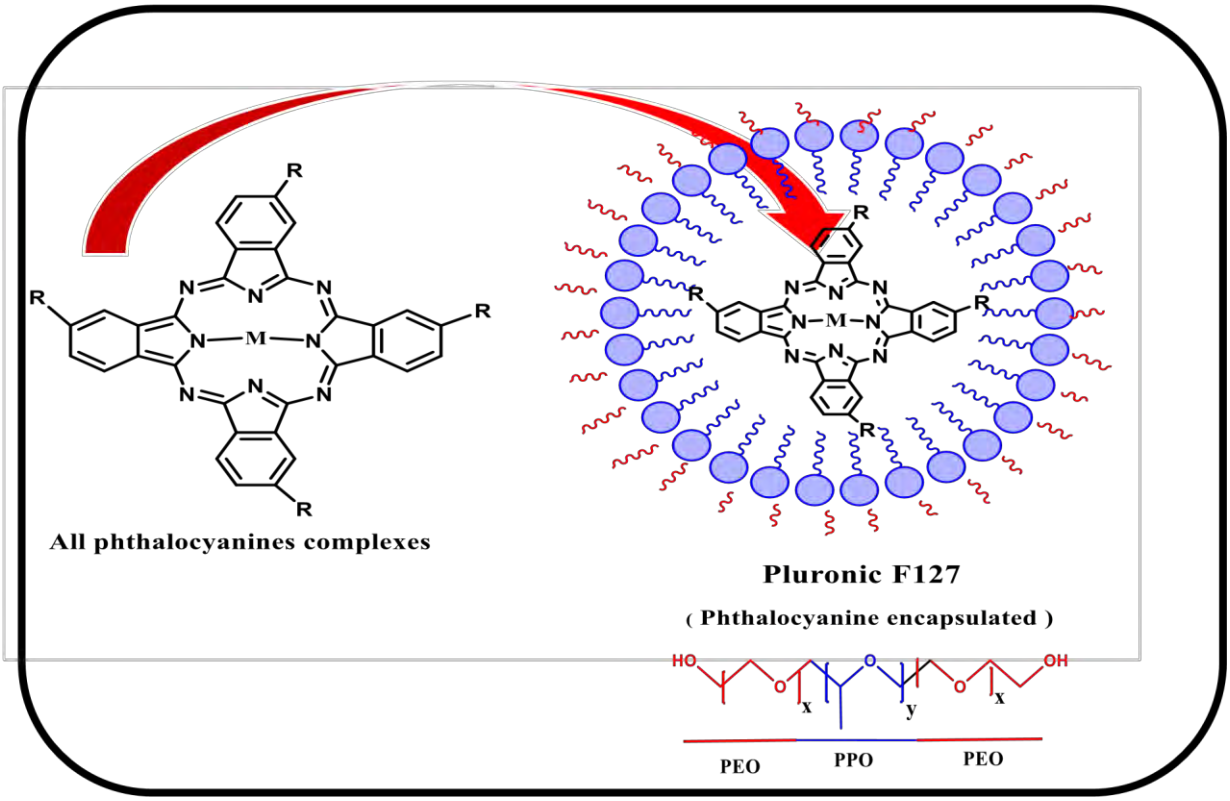

Scheme 4.3: Representation of the incorporation of phthalocyanine into Pluronic F127 micelles

The Q bands of complexes **1, 2, 3, 4, 5** and **6** in F127 and **5** and **6** in F127/L121 micelles were observed at 693, 683, 686, 675, 690, 677, 716 and 672 nm in water, respectively, **Table 4.1** and **Fig. 4.3** (the latter using complexes **1** and **2** as examples). The Q bands are broadened for Pcs incorporated into micelles in water compared to Pcs alone in DMSO. The broadening in water could be due to aggregation.

Aggregation (the so called "H" aggregates) in phthalocyanines is judged by broadening or splitting of the Q band, with the low energy band being due to the monomer and the high the energy band due to the aggregate **[117].** The aggregation was also observed in mixed micelles, **Fig**. **4.4.**

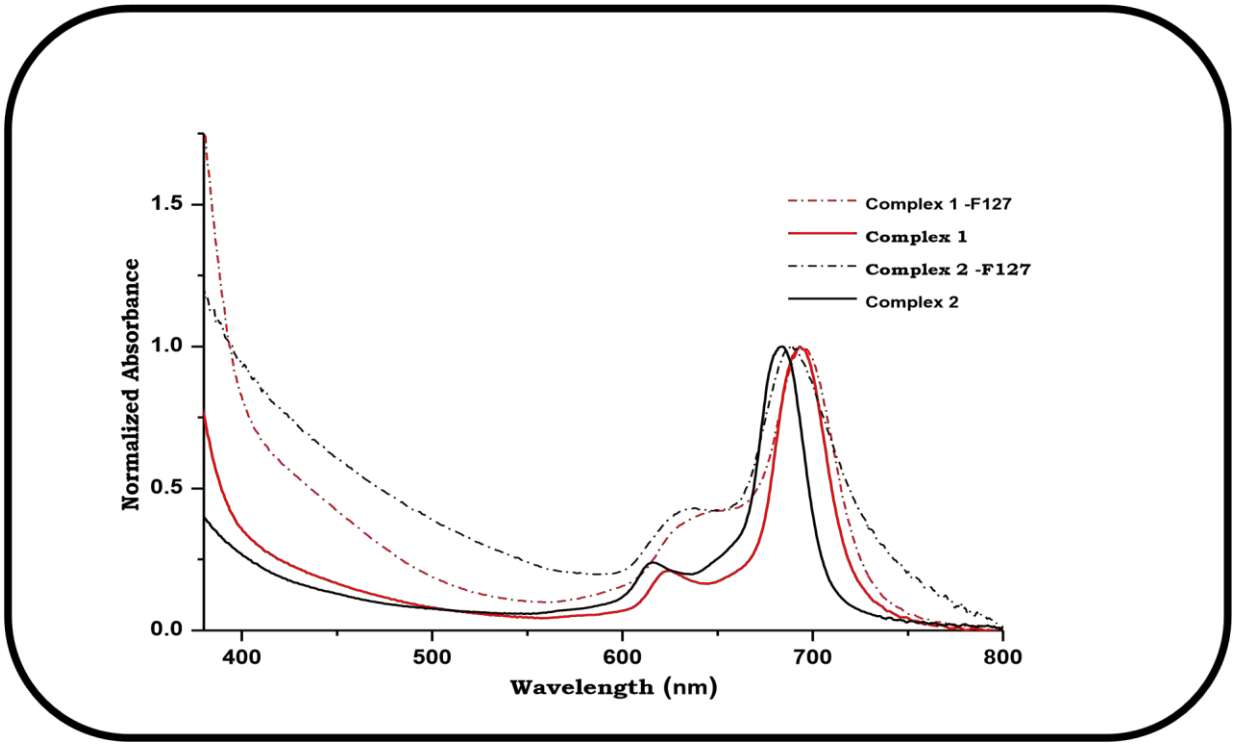

Figure 4.3: Normalized electronic absorption spectra of complexes 1 and 2 (in DMSO) when loaded in Pluronic F127 in water.

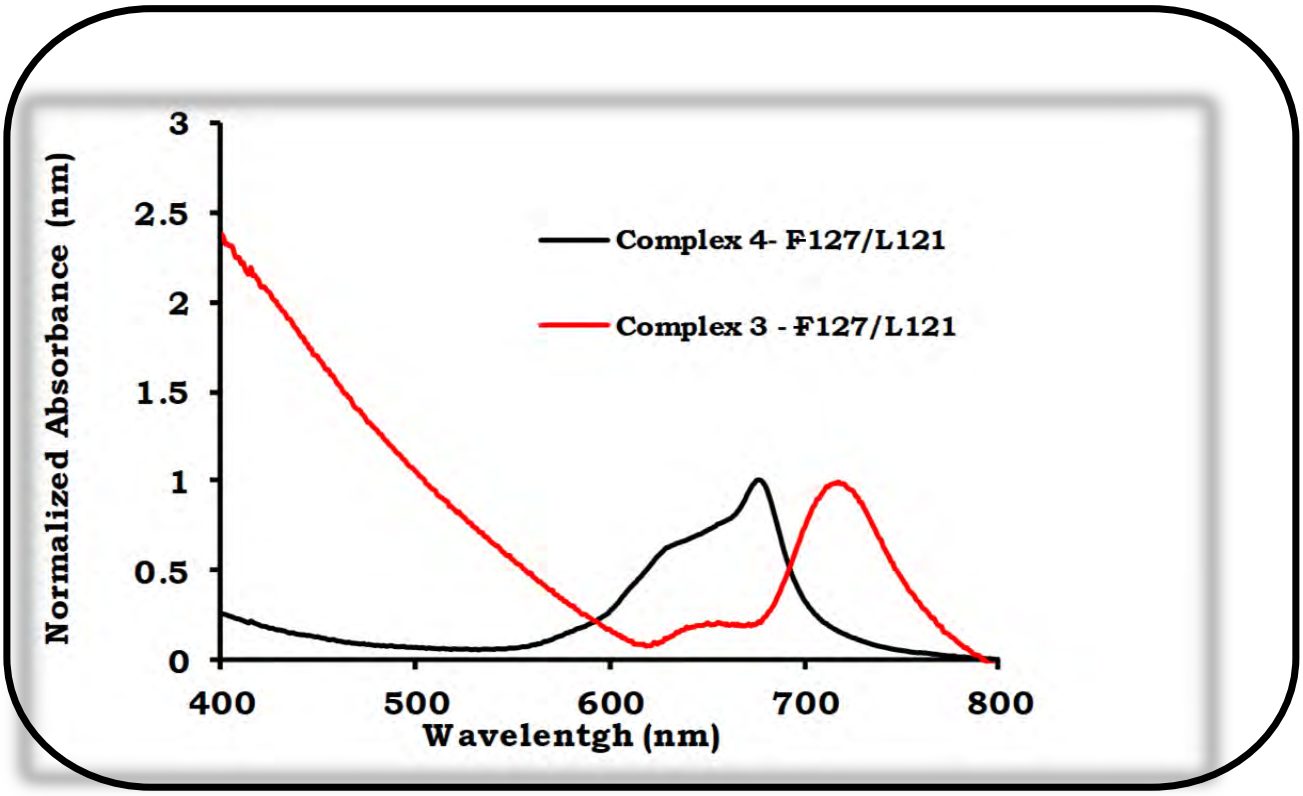

Figure 4.4: Electronic absorption spectra of 5–F127/L121 and 6–F127/L121 in H_2O.

4.2.2 Partition coefficients (Kp)

The K_p values were determined to be 146, 114, 158, 102, 145,143, 112 and 128 for complexes **1**–F127, **2**–F127, **3**–F127, **4**–F127, **5**–F127, **5**–F127/L121**, 6**–F127 and **6** –F127/L121, respectively, **(Table 4.1)**. The over expression of low-density lipoproteins (LDL) in cancer has been reported **[118]**. LDL have been shown to be the major localization target for hydrophobic drugs **[118]**. Thus, all the hydrophobic complexes **1**, **2**, **3**, **4**, **5** and **6** with Pluronic micelles carrier employed in this work could be preferentially localized in the LDL, hence enhancing selectivity and targeting **[118,119]**.

As reported in literature **[84]**, a high K_p value demonstrates a preferential partition for organic phase. **1**–F127, **3**–F127, **5**–F127 and **5**–F127/L121 have a larger K_p value compared to complexes **2**–F127 and **4**–F127, and **6**–F127 and **6**–F127/L121 suggesting that the former is more likely to be taken up by cancer cells. This shows that InPc complexes (**1, 3** and **5**) with axial ligands, are taken up by cells more readily than ZnPc complexes (**2, 4** and **6**).

4.2.3 Size determination by DLS

In order to ascertain the sizes of the nanoconjugates, dynamic light scattering (DLS) measurements were carried out **Fig. 4.5** As stated above, it has been reported that micelles should be small enough to evade detection and destruction by the reticular endothelial system therefore increasing the efficacy and circulation in the blood of the incorporated drug, hence the determination of micelle size is of crucial for this work **[120]**. The sizes of F127 alone were determined to be 14.10 nm. The sizes of the phthalocyanine contained in F127 micelles were determined to be 18.52 nm, 18.25 nm, 27.14 nm, 21.23 nm, 28.13 nm and 20.25 nm for **1**–F127, 2–F127, **3**–F127, **4**–F127, **5**–F127 and **6**–F127, respectively. The size of F127/L121 alone was determined to be 32.86 nm. The sizes determined for complexes **5** – F127/L121 and **6**–F127/L121 were determined to be 36.03 nm and 37.81 nm, respectively. The sizes of **5**–F127/L121 and **6**–F127/L121 are slightly larger than **5**–F127 and **6**–F127, respectively probably due to the micellization of the two polymers. The sizes of the micelles alone increased when they were physically entrapped with the complexes **(Table 4.1)**, showing the formation of supramolecular assemblies of the complexes with micelles.
It has been reported that micelles with diameters below 50 nm are able to deeply penetrate tumor tissue despite elevated interstitial pressure **[95]**. The micelle sizes obtained in this work are all below 50 nm.

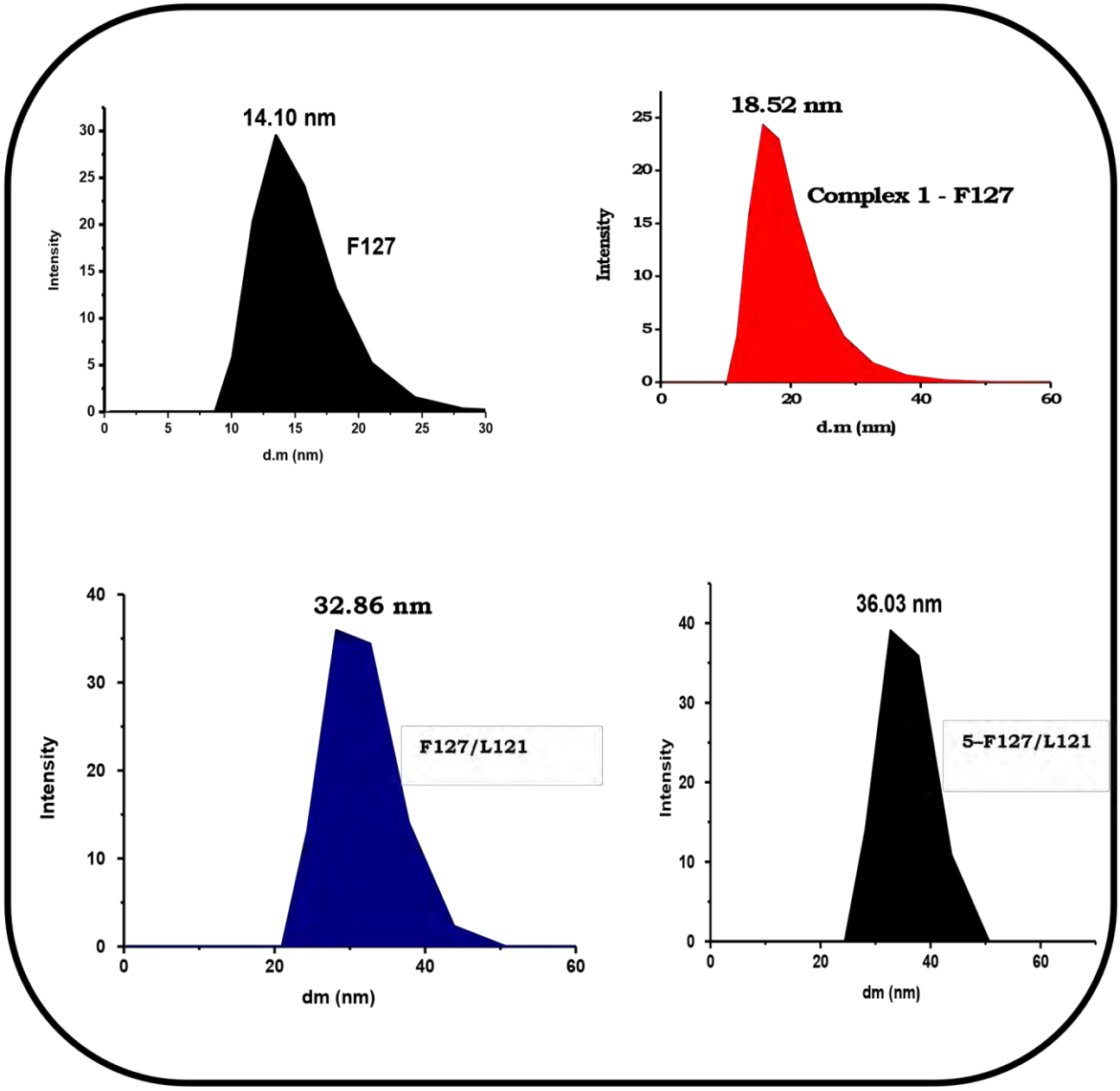

Figure 4.5: Dynamic Light Scattering (DLS) for Pluronic F127 alone, 1–F127, F127/L121 alone and 5–F127/L121.

4.2.4. Transmission Electron Microscopy (TEM)

Fig. 4.6 shows the micrographs of Pluronic® F–127 micelles alone (A) and F127/L121 alone (B) complex **5**–F127 (C) and **5**–F127/L121 (D) (as examples). The Pluronic® F–127 micelles are relatively spherical with a size range of 12.7 – 14.6 nm while the conjugates afforded similar morphology with a size range of 16.91– 18.83 nm. Pluronic® F127/L121 are also relatively spherical with a size range of 27.74 nm – 29.08 nm while the conjugates afforded a slightly aggregated morphology with a size range of 30.74 nm and 31.87 nm. There is an increase in micelle size after the encapsulation of complexes **1**, **2**, **3, 4, 5** and **6** as observed with DLS sizes (**Table 4.1**). The sizes determined by DLS have been reported to be larger than those determined by other techniques since DLS results tend to be skewed toward larger particles **[121]**, hence TEM values are lower than for DLS in **Table 4.1**.

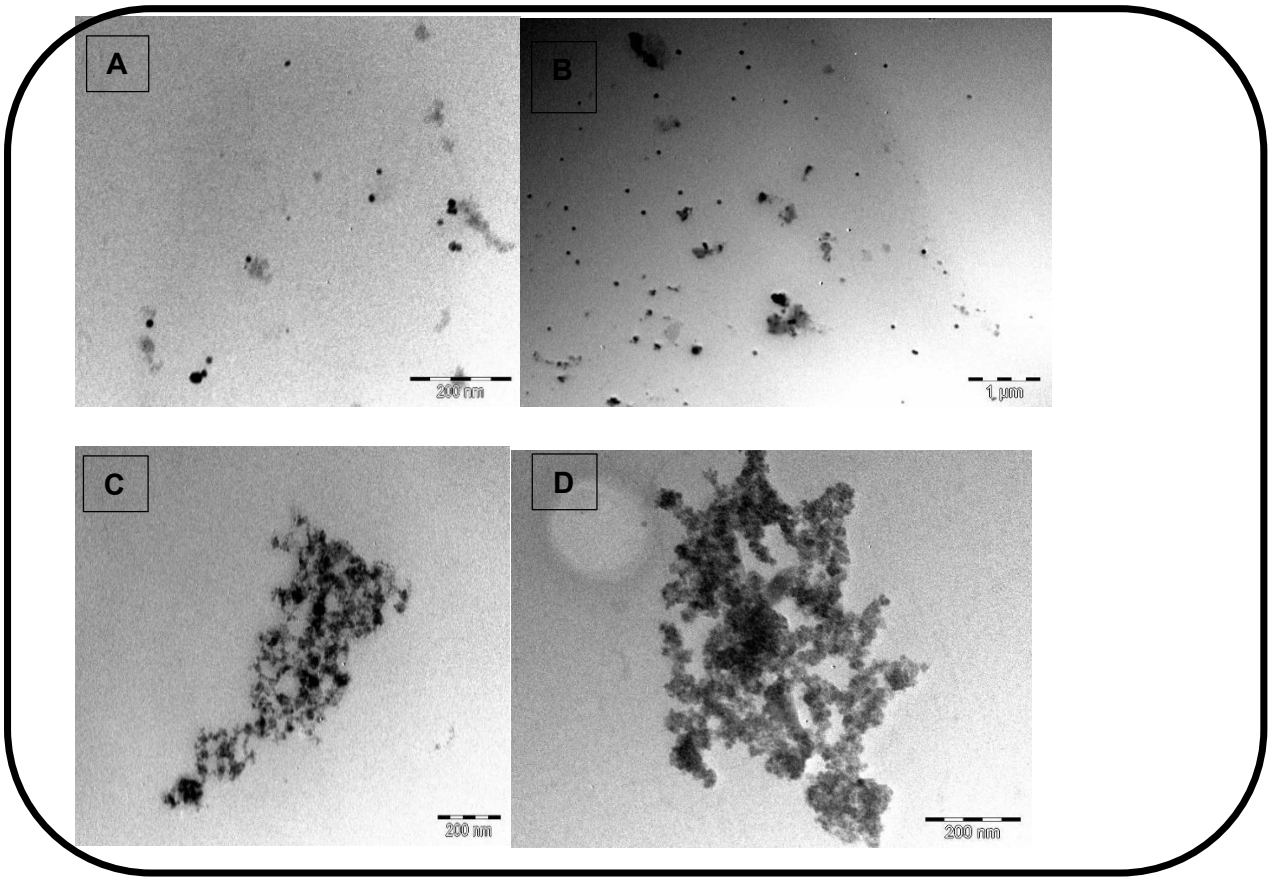

Figure 4.6: Tem micrographs for F127 alone (A), F127/L121 alone (B), 5–F127 (C) and 5–F127/L121 (as an example) (D). Solvent = water.

4.3 Conclusion

Complexes 1–6 *were successfully synthesized and characterized using* ^{1}H *NMR, IR, and mass spectroscopies as well as elemental analysis. These complexes were embedded into Pluronic micelles and further characterized using UV/Vis, DLS and TEM etc.* ***Complexes 5*** *and* ***6*** *were embedded into binary mixture micelles of F127/L121. These results showed a promising trend to be potential drug candidates for PDT.*

CHAPTER 5
Photophysicochemical properties

5. Photophysical and Photochemical Properties

The chapter discusses the photophysical and photochemical behaviour; fluorescence quantum yields and lifetimes, triplet quantum yields and lifetimes, and singlet oxygen quantum yields of phthalocyanines when alone and when incorporated into Pluronic micelles.

5.1 Fluorescence lifetimes (τ_F) and quantum yields (Φ_F)

All samples and standards were excited at the same wavelength. The absorbances of the solutions at the excitation source were about 0.05 to avoid any filter effects. The fluorescence quantum yields (Φ_F) were determined by a comparative method **[98, 99]** and calculated according to Equation 1.1, using unsubstituted ZnPc in DMSO ($\Phi_F = 0.2$) **[41]** as a standard. The fluorescence lifetimes (τ_F) were obtained using the time correlated single photon counting (TCSPC) method.

The fluorescence decay curve for complex **3** is shown as an example in **Figure 5.1**, and this is used as a representative for all the Pcs and their nanocomposites.

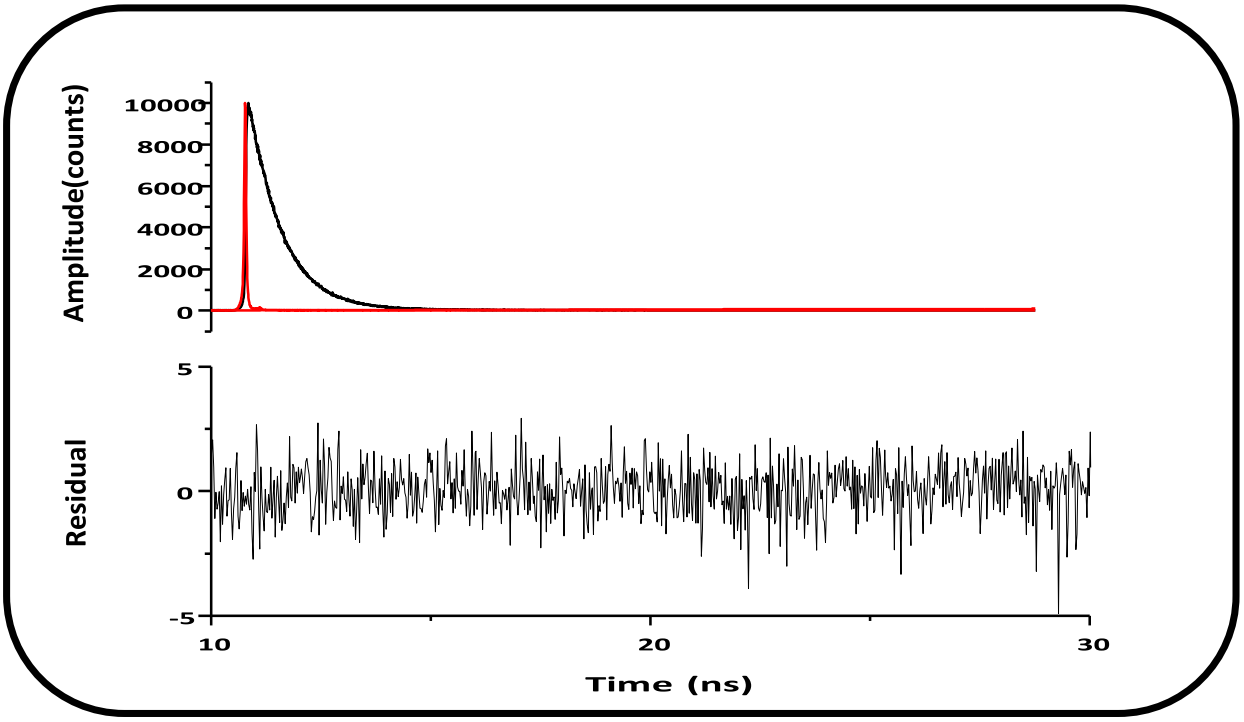

Figure 5.1: Fluorescence decay (black), χ2 fitting (red) and IRF (Instrument Response Factor) (black) curves for complex 3 in DMSO.

Table 5.1: Physicochemical properties of complexes 1–6 and their conjugates in DMSO and water.

Complex/ Conjugate	Solvent	Φ_F (±0.01)	τ_F (ns) (±0.01)	Φ_T (±0.01)	τ_T (μs) (±1)	Φ_Δ (±0.01)
1	DMSO	< 0.01	0.59	0.92	222	0.47
1-F127	Water	0.09	0.98	-	-	0.31
2	DMSO	< 0.01	0.38	0.32	105	0.20
2-F127	Water	0.07	0.31	-	-	0.09
3	DMSO	< 0.01	0.52	0.82	245	0.76
3-F127	Water	0.02	0.03	-	-	0.39
4	DMSO	0.07	1.19	0.75	128	0.47
4-F127	Water	0.018	0.02	-	-	0.23
5	DMSO	0.03	0.75	0.79	202	0.68
5-F127	Water	< 0.01	0.01	-	-	0.42
5-F127/L121	Water	0.03	< 0.01	-	-	0.51
6	DMSO	0.18[a]	1.92[a]	0.68[a]	148[a]	0.44[b]
6-F127	Water	< 0.01	< 0.01	-	-	0.37
6-F127/L121	Water	0.01	< 0.01	-	-	0.29

[a] from reference **[36]**

The MPc complexes showed a mono exponential fluorescence decay as expected **[122],** while the corresponding MPcs in micelles displayed bi-exponential decays and hence there are two lifetime values for the MPcs in micelles. Only the average lifetimes are presented in **Table 5.1**

The bi-exponential lifetimes observed when Pcs are in micelles, could be associated with the monomeric non-interacting MPc molecules, and the interaction between the MPc framework and the Pluronic polymer micelles resulting in unquenched and quenched photo-excited singlet states, respectively **[122,123].** Different orientations of the phthalocyanines on the micelles could also be responsible for the two lifetimes **[124].** Metal centres **[38, 39]**, substituents **[40, 41]** and symmetry **[125,126]** of the Pcs together with the shape and size of the nanocomposites **[127]** influence the fluorescence/triplet lifetimes and quantum yields of the complexes. **Table 5.1** shows the Φ_F and τ_F values of the complexes and their respective conjugates in DMSO and water.

i) Effect of central metal

Complexes **1** and **2**, have a similar ring substituents but differ in the central metal and this is the same for complexes **3** and **4** as well as **5** and **6**. Complexes **1** (Φ_F = < 0.01), **3** (Φ_F = < 0.01) and **5** (Φ_F = 0.03) containing indium as the central metal displayed lower fluorescence quantum yields than their zinc counterparts complexes **4** (Φ_F = 0.07) and **6** (Φ_F = 0.18) except for complex **2** (Φ_F = < 0.01). This shows that indium quenches the fluorescence lifetime and lowers the fluorescence quantum yield of Pcs more than zinc, **Table 5.1**. This is because indium is a heavier atom than zinc. Heavy atoms are known to encourage intersystem crossing to the triplet state through spin orbit coupling. The Φ_F and τ_F values for **1**–F127, **2**–F127, **3**–F127, **4**–F127, **5**–F127, **5**–F127/L121, **6** –F127 and **6** – F127/L121 are also low and cannot be compared to those for the Pc complexes alone due to differences in solvents.

ii) Effect of substituents

Complexes **2**, **4** and **6** have zinc as a central metal, however they differ in their substituents. Complex **2** (Φ_F = < 0.01) has phenyldiazenyl group (azo group), complex **4** (Φ_F = 0.07) has a pyridyloxy group and complex **6** (Φ_F = 0.18) has a benzothiazol2-ylthio group (**Table 5.1).** The low Φ_F for complex **2** suggest that the phenyldiazenyl group quenches fluorescence more than the pyridyloxy and benzothiazol-2-ylthio groups.

Complexes **1**, **3** and **5** contain indium as a central metal in the cavity, however, these complexes have different ring substituents, but there were insignificant differences in Φ_F values (< 0.01, < 0.01, 0.03). The low Φ_F values are due to the heavy atom effect of indium as previously explained.

5.2 Triplet quantum yields (Φ_T), lifetimes (τ_T).

Laser flash photolysis technique was employed to study the properties of complexes **1, 2, 3, 4, 5** and **6** at the triplet excited state. The triplet state properties of a complex such as long triplet lifetime and high triplet quantum yield are key parameters that determine its functionality and efficacy in PDT**.** The triplet state quantum yield Φ_T represents the fraction of molecules that undergoes intersystem crossing to the excited triplet state. A high triplet state quantum yield corresponds to low fluorescence quantum yield suggesting high efficiency of intersystem crossing, which is an attractive feature for MPcs intended for PDT as photosensitizers. A high triplet quantum yield is of great importance since it influences the singlet oxygen production. The Φ_T and τ_T values were measured by laser flash photolysis system in argon saturated solutions of the complexes or their conjugates in DMSO. The triplet quantum yield in aqueous media could not be obtained due to the plausible aggregation of Pcs, since aggregation is known to deactivate the photoactivity of molecules **[128]. Figure 5.2 B** shows the triplet decay curve of complex **2** in DMSO (as a representative) together with its transient curve **(Figure 5.2 A).** All the complexes decayed mono exponentially.

The transient absorption spectrum shows a broad band between 400–600 nm with a maximum absorption at 500 nm, attributed to the excited triplet-triplet state absorption ($T_1 \rightarrow T_n$). The negative peaks were also shown between 325 and 380 nm, and between 600 and 700 nm. The negative signals can be attributed to the depletion or photobleaching of the phthalocyanine ground state **[129]**.

Fitting the decay curve at the absorption maximum produced the triplet lifetimes and the obtained values together with the triplet quantum yield are summarized in **Table 5.1.**

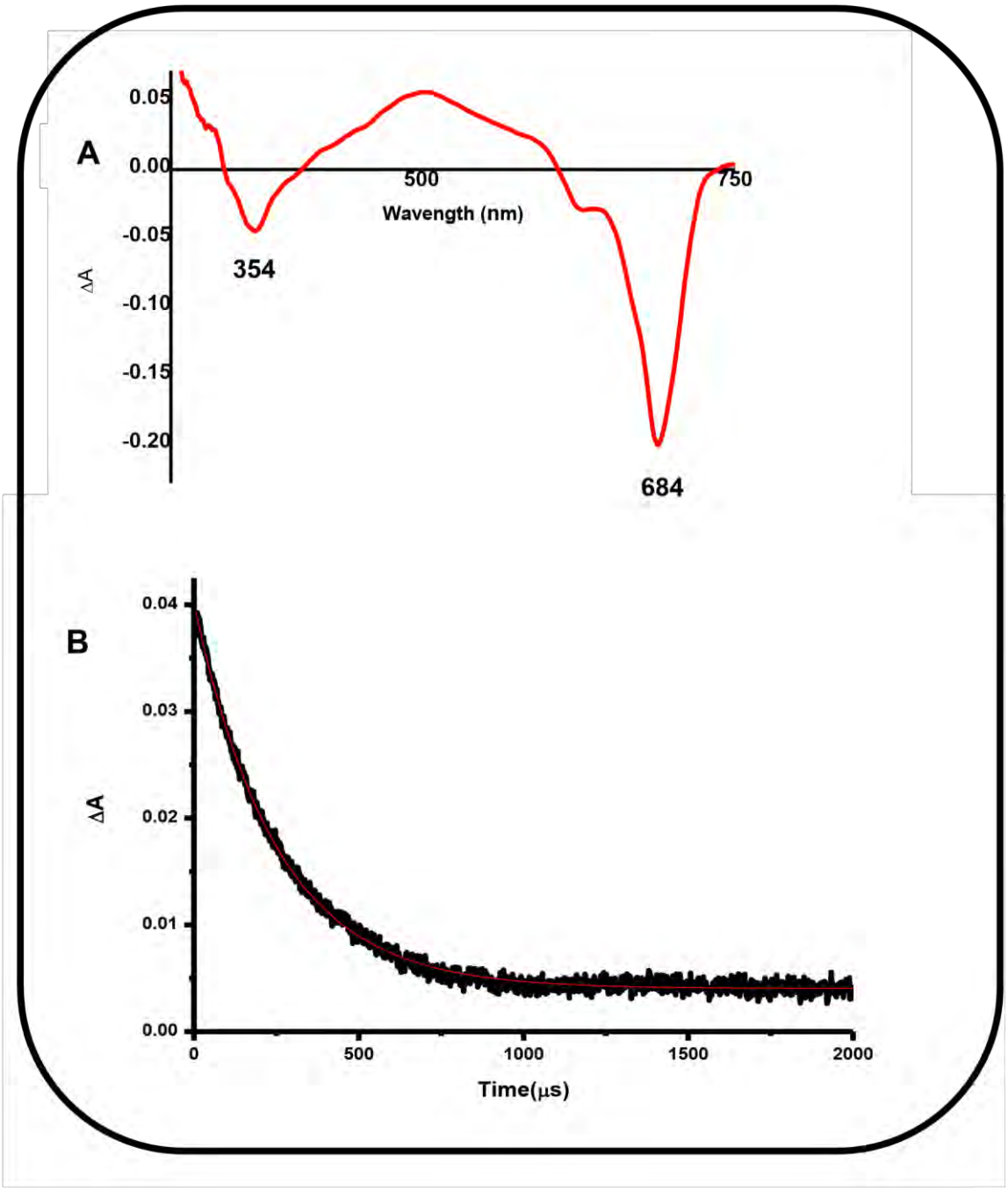

Figure 5.2: (A) Transient curve and (B) Triplet absorption decay curve (black) and fitting (red) for complex 2 in DMSO.

The Pc complexes displayed high triplet quantum yields (Φ_T = 0.92 for **1,** 0.82 for **3**, 0.75 for **4,** 0.79 for **5,** and 0.68 for **6**), (**Table 5.1**) corresponding to their low Φ_F , due to the presence of heavy atoms, Zn and In, as previously explained. The triplet quantum yields were higher for In Pcs due to heavier metal than Zn. **2** gave a very low value, the triplet lifetimes were longer for complexes **1**, **3** and **5**. Values in Pluronics could not be determined due to reasons explained above. There was no clear trend with substituents.

5.3 Singlet Oxygen quantum yield (Φ_{Δ})

Efficient interaction of the triplet state of the photosensitizer with the ground state molecular oxygen can result in generation of singlet oxygen due to energy transfer from the photosensitizer to the molecular oxygen. In order to determine the singlet oxygen quantum yield (Φ_{Δ}) the chemical photodegradation of the singlet oxygen quenchers: DPBF in DMSO and ADMA in water was monitored over a period as shown in **Fig. 5.3.** The experiments were conducted at room temperature using 1.5 mL of each MPc, MPc–F127 and MPc–F127/L121 mixed with equal volumes of ADMA or DPBF. Absorbance of the MPcs, MPc–F127 and MPc–F127/L121 was at 1.5 the Q_{band} and for DPBF/ADMA absorbance was at 2. The absorbance profiles of DPBF and ADMA **Fig. 5.3** (using **2** as an example). A gradual decrease in the absorbance of DPBF and ADMA was observed suggesting singlet oxygen was produced, **Fig. 5.3.** The was no decrease in the Q-band for the MPc, this therefore proves that the MPc was very stable during irradiation. It is expected that when Φ_T values increase, Φ_{Δ} values will also increase. Singlet oxygen quantum yield values are summarized in **Table 5.1** Complex **1** had the largest triplet quantum yield, but complex **3** had the largest singlet oxygen quantum yield in DMSO this is probably due to inefficient energy transfer in complex **1.**

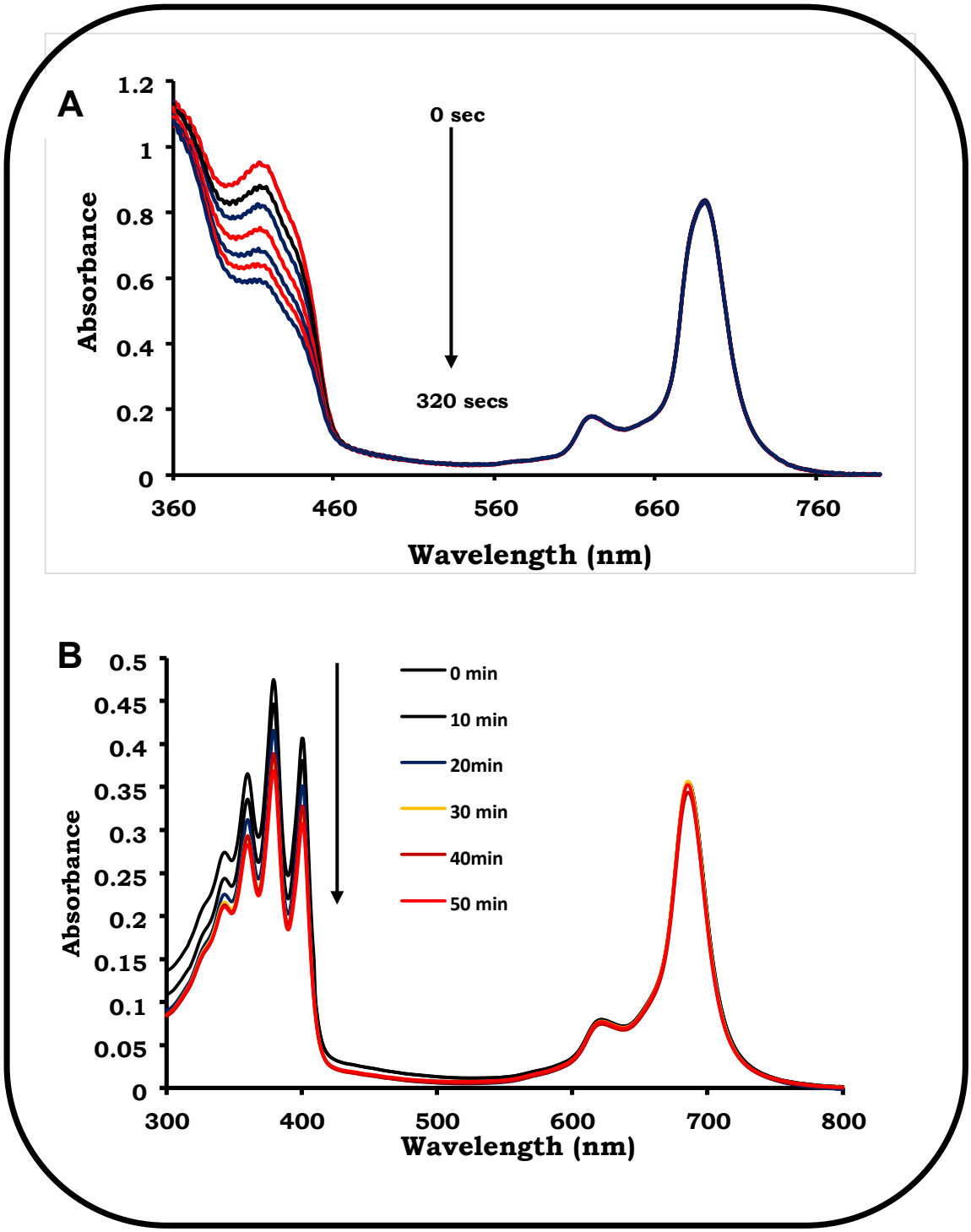

Figure 5.3: DPBF (A) and ADMA (B) decay profile of complex 2 in DMSO and 2 F127 in water.

A larger Φ_{Δ} was obtained for complexes **1, 3** and **5** in DMSO and in water in the presence of micelles (compared to complexes **2, 4** and **6**), due to the larger central In metal which encourages intersystem crossing to the triplet state. Complex **5** in the presence of mixed micelles (F127/L121) gave larger Φ_{Δ} value than for **5** with only F127. However, this was not the case for complex **6**. The low value for **6** in F127/L121 could be related to the large DLS size **(Table 4.1)** of the micelles which could have

resulted in screening effect, which could have prevented the interaction of the excited triplet state of the nanoconjugates and the ground state molecular oxygen **[130]**.

5.4 Conclusions

Physico-chemical properties of MPcs, MPc– F127 or MPc –F127/L121 conjugates are reported. An improvement in the photophysical properties of some MPcs following incorporation into Pluronic polymer micelles was observed. The singlet oxygen quantum yields generally higher for indium containing complexes compared to their zinc counterparts.

CHAPTER 6
Photodynamic therapy

6. *In-vitro* dark cytotoxicity and photodynamic therapy of against epithelial breast cancer cell lines (MCF7).

This chapter discusses the *in-vitro* dark cytotoxicity and photodynamic therapy activity of phthalocyanines when alone and when incorporated into Pluronic polymer micelles against epithelial breast cancer cell lines (MCF7).

6.1 Dark Toxicity

Dark cytotoxicity studies were performed at 5, 10, 20, 40, 80 and 100 µg/ml, **Fig. 6.1** for all. At all concentrations studied the percentage cell viabilities were all above 80%. *In vitro* dark toxicity is undesirable for photosensitizers aimed for use in PDT. The dark toxicities of the photosensitizers were determined in DMSO (1% v/v); relative to the test concentrations the vehicle control, DMSO (1% v/v) had negligible effect on the cells shown here and as reported previously **[131].**

Upon analysis of the triplicate replicate data of each concentration, no statistically significant difference was observed as the p-value was found to be greater than 0.05 (**Fig 6.1**).

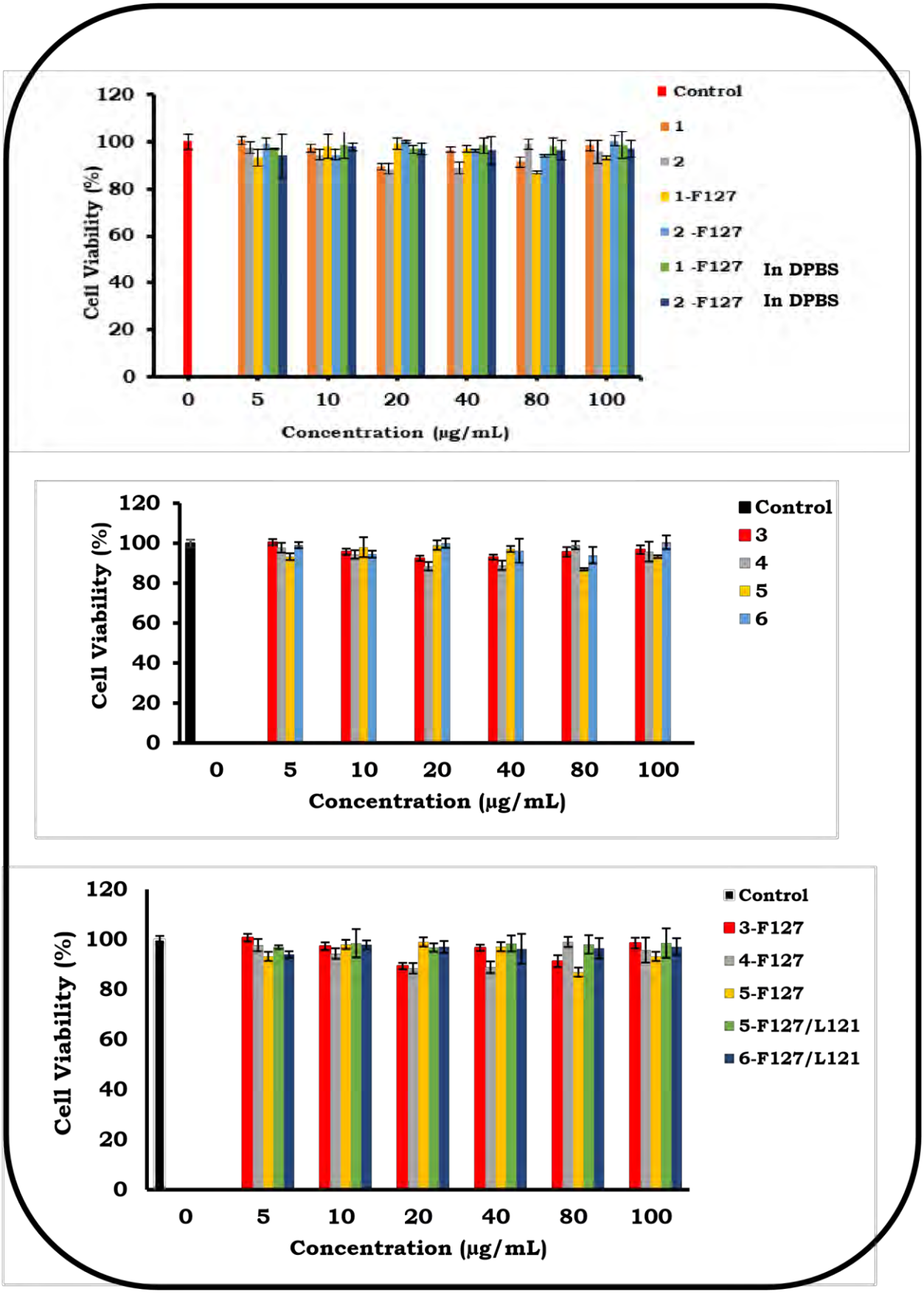

Fig 6.1: Dark toxicity plots for all complexes in 1% DMSO except where indicated.

6.2 Photodynamic therapy

In PDT, an excited triplet state of the photosensitizer transfers its energy to the ground state molecular oxygen resulting in the production of singlet oxygen which is the main cytotoxic species in PDT. Thus, the PDT activity is expected to follow the same trend as the singlet oxygen quantum yields, as observed in this work. There were no changes in the spectra of the complexes following irradiation for PDT studies, thus confirming stability. The phototoxicity of the complexes increased from 0 µg/mL to 100 µg/mL. When comparing **1** and **2, 3** and **4** as well as **5** and **6**, InPc (**1**, **3** and **5**) show the highest PDT activity corresponding to the high singlet oxygen quantum yield.
The following conclusion can be drawn from **Fig. 6.2**, and **Table 6.1**

(a) The effect of Pluronic F127 can be determined by comparing Pcs alone and Pcs with micelles, all in 1% (v/v) DMSO. In all cases the PDT activity is higher in the presence of micelles **(Table 6.1)**. This could be attributed to the small micellar size (~ 10 -100 nm) which allows tumour accumulation after administration due to the enhanced permeation and retention (EPR) effect **[131]**. F127 alone (without **1**, **2**, **3**, **4**, **5** and **6**) and F127/L121 (without 5 and **6**) had no PDT effect.

(b) The effect of PBS only compared to 1% (v/v) DMSO, may be determined by comparing **1**–F127 and **2**–F127 in the different solvents -there is no significant difference.

(c) Complex **5**–F127/L121 showed a slightly better PDT activity than complex **5** F127, the same trend was observed for complex **6**–F127/L121 and **6**–F127 this could be attributed to the higher solubilization capacity of mixed micelles in comparison to individual systems **[95].**

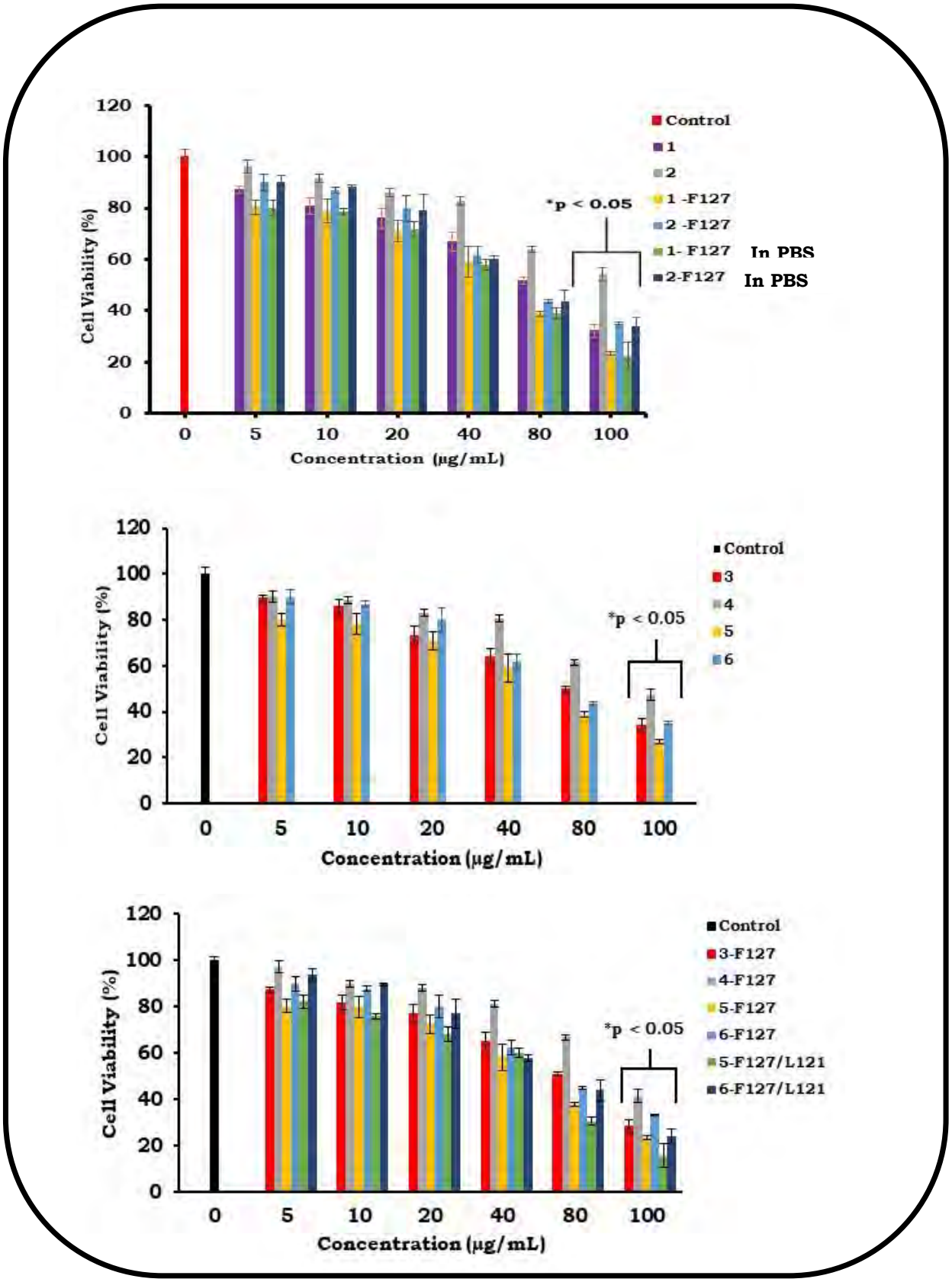

Fig 6.2: PDT Plots for all complexes in 1% DMSO except where indicated.

Table 6.1: Summary of PDT activities at 100 µg/mL of Pcs alone and Pcs with micelles on MCF7 *in vitro* in 1% DMSO.

Complex	Cell viability (%)
1	32.04
1-F127	23.26
1-F127 in DPBS	22.00
2	54.00
2-F127	35.06
2-F127 in DPBS	34.02
3	34.00
3-F127	28.14
4	47.30
4-F127	41.30
5	26.89
5-F127	23.00
5-F127/L121	15.58
6	35.06
6-F127	33.44
6-F127/L121	24.02

6.3 Conclusions

In vitro dark cytotoxicity and photodynamic therapy of complexes **1, 2, 3, 4, 5, 6** and **1**–F127, **2**–F127, **3**–F127**, 4**–F127, **5**–F127, **5**–F127/L121**, 6**–F127 and **6**–F127/L121 *against MCF7 cells were presented. The complexes were relatively non-toxic in the dark. The complexes displayed cell viability of 80% at the studied concentrations in the dark. The complexes in micelles showed an improved phototoxicity at 100 µg/mL. Complexes **1**–F127, **3**–F127 and **5**–F127 showed 23%, 28% and 23% viable cell at 100 µg/mL. The mixed micelles showed a slightly better phototoxicity compared to the individual micelles with **5**–F127/L121 showed 15% viable cells. This makes the complexes good candidates for real life applications in PDT.*

CHAPTER 7
General conclusions

7.1 General conclusions

This work presents the successful synthesis and characterization new symmetric MPcs. The MPcs were characterised using FTIR, UV-Vis, ^{1}HNMR, MALDI-TOF mass spectroscopies and elemental analyses. The prepared Pcs were soluble in DMSO and exhibited monomeric behaviour. These were further physically entrapped into Pluronic polymer micelles. The MPcs became water soluble after incorporation into Pluronic polymer micelles. The effect of metal centres and substituents of MPcs physically entrapped to Pluronic polymer micelles on the photochemical and photophysical behaviour of MPcs was studied.

Furthermore, *in vitro* dark cytotoxicity and photodynamic therapy of complexes **1, 2, 3, 4, 5, 6** and **1**–F127, **2**–F127 **3**–F127**, 4**–F127, **5**–F127, **5**–F127/L121**, 6**–F127 and **6**–F127/L121 against MCF7 cells was tested. Complexes alone and with micelles showed minimum dark toxicity making them applicable for PDT. All complexes displayed good phototoxicity with < 50% cell viability (except for complex **2 >** 50 %) at concentrations = 100 µg/mL, however complexes with micelles showed < 45% cell viability at concentrations = 100 µg/mL probably due to the small micellar size (~ 10 100 nm) which allows tumour accumulation after administration due to the enhanced permeation and retention (EPR) effect. The complexes with micelles showed both minimum dark toxicity and better PDT activity than Pc complexes alone making them good candidates for real life PDT applications, however 5–F127/L121 displayed the best PDT activity of all complexes alone and with micelles studied.

7.2 Future

Physical entrapment of MPcs to Pluronic micelles has been proven to enhance physicochemical properties and photodynamic therapy activities of MPcs when incorporated into Pluronic micelles. It would be interesting to study the antimicrobial properties of these MPcs when incorporated into Pluronic micelles.

References

1. G. De La Torre, C.G. Claessens, T. Torres, Chem. Commun. 20 (**2007**) 2000.
2. T. Fukuda, N. Kobayashi, in: K.M. Kadish, K.M. Smith, R. Guilard (Eds.), Handbook Porphyrin. Science, 9th ed., World Scientific Press, Singapore, **2010**, pp. 1- 644.
3. L.M. Moreira, F.V. Dos Santos, J.P. Lyon, M. Maftoum-Costa, C. Pacheco-Soares, N. Soares Da Silva, Aust. J. Chem 61 (**2008**) 741.
4. R. Bonnett, In Chemical Aspects of Photodynamic Therapy, Gordon and Breach Science Publishers, Amsterdam, **2000**.
5. S.B. Brown, E.A. Brown, I. Walker, Lancet Oncol. 5 (**2004**) 497.
6. V. Mantareva, I. Angelov, V. Kussovski, D. Woehrle, S. Dimitrov, Comptes Rendus L'Academie Bulg. Des Sci. 63 (**2010**) 77.
7. D. Mondal, S. Bera, Adv. Nat. Sci. Nanosci. Nanotechnol. 5 (**2014**) 033002 (12 pages).
8. M. Wainwright, Chemother. 42 (**1998**) 13.
9. R. Zugle, T. Nyokong, Appl. Polym. Sci. 128 (**2013**) 1131.
10. M. Hanack, T. Schneider, M. Barthel, J.S. Shirk, S.R. Flom, R.G.S. Pong, Coord. Chem. Rev. 219 (**2001**) 235.
11. P. Gregory, High-Technology Applications of Organic Colourants, 7th ed., Plenum Press, New York, **1991**.
12. I. Okura, Photosensitization of Porphyrins and Phthalocyanines, Gordon and

Breach Science Publishers, Netherlands, **2000**.

13. D. Dini, M. Hanack, in: K.M. Kadish, K.M. Smith, R. Guilard (Eds.), Porphyrin. Handbook, 17th ed., Academic Press, New York, **2003**, pp. 1.

14. E. Ben-Hur, W.S. Chan, in: K.M. Kadish, K.M. Smith, R. Guilard (Eds.), Porphyrin. Handbook, 19th ed., Academic Press, New York, **2003**, pp. 1–35.

15. P. Gregory, J. Porphyrins Phthalocyanines 4 (**2000**) 432.

16. T. Fukuda, K. Ono, S. Homma, N. Kobayashi, Chem. Lett. 32 (**2003**) 736.

17. T. Nyokong, in: J. Jiang (Ed.), Funct. Phthalocyanines Mol. Mater. Struct. Bond, 135th ed., Springer, New York, **2010**, pp. 45.

18. N. Kobayashi, H. Ogata, N. Nonaka, E.A. Luk'yanets, Chem. Eur. J. 9 (**2003**) 5123.

19. N. Kobayashi, H. Konami, in: C.C. Leznoff, A.B.P. Lever (Eds.), Phthalocyanines Properties. Applications, 4th ed., VCH, New York, **1996**, pp. 343 - 404.

20. L. Edwards, M. Gouterman, Porphyrins: XV, J. Mol. Spectrosc. 33 (**1970**) 292.

21. M. Gouterman, The Porphyrins, Part A. Physical Chemistry, 3rd ed., Academic Press, New York, **1978**.

22. A. Henriksson, M. Sundbom, Theor. Chim. Acta 27 (**1972**) 213.

23. C.G. Claessens, U. Hahn, T. Torres, Chem. Rec. 8 (**2008**) 75.

24. P. Yiru, H. Fenghua, L. Zhipeng, C. Naisheng, H. Jinling, Inorg. Chem. Commun. 7 (**2004**) 967.

25. N.B. McKeown, Phthalocyanine Materials: Synthesis, Structure, and Function. Chemistry of Solid-State Materials, Cambridge University Press, New York, **1998**.

26. F. Dumoulin, M. Durmuş, V. Ahsen, T. Nyokong, Coord. Chem. Rev. 254 (**2010**) 2792.

27. V.N. Nemykin, E.A. Luk'yanets, Arkivoc. i (**2010**) 136.

28. W. Liu, C. Lee, H. Chan, T.C.W. Mak, D.K.P. Ng, J. Inorg. Chem. (**2004**) 286.

29. V. Novakova, J. Roh, P. Gela, J. Kuneš, P. Zimcik, Chem. Commun. 48 (**2012**) 4326.

30. W.M. Sharman, J.E. Van Lier, in: K.M. Kadish, K.M. Smith, R. Guilard (Eds.), Porphyrin. Handbook. 15th ed., Academic Press, San Diego, **2003**, pp. 1-53.

31. V.N. Nemykin, S. V. Dudkin, F. Dumoulin, C. Hirel, A.G. Gürek, V. Ahsen, Arkivoc. i (**2014**) 142.

32. S.M. RodríGuez-Morgade, G. De La Torre, T. Torres, in: K.M. Kadish, K.M. Smith, R. Guilard (Eds.), Porphyrin. Handbook. Phthalocyanines Synth. 15th ed., Academic Press, San Diego, **2003**, pp. 125 - 155.

33. Y. Liu, Y. Xu, D. Zhu, T. Wada, H. Sasabe, L. Liu, Thin Solid Films 244 (**1994**) 943.

34. Y. Liu, D. Zhu, T. Wada, A. Yamada, H. Sasabe, J. Heterocycl. Chem. 31 (**1994**) 1017.

35. W. Chidawanyika, A. Ogunsipe, T. Nyokong, New J. Chem, 31 (**2007**) 377.

36. N. Njwaji, O.M. Bankole, J. Britton, T. Nyokong, J. Porphyrins Phthalocyanines 21(**2017**) 263.

37. N. Njwaji, B. Jones, J. Mack, D.O. Oluwole, T. Nyokong, J. Photochem. Photobiol A: Chem 346 (**2017**) 46.

38. K. Hayashi, M. Nakamura, H. Miki, S. Ozaki, Adv. Funct. Mater. 24 (**2014**) 503.

39. A. Gorman, J. Killoran, C. O'Shea, T. Kenna, W.M. Gallagher, D.F. O'Shea, J. Am. Chem. Soc. 126 (**2004**) 10619.

40. T. Nyokong, Coord. Chem. Rev. 251 (**2007**) 1707.

41. A. Ogunsipe, J.-Y. Chen, T. Nyokong, New. J. Chem. 28 (**2004**) 822.

42. Z. Chen, S. Dong, C. Zhong, Z. Zhang, L. Niu, Z. Liu, F. Zhang, Photochem. Photobiol A: Chem. 206 (**2009**) 213.

43. M. Auzios, B. Therrien, G. Suss – Fink, P. Stephicka, W. H. Ang, P.J. Dyson, Inorg. Chem. 47 (**2008**) 578.

44. V.E. Kuz'min, V.P. Lozitsky, G.L. Kamatov, R.N. Lozitskaya, A.I. Zheltvay, A.S. Fedtchouk, D.N. Kryzhanovsky, Acta. Bio. Pol. 47 (**2000**) 867.

45. M.T. Colvin, A.B. Ricks, A.M. Scott, D.T. Co, M.R. Wasielewski, J. Phys. Chem. A 116 (**2012**) 1923.

46. C.G. Mortimer, G. Wells, J. Crochard, E.L. Stone, T.D. Bradshaw, M.F.G. Stevens, A.D. Westwell, J. Med. Chem 49 (**2006**) 179.

47. D. Havrylyuk, L. Mosula, B. Zimenkovsky, O. Vasylenko, A. Gzella, R. Lesyk, Eur. J. Med. Chem. 45 (**2010**) 5012.

48. P.C. Sharma, A. Sinhmar, A. Sharma, H. Rajak, D.P. Pathak, J. Inhib. Med. Chem. 28 (**2013**) 240.

49. S. Anand, B.J. Ortel, S.P. Pereira, T. Hasan, E.V. Maytin, Cancer Lett. 326 (**2012**) 8.

50. R. Ackroyd, C. Kelty, N. Brown, M. Reed, Photochem. Photobiol. 74 (**2001**) 656.

51. J.P. Celli, B.Q. Spring, I. Rizvi, C.L. Evans, K.S. Samkoe, S. Verma, B.W. Pogue, T. Hasan, Chem. Rev. 110 (**2010**) 2795.

52. Á. Juarranz, P. Jaén, F. Sanz-Rodríguez, J. Cuevas, S. González, Transl. Oncol. 10 (**2008**) 148.

53. M. Alemany-Ribes, M. García-Díaz, P. Acedo, M. Agut, S. Nonell, M.L. Sagristá, M. Mora, M. Cañete, Á. Villanueva, J.C. Stockert, C.E.J. Semino, J. Anal. Bioanal. Tech. S 1. (**2013**) doi: 10.4172/2155-9872.51-004 (6 pages).

54. P.C. Lo, S.Y.S. Chow, D.K.P. Ng, in, K.D.P Ravindra, T.J Dougherty (Ed.), Handbook. Photodynamic. Therapy. Recent Applications. World Scientific Press, Singapore, **2016**, pp. 237- 272.

55. R.R. Allison, G.H. Downie, R. Cuenca, X.-H. Hu, C.J. Childs, C. Sibata, Photodiagnosis Photodyn. Ther. 1 (**2004**) 27.

56. L.B. Josefsen, R.W. Boyle, Theranostics 2 (**2012**) 916.

57. K. Plaetzer, B. Krammer, J. Berlanda, F. Berr, T. Kiesslich, Med. Sci. 24 (**2009**) 259.

58. B.W. Henderson, T. Dougherty, Photochem. Photobiol. 55 (**1992**) 145.

59. T.J. Dougherty, C.J. Gomer, B.W. Henderson, G. Jori, D. Kessel, M. Korbeilk, J. Moan, Q. Peng, J. Natl. Cancer Inst. 90 (**1998**) 899.

60. K. S. Oh, J. Y. Song, S. H. Cho, B. S. Lee, S. Y. Kim, K. Kim, H. Jeon, I. C. Kwon, S. H. Yuk, J. Contr. Release. 148 (**2010**) 344.

61. A. V. Kabanov, E. V. Batrakova, Curr. Pharm. Des. 10 (**2004**) 13.

62. U. Kedar, P. Phutane, S. Shidhaye, V. Kadam, Nanomed Nanotech Biol Med. 6 (**2010**) 71.

63. S. R. Croy, G. S. Kwon, Curr. Pharm. Des. 12 (**2006**) 4669.

64. G. S. Kwon and K. Kataoka, Adv. Drug Deliv. Rev. 16 (**1995**) 295.

65. D. Missirlis, N. Tirelli, and J. A. Hubbell, Langmuir 21 (**2005**) 2605.

66. H. S. Yoo and T. G. Park, J. Control. Release, 96 (**2004**) 273.

67. A. V. Kabanova. E. V. Batrakovaa, V. Y. Alakhovb, J. Control. Release 82 (**2002**) 189.

68. R. Nagarajan, Colloids Surfaces B. Biointerfaces 16 (**1999**) 55.

69. A. Venne, S. Li, R. Mandeville, A. V. A. Kabanov, Cancer Res. 56 (**1996**) 3626.

70. D. Sutton, N. Nasongkla, E. Blanco, J. Gao, Pharm. Res. 24 (**2007**) 1029.

71. G. S. Kwon, Critical Rev 20 (**2003**) 357.

72. V. Alakhov, E. Klinski, S. Li, G. Pietrzynski, A. Venne, E. V. Batrakova, T. Bronitch, A. V. Kabanov, Colloids Surf, B: Biointerfaces 16 (**1999**) 113.

73. W. Zhang, Y. Shi, Y. Chen, J. Ye, X. Sha, X. Fang, Biomaterials 32 (**2011**) 2894.

74. M. Yokoyama, P. Opanasopit, T. Okano, K. Kawano, Y. Maitani, J. Drug Target., 12 (**2004**) 384.

75. Z. Sezgin, N. Yüksel, T. Baykara, Int. J. Pharm. 332 (**2007**) 161.

76. L, Liu, K.T, Yong, I. Roy, W.C, Law, L. Ye, J. Liu, J. Liu, R. Kumar, X, Zhang, P.N. Prasad, Theranostics 7 (**2012**) 705.

77. B. H. Vilsinski, J. L. Aparicio, P. C. de Souza Pereira, S. L. Fávaro, K. S. S. Campanholi, A. P. Gerola, A. L. Tessaro, N. Hioka, W. Caetano, Quim. Nova, 37 (**2014**) 1650.

78. A. B. Solovieva, N. S. Melik-Nubaro, T. M. Zhiyentayev, P. I. Tolstih, I. I. Kuleshov, N. A. Aksenova, E. A. Litmanovich, N. N. Glagolev, V. A. Timofeeva, A. V. Ivanov, Laser Physics 19 (**2009**) 817.

79. T. M. Zhientaeva, N. S. Melik-Nubarova, E. A. Litmanovicha, N. A. Aksenovab, N. N. Glagolevb, A. B. Solov'evab. Poly. Sci. Series A 51 (**2009**) 502.

80. Y. T. Yang, C. T. Chen, T. Tsai, Dyes Pigm 96 (**2013**) 763.

81. H. Park, K. Na, Biomaterials 34 (**2013**) 6992.

82. Z. Sezgin, N. Yüksel, T. Baykara, Eur. J. Pharm. Biopharm. 64 (**2006**) 261.

83. J. Sobczyński, S. Kristensena, K. Berga, Photochem. Photobiol. Sci. 13 (**2014**) 8.

84. A.C. Wenceslau, G.L.Q.C. Ferreira, N. Hioka, W. Caetano, J. Porphyrins Phthalocyanines 19 (**2015**) 1168.

85. K.R. Py-Daniel, J. S. Namban, L. R. de Andrade, P. E.N. de Souza, L. G. Paterno, R. B. Azevedo, M. A.G. Soler, European J. Pharm. Biopharm. 103 (**2016**) 23.

86. B. H. Vilsinski, A. P. Gerola, J. A. Enumo, K. da Silva Souza Campanholi, P. C. de Souza Pereira, G. Braga, N. Hiok, E. Kimura, A. L. Tessaro, W. Caetano, Photochem. Photobiol. 91 (**2015**) 518.

87. Ł. Lamch, M. Tsirigotis-Maniecka, J. Kulbacka, K. A. Wilk, Arkivoc. ii (**2017**) 433.

88. R. Trivedi, U. B Kompella, Nanomedicine (Lond). 5 (**2010**) 485.

89. E. S. Lee, Y.T. Oh, Y.S. Youn, M. Nam, B. Park, J. Yun, J.H. Kim, H.T. Song, K.T. Oh, Colloids Surf. B: Bio. 82 (**2011**) 190.

90. D. S. Pellosi, A. L. Tessaro, F. Moret, E. Gaio, E. Reddi, W. Caetano, F. Quaglia, N. Hioka, J. Photochem. Photobiol A: Chemistry 314 (**2016**) 143.

91. F. Moret, E. Redd, J. Porphyrins Phthalocyanines 21 (**2017**) 239.

92. L. Lamch, U. Bazyli'nska, J. Kulback, J. Pietkiewicz, K. Bieżu'nska-Kusiak, K.A. Wilk. Photodiagnosis Photodyn. Ther. 11 (**2014**) 570.

93. M. Managa, B.P. Ngoy, T. Nyokong, J. Photochem. Photobiol. A: Chem. 339 (**2017**) 49.

94. A. Seth, D.S Katti, Int. J. Nanomedicine. 7 (**2012**) 5129.

95. K. T. Oh, T. K. Bronich, A. V. Kabanov, J. Controlled Release 94 (**2004**) 411.

96. A. Gilbert, J. Baggot, Essentials of Molecular Photochemistry, 1st ed., Blackwell Science Ltd., Oxford, **1991**.

97. E.T. Saka, C. Göl, M. Durmus, H. Kantekin, Z. Biyiklioglu, J. Photochem. Photobiol. A Chem. 241 (**2012**) 67.

98. S. Fery-Forgues, D. Lavabre, J. Chem. Educ. 76 (**1999**) 1260.

99. D.M. Maree, T. Nyokong, K. Suhling, D. Phillips, J. Porphyrins Phthalocyanines 6 (**2002**) 373.

100. H.C. Gerritsen, R. Sanders, A. Draaijer, Proc. SPI 2329 (**1994**) 260 (8 pages).

101. A.G. Ryder, S. Power, T.J. Glynn, J.J. Morrison, Proc. SPI 4529 (**2001**) 102.

102. T.H. Tran–Thi, C. Desforge, C. Thiec, S.J. Gaspard, J. Phys. Chem. 93 (**1989**) 1226.

103. L. Deboni, E. Piovesan, L. Gaffo, C.R. Mendonca, J. Phys. Chem. A. 112 (**2008**) 6803.

104. K.R. Weishaupt, C.J. Gomer, J. Dougherty, Cancer Res. 36 (**1976**) 2326.

105. N.A. Kuznetsova, N.S. Gretsova, V.M. Derkacheva, O.L. Kaliya, E.A. Luk'yanets, Porphyrins Phthalocyanines. 7 (**2003**) 147.

106. A.A. Gorman, Chem Soc Rev 10 (**1981**) 205.

107. N.A. Kuznetsova, N. Gretsova, O. Yuzhakova, V. Negrimovsky, O. Kaliya, E. Luk'yanets, Russ. J. Gen. Chem. 71 (**2001**) 36.

108. T. Nyokong, E. Antunes, in: K.M. Kadish, K. Smith, R. Guilard (Eds.), Handbook. Porphyrin. Science, 7th ed., Academic Press, New York, **2010**, pp. 247- 349.

109. T. Nyokong, Pure Appl. Chem. 83 (**2011**) 1763.

110. C.S. Foote, Singlet Oxygen, Academic Press, New York, San Francisco, London, **1979**.

111. J.R. Lakowicz, Principles of Fluorescence Spectroscopy, 2nd ed., Kluwer Academic/Plenum Publishers, New York, **1999**.

112. M. Ambroz, A. Beeby, A. McRobert, M. Simpson, R. Svensen, D. Phillips, J. Photochem. Photobiol B. Biol. 9 (**1991**) 87.

113. E.A. Mohamed, I. I. A. Hashim, R.M. Yusif, G.M. Suddek, A.A.A. Shaaban, F.A.E. Badria, Eur. J. Pharm. Sci. 96 (**2017**) 232.

114. M. J. Ruiz – Angel, R.D. Caballero, E.F. Simo- Alfonso, M.C. Garcia – Alvarez – Coque, J. Chromatogr. A 947 (**2002**) 31.

115. J.A. Menard, H.C. Christianson, P. Kucharzewska, E. Bourseau- Guilman, K.J. Svensson, E. Lindqvist, V.I. Chandran, L. Kjelle, C. Welinder, J. Bengzon, M.C. Johansso, M. Belting Cancer Res. 76 (**2016**) 4828.

116. L.C. Nene, M.E. Managa, D.O. Oluwole, D.M. Mafukidze, A. Sindelo, T. Nyokong, Inorg. Chim. Acta 488 (**2019**) 304.

117. T. Nyokong, Electronic Spectral and Electrochemical Behavior of Near Infrared Absorbing Metallophthalocyanines. In: Jiang J. (eds) Functional Phthalocyanine Molecular Materials. Structure and Bonding, vol 135. Springer, Berlin, Heidelberg strict bond. Springer. Berlin. Heidelberg: **2010**.

118. A.P. Castano, T.N. Demidova, M.R., Photodiag. Photodyn. Ther. 2 (**2005**) 91.

119. G. Jori, E. Reddi, Int.J. Biochem. 25 (**1993**) 1369.

120. A. T. Press, A. Ramoji, M. Lühe, A. C Rinkenauer, J. Hoff, M. Butans, C. Rössel, C. Pietsch, U. Neugebauer, F. H Schacher, M. Bauer. NPG Asia Materials, 9 (**2017**) 13.

121. C.M. Hoo, N. Starostin, P. West, M.I. Mecartney, J Nanoparticle Res. 2008; 10 (**2016**) 89.

122. J.W. Owens, M.J. Robins, J. Porphyrins Phthalocyanines 5 (**2001**) 460.

123. Z. Petrásek, D. Phillips, Photochem. Photobiol. Sci. 2 (**2003**) 236.

124. C. Geddes, Topics in Fluorescence Spectroscopy, 10th ed., Springer, New York, **2005**.

125. C.C. Byeon, M.M. McKerns, W. Sun, T.M. Nordlund, C.M. Lawson, G.M. Gray, Appl. Phys. Lett. 84 (**2014**) 5174.

126. T. Fukuda, S. Homma, N. Kobayashi, Chem. Eur. J. 11 (**2005**) 5205.

127. C. Xue, Y. Xue, L. Dai, A. Urbas, Q. Li, Adv. Opt. Mater. 1 (**2013**) 581.

128. G.J. Smith, Photochem. Photobiol. 41 (**1985**) 123.

129. Z.N. Erol, P. Atienzar, Y. Arslanołlu, E. Hamuryudan, H. García, RSC Adv. 5 (**2015**) 55901.

130. E. I. Sagun, E. I. Zenkevich, V. N. Knyukshuto, A. M. Shulga, D. A. Starukhin, C. von Borczyskowski, Chem. Phys. 275 (**2002**) 211.

131. R.O. Ogbou, J.L. Limson, E. Prinsloo, T. Nyokong, Synth. Met. 204 (**2015**) 122.

Appendix

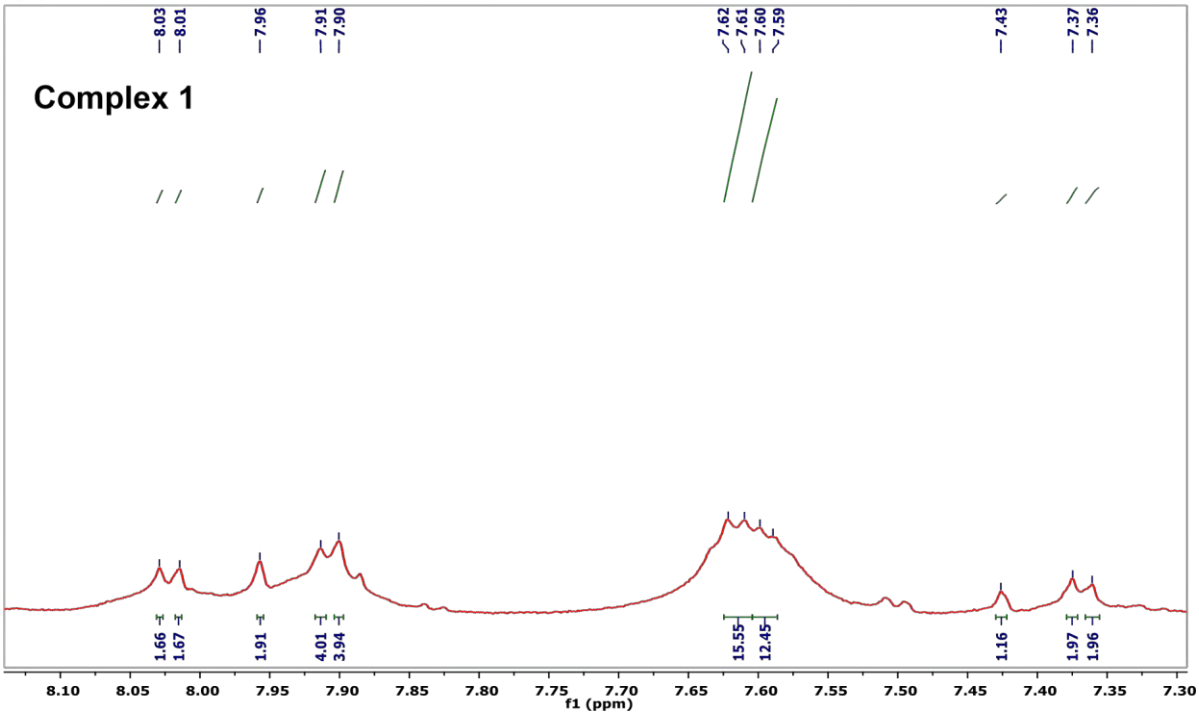

Fig A1: Fig A1: ^{1}H-NMR spectrum of complex 1 at 600MHz in $CDCl_3$.

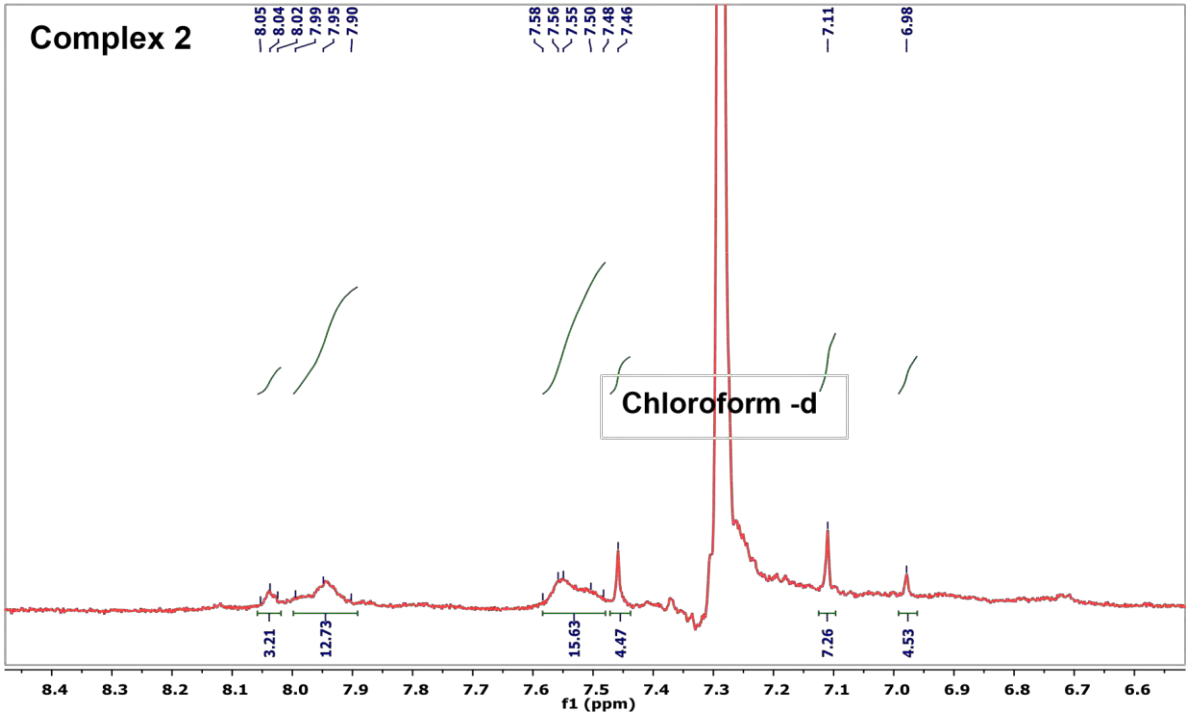

Fig A2: ^{1}H-NMR spectrum of complex 2 at 600MHz in $CDCl_3$.

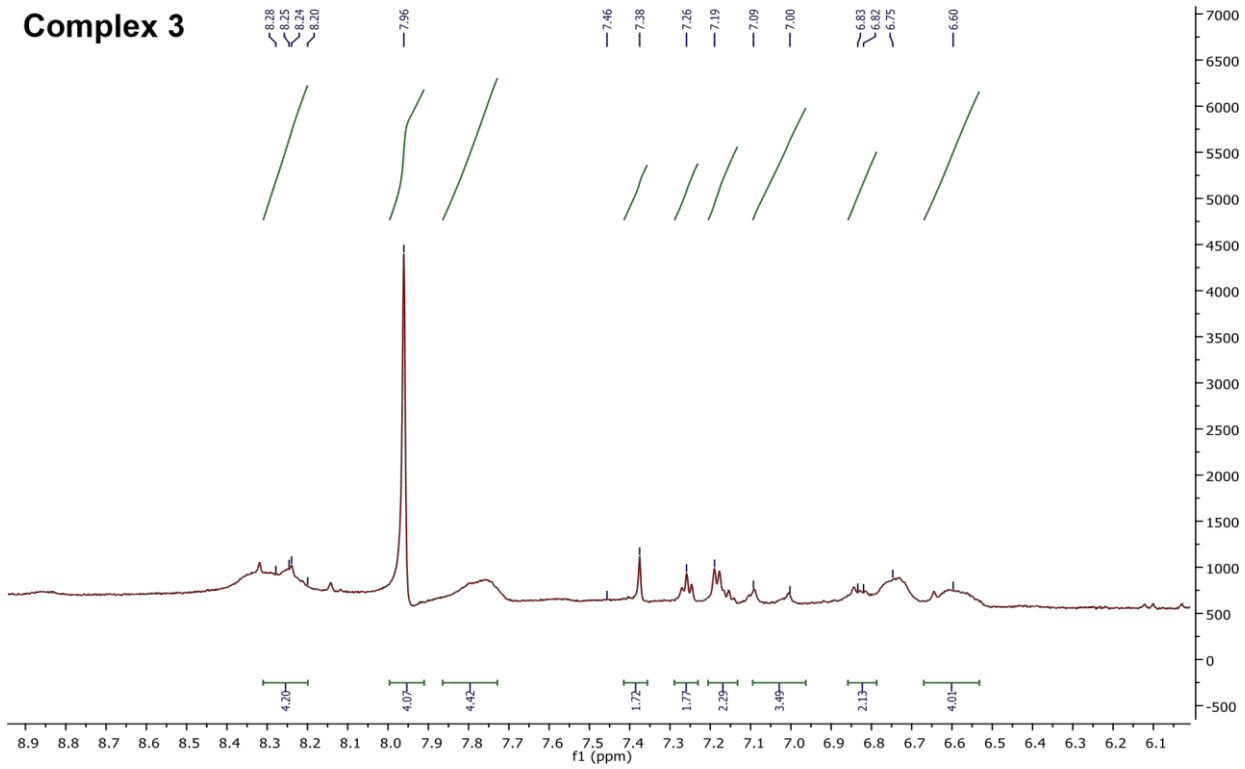

Fig A3: ^{1}H-NMR spectrum of complex 3 at 600MHz in DMSO.

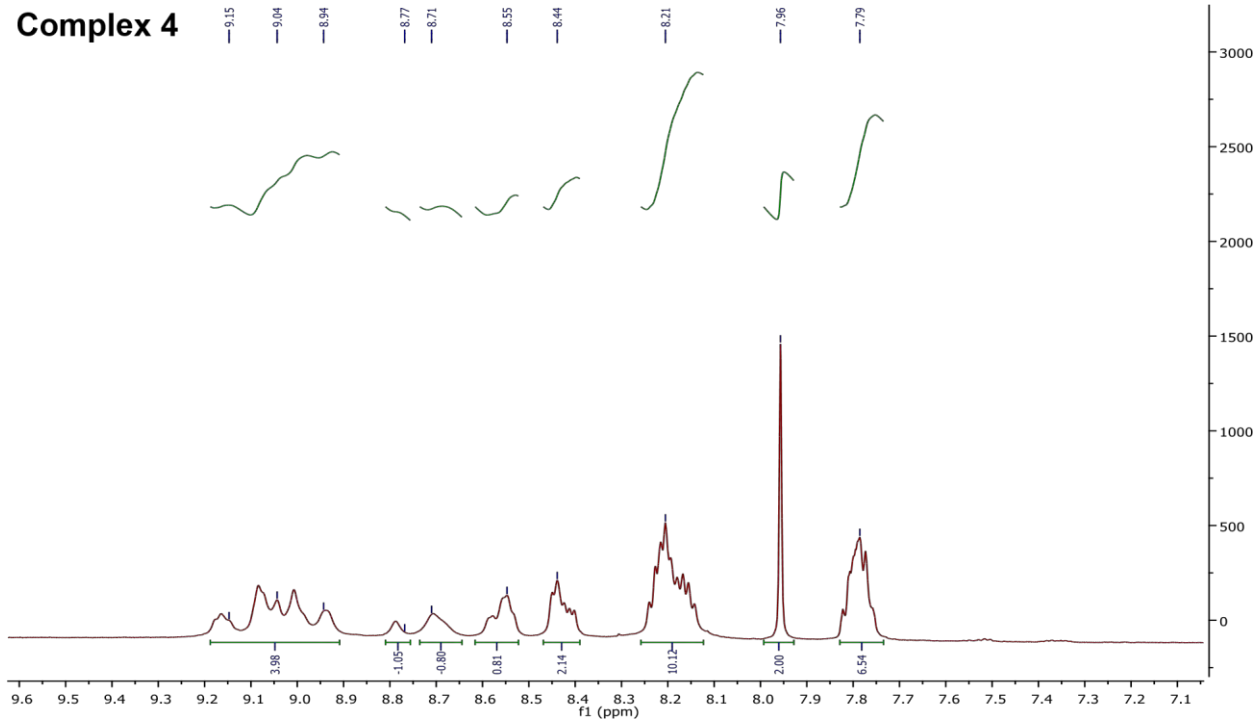

Fig A4: ^{1}H-NMR spectrum of complex 4 at 600MHz in DMSO.

(4) Yield: 73 %; UV/ Vis (DMSO): λ_{max}/nm (log ε): 340 (4.48), 615 (4.29), 680 (5.34). FTIR (KBr, cm^{-1}) 3040 (C–H), 1582, 1244, 1554 (C–O), 1135, 1093, (C–O–C) 865, 765 ^{1}H NMR (600, DMSO-d_6) ppm: 9.15 – 8.94 (m, 4H, pyridyloxy), 8.77 (s, H, pyridyloxy), 8.71 (s, H, pyridyloxy), 8.55 (s, H, pyridyloxy), 8.44 (m, 2H, pyridyloxy), 8.21 (m,10H, Pc), 7.96 (s, 2H, Pc), 7.79 (m, 7H, pyridyloxy), Calc for $C_{52}H_{28}N_{12}O_4Zn$ (%): C, 65.53, H, 2.97, N, 17.69; Found C: 65.28, H 2.90, N 17.62. MALDI TOF MS *m/z*: 949.43 amu. Found: 948.34 amu $[M - H]^+$.

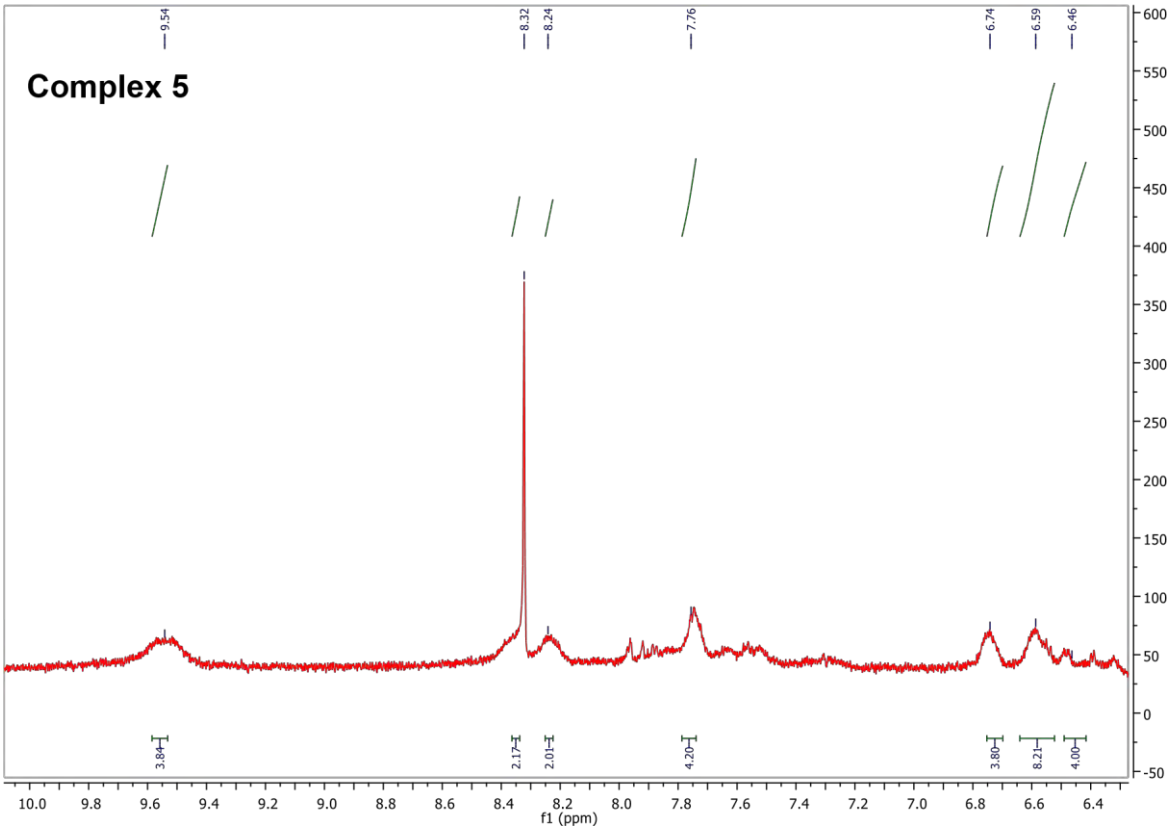

Fig A5: ^{1}H-NMR spectrum of complex 5 at 600MHz in DMSO.

(5) Yield: 68 %; UV/ Vis (DMSO): λ_{max}/nm (log ε): 314 (4.48), 618 (4.39), 693 (5.11). FTIR (KBr, cm^{-1}) 3071 (C-H), 1620 (C=N/C=C), 1634, 1554, 1480, 1344, 1255 (C–O–C) 1183, 1062 and 1011. ^{1}H NMR (600, DMSO–d_6) ppm: 8.94 (m, 4H, Pc), 8.32 (m, 2H, Pc), 8.24 (m, 2H, Pc), 7.76 (s, 4H, Pc), 6.74 (s, 4H, benzo[d]thiazole-2-ylthio), 6.59 (m, 8H, benzo[d]thiazole-2-ylthio), 6.46 (m, 4H, benzo[d]thiazole-2-ylthio), Calc (%) for $C_{60}H_{28}InClS_8N_{12}O_4$: C, 58.24, H, 2.44, N, 8.49, S, 19.44 Found C: 57.99, H 2.45, N 8.50 S, 19.37 MALDI TOF MS *m/z*: 1324.43 amu. Found: 1322.74 amu $[M - 2H]^+$

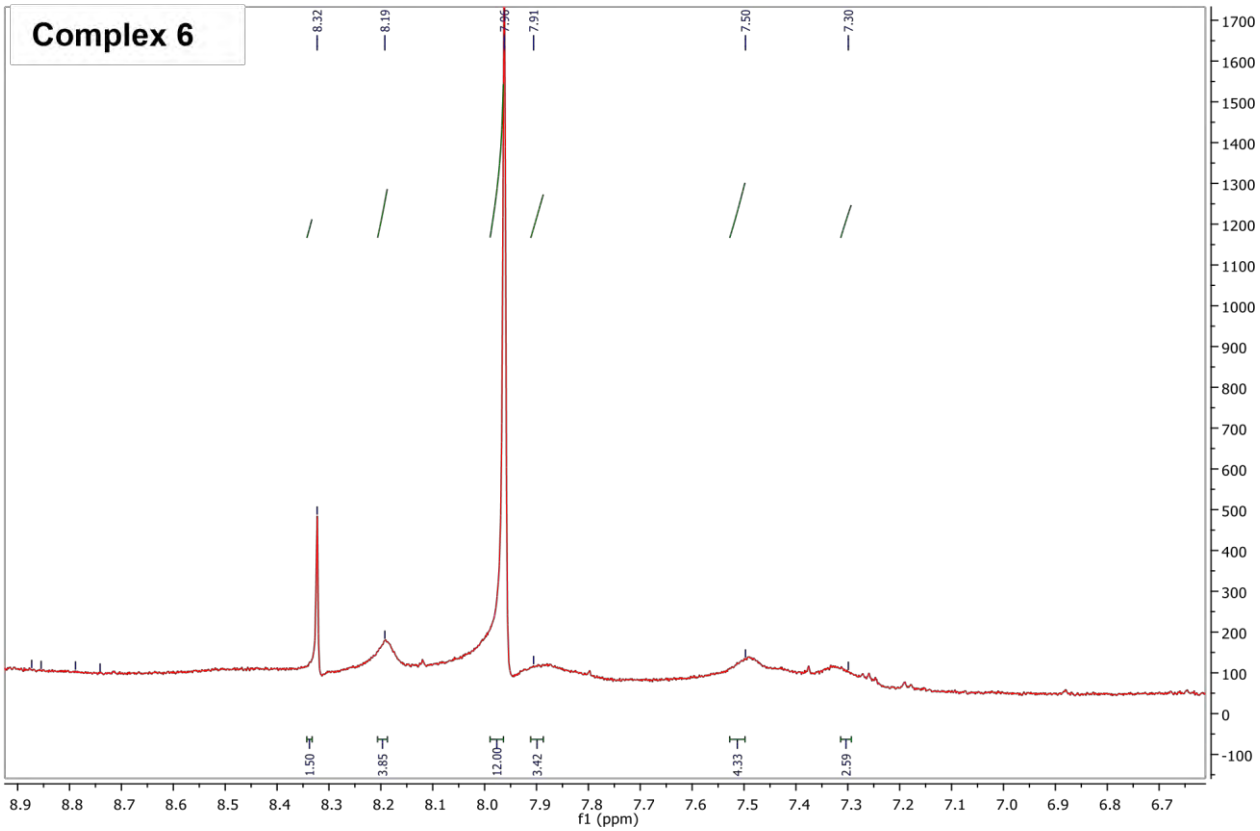

Fig A6: ^{1}H-NMR spectrum of complex 6 at 600MHz in DMSO.

(6) Yield: 75%; UV/ Vis (DMSO): λ_{max}/nm (log ε): 365 (4.86), 664 (4.92), 689 (5.52). FTIR (KBr, cm^{-1}) 3064 (C-H), 1622 (C=N/C=C) 1632,1550, 1469, 1343, 1252 (C-O-C) 1180, 1061 and 1010. ^{1}H NMR (600, DMSO-d_6) ppm: 8.32 (s, 2H, benzo[d]thiazole2-ylthio), 8.19 (s, 4H, benzo[d]thiazole-2-ylthio), 7.96 (m,12H, Pc), 7.91 (m, 3H, benzo[d]thiazole-2-yithio), 7.50 (s, 4H, benzo[d]thiazole-2-ylthio), 7.30 (s, 3H, benzo[d]thiazole-2-ylthio), Calc (%) for $C_{60}H_{28}N_{12}S_8O_4$: C, 58.17, H, 2.40, N, 13.24, S, 20.17. Found C: 58.14, H 2.36, N 13.18, S 20, 09. MALDI TOF MS *m/z*: 1239.43 amu. Found: 1238.66 amu $[M - H]^+$.

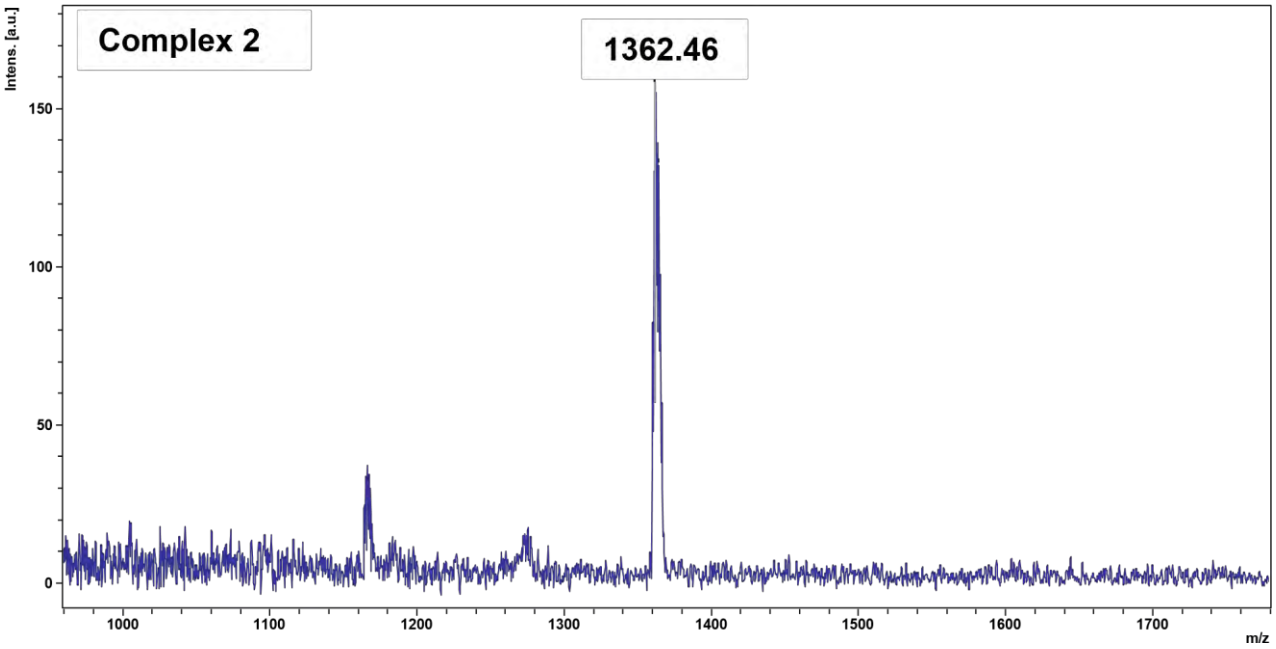

Fig A7: The MS (Maldi-TOF) for 2

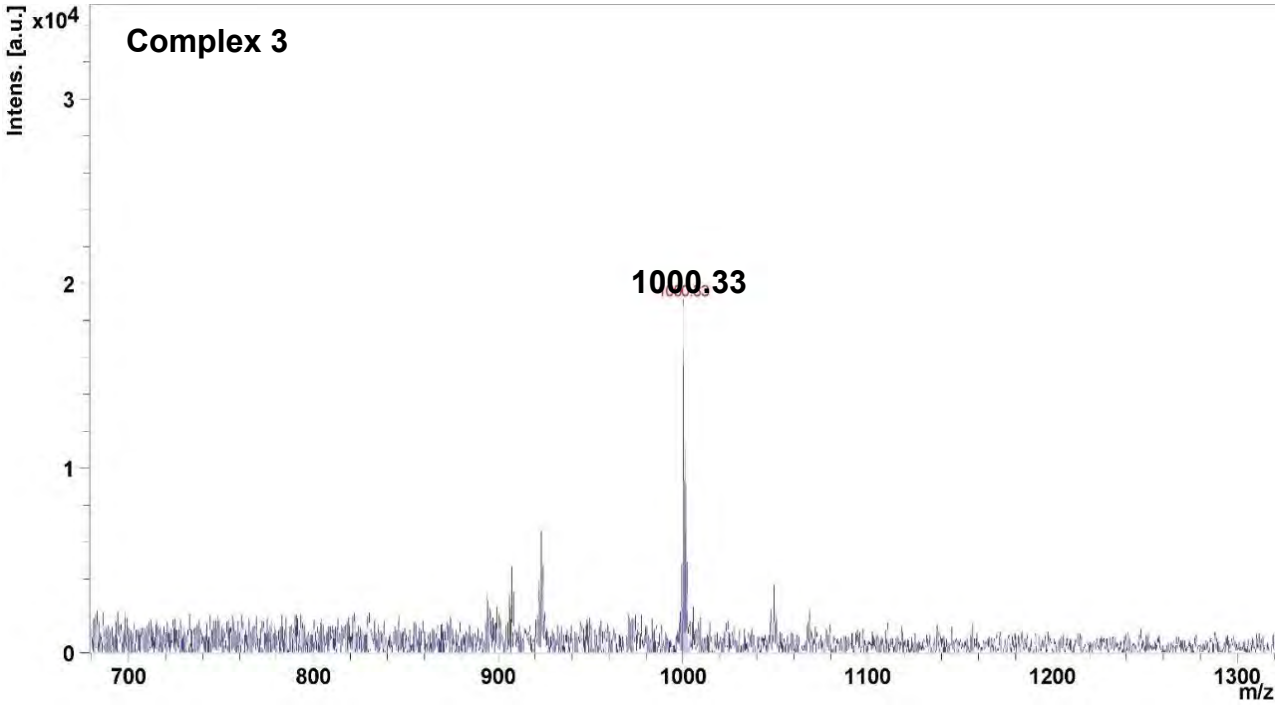

Fig A8: The MS (Maldi-TOF) for 3.

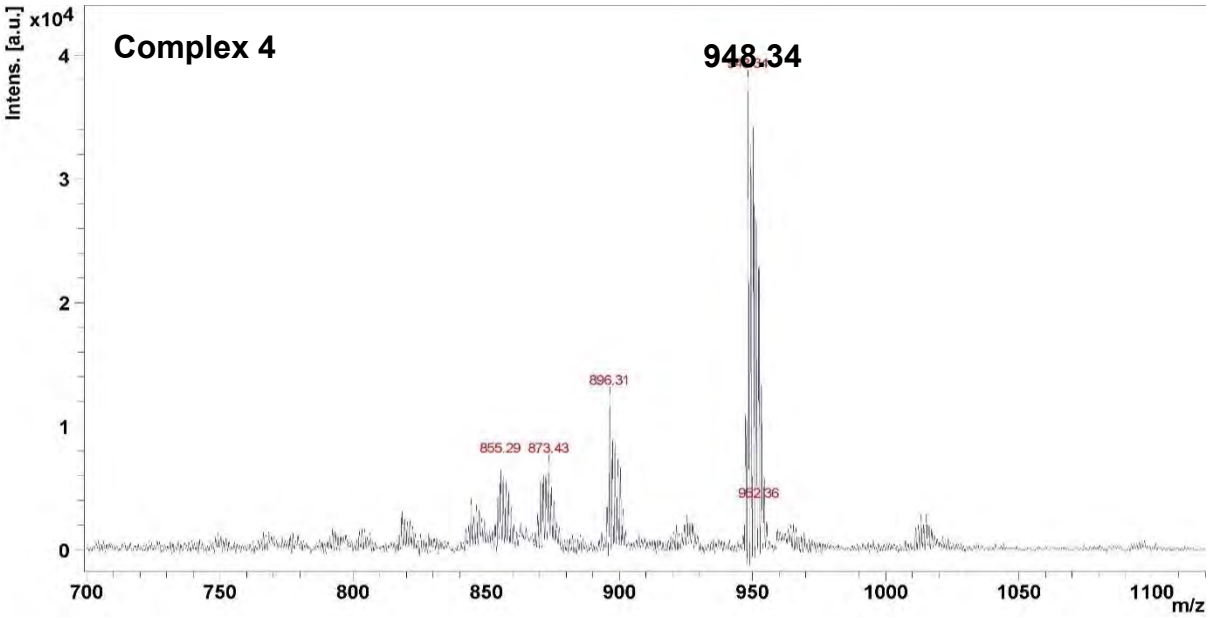

Fig A9: The MS (Maldi-TOF) for 4

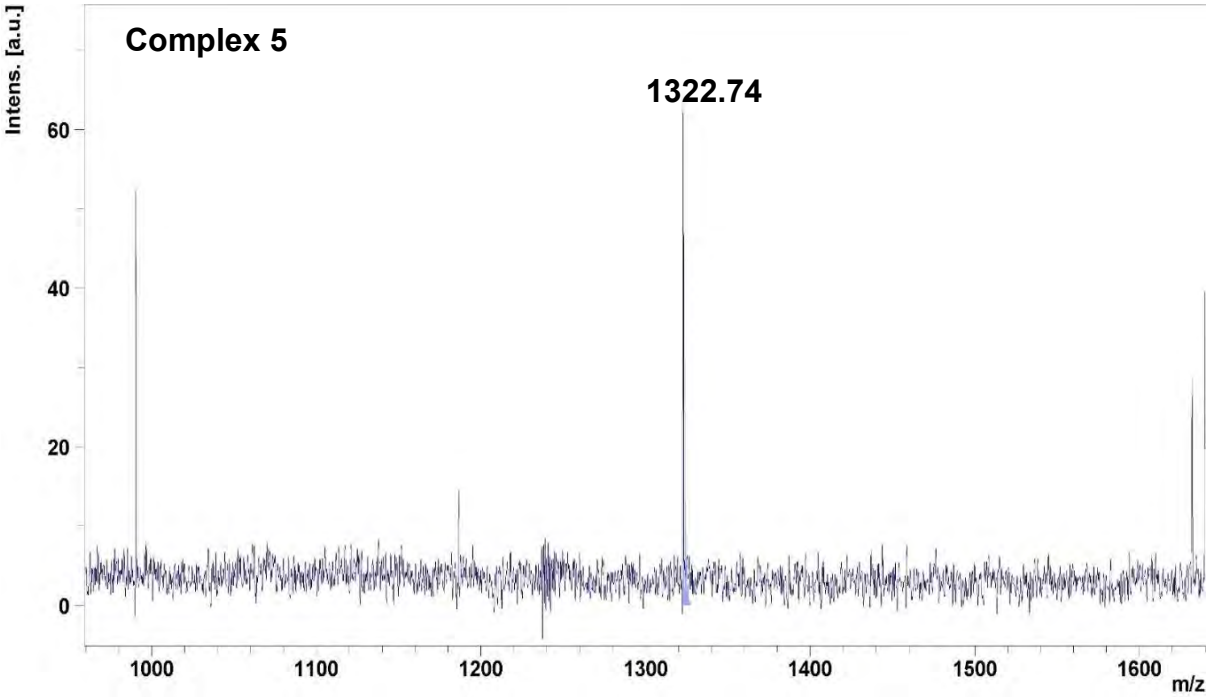

Fig A10: The MS (Maldi-TOF) for 5.

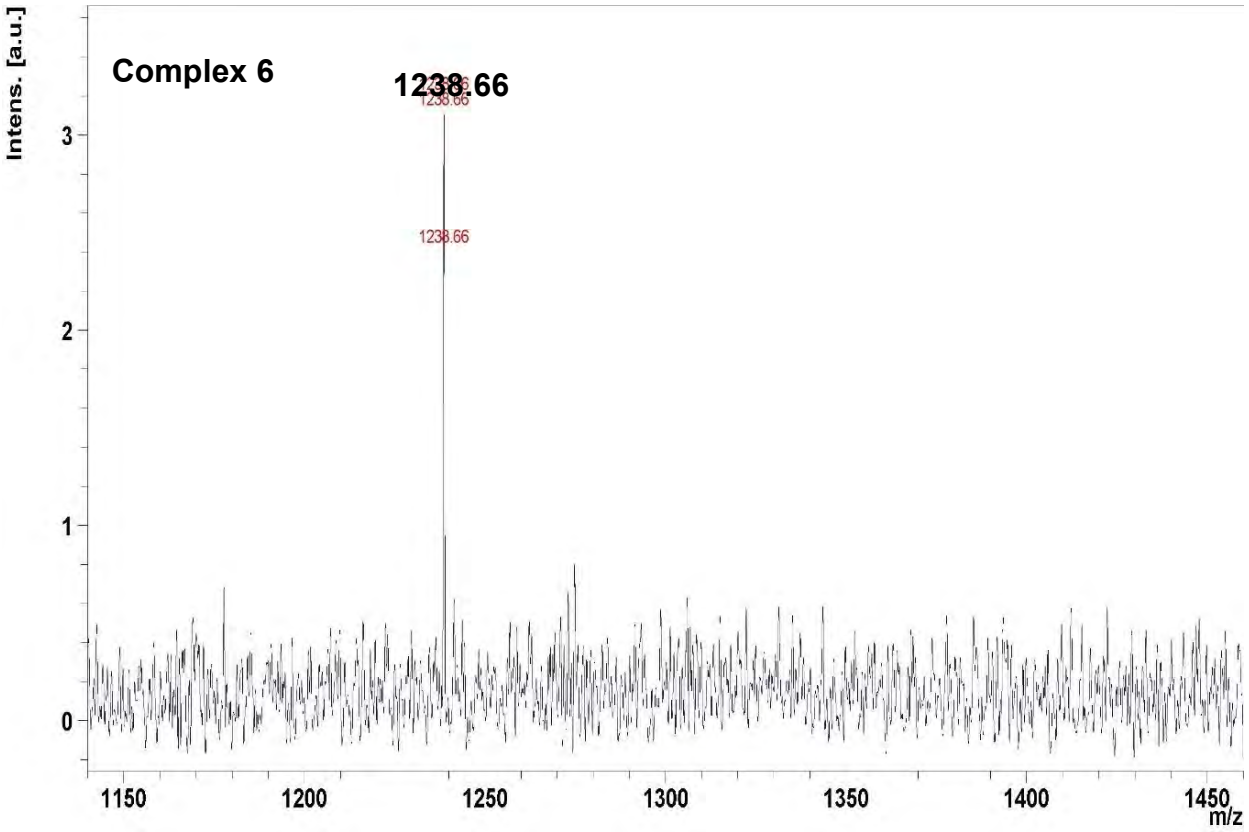

Fig A11: The MS (Maldi-TOF) for 6.